The Coupling of Dynamics and Chemistry in the Antarctic Stratosphere

A thesis
submitted in partial fulfilment
of the requirements for the Degree
of
Doctor of Philosophy in Physics
in the
University of Canterbury

by

Petra E. Huck

University of Canterbury
2007

Abstract

This thesis addresses the parameterisation of chemical and dynamical processes in the Antarctic stratosphere. Statistical models for the inter- and intra-annual variability in Antarctic stratospheric ozone depletion were developed based on theory and an understanding of the coupling of dynamics and chemistry in the atmosphere.

It was confirmed that the primary driver of the long-term trend in the severity of the Antarctic ozone hole is halogen loading in the stratosphere. The year-to-year variability in ozone mass deficit, a measure of the severity of Antarctic ozone depletion, could be described by a linear combination of South Pole temperatures and midlatitude wave activity. A time lag of two weeks between wave activity effects and ozone depletion indicates the predictive capability of meteorological parameters for seasonal projections of the severity of the Antarctic ozone hole. The statistical model describing the inter-annual variability in ozone mass deficit was regressed against observations from 1979 to 2004. The resulting regression coefficients were applied to South Pole temperature and wave activity fields from 28 chemistry-climate models. This analysis indicates a slight increase in the year-to-year variability in the severity of Antarctic ozone depletion.

As a prelude to analysing the seasonal evolution of Antarctic ozone depletion, an improved ozone mass deficit measure was derived by replacing the constant 220 DU threshold with a seasonal varying pre-ozone hole background which leads to better capturing the true extent of the depleted ozone. Furthermore, it was shown that the new measure represents the chemical ozone loss within the Antarctic vortex provided that no mixing occurs through the vortex boundary. This new measure has many advantages over previous stratospheric ozone depletion indices. The conventional ozone mass deficit omits large amounts of depleted mass of ozone, and the onset of ozone depletion does not coincide with the timing of when sunlight first reaches areas of polar stratospheric clouds as expected from

theory. Chemical ozone loss derived with a tracer-tracer correlation technique depends on ozone and passive tracer profile measurements which are not as readily available as the total column ozone fields required for the new ozone mass deficit presented in this thesis. As such, the new ozone depletion measure combines the simplicity of the old ozone mass deficit index with higher accuracy of the actual amount of chemically depleted stratospheric ozone. Furthermore, when applying the new definition of ozone mass deficit to chemistry-climate model outputs, model intercomparisons should become easier to interpret because biases in the models can be avoided.

Based on theory and understanding of the coupling of chemistry and dynamics in the Antarctic stratosphere, two semi-empirical models were developed to describe the intra-seasonal evolution of chlorine activation and ozone depletion. Regression of the models against chlorine monoxide and ozone mass deficit from observations results in coefficients that capture key sensitivities in the real atmosphere. The seasonal evolution of ozone mass deficit can be described with these coefficients and readily available meteorological fields (temperature and wind fields). The predictive capability of these models was demonstrated for 2005 and 2006. Given temperature and wind fields, which for example can be obtained from general circulation models, these models can predict the size and depth of the Antarctic ozone hole. Important applications of the semi-empirical models could be chemistry-climate model validation by comparing the sensitivities from observations and models which may provide new insights into potential sources of differences in chemistry-climate model projections of Antarctic ozone depletion. Furthermore, projection of the inter-annual and intra-seasonal evolution of the Antarctic ozone hole into the future can help to assess the potential recovery of the Antarctic ozone hole.

Acknowledgements

It is my great pleasure to thank everybody who made this thesis possible and enjoyable. I would like to thank my supervisors Adrian McDonald and Greg Bodeker for always having their doors and email accounts open, for their infinite support and encouragement, their knowledge and perceptiveness, and for barbecues, bunny sitting and farm stays. Thank you to my examiners Ulrike Langematz and Jim Renwick for reading through the thesis and adding helpful comments. I would also like to thank Peter Cottrell for his interest in my work and for asking "How is it going?" when I needed someone to ask me that. Thank you to my office mate Kate Monahan for many cheerful moments, the best chocolate brownies and for always listening to my minor and not so minor problems. I would also like to thank the Atmospheric group and everybody else in the department who was part of my three years at the University of Canterbury. I had the privilege to spend some time at NIWA in Lauder and I would like to thank everybody from the Lauder team for making my visits down South always very enjoyable. Thanks to Bill Randel at NCAR in Boulder for inviting me to visit for six weeks and having some valuable thoughts on the project and to Simone Tilmes for a great collaboration and good times in and around Boulder.

Furthermore, I would like to thank my friends here in Christchurch and all around the world for being there, thinking of me and supporting me throughout the past three years. Thank you to my family for your encouragement and support and all your mail and phone calls. Special thanks to my parents for always believing in me and staying so close over such a long distance. And the greatest thanks go to my husband Thomas for his incredible amount of patience and understanding, for always knowing how to motivate me during a time when we were both very busy.

Contents

List of Figures

List of Tables

Chapter 1

Introduction

Trends and variability in global ozone impact life on Earth. Without the protection of stratospheric ozone, life-threatening ultraviolet irradiation at the surface would increase. This has important consequences for the biosphere, human health and economic sustainability [e.g. *McKenzie et al.*, 1999, and references therein]. After the discovery of the Antarctic ozone hole in 1985 [*Farman et al.*, 1985] the severity and the size of the ozone hole has increased steadily. However this increase has shown significant year-to-year fluctuations. It has been suggested that these variations are strongly linked to atmospheric dynamics and in particular planetary-scale waves in the atmosphere [*Shindell et al.*, 1997; *Randel et al.*, 2002, and others]. In addition, each year has specific dynamical events which cause variation in the rate of change of ozone depletion over the course of the year. To answer the questions about the future development and consequences of the Antarctic ozone hole, it is essential to understand the dynamical and chemical processes leading to the long-term trend as well as the inter- and intra-annual variability in stratospheric ozone depletion.

In this thesis, the coupling of dynamics and chemistry in the Antarctic stratosphere is examined to describe inter- and intra-annual variability in Antarctic ozone depletion. Dynamics in the form of planetary-scale atmospheric waves can affect the ozone distribution directly through transport of trace gases. In addition, indirect effects such as heat transport causing temperature changes which in turn modify ozone destruction have to be considered. Planetary waves can change the dynamical conditions in the Antarctic stratosphere and thereby change the

conditions necessary for ozone destruction. Chemical ozone depletion depends on the abundance of halogens in the stratosphere, temperature and the availability of sunlight. In particular, low temperatures (<195 K) are necessary for the formation of polar stratospheric clouds which lead to heterogeneous chemistry and chlorine activation which is a basic requirement for ozone depletion. Based on this theory, statistical models are developed which can then be used to project inter-annual variability and the intra-seasonal evolution of Antarctic stratospheric ozone depletion into the future.

1.1 Structure and Composition of the Atmosphere

In the vertical, the atmosphere can be classified by different physical properties. Most commonly the atmosphere is classified by changes in temperature with altitude [e.g. *Brasseur and Solomon*, 1984; *Kraus*, 2000]. The schematic in Figure 1.1 illustrates the different regions of the atmosphere including the most important phenomena in those regions and the corresponding temperature characteristics.

The lowest layer in this classification scheme is the **troposphere**. It reaches an altitude of up to 15 km in equatorial regions, 10-12 km in midlatitudes, and about 8 km in polar regions. The layer is characterised by temperature decrease with altitude of an average value of 6.5 K/km. It is primarily composed of nitrogen (78 %) and oxygen (21 %) and small concentrations of trace gases. Nearly all atmospheric water vapour or moisture is found in the troposphere. This is the region where most of the World's weather occurs, for example cloud formation and precipitation as a result of high water content and strong vertical mixing. The boundary between the troposphere and the region above is called the **tropopause**. It can be defined as the lowest level where the temperature decrease with altitude is 2 K/km or less and is therefore characterised by an increase in the static stability (stability of the atmosphere in hydrostatic equilibrium with respect to vertical displacements) [*Holton et al.*, 1995]. The rate of transport between tropospheric and stratospheric source gases is determined here [*Andrews et al.*, 1987].

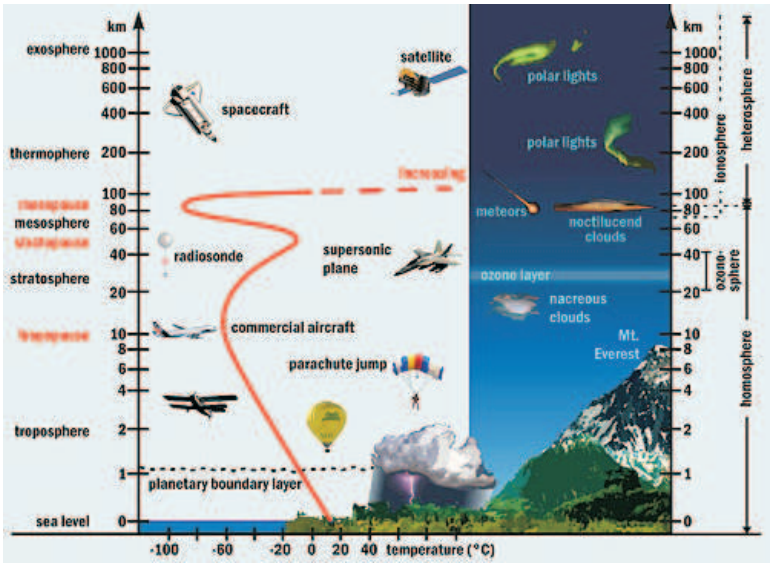

Figure 1.1: Schematic of the structure of the atmosphere, the most important phenomena in each region and the different ways of classification. (Source: http://www.kowoma.de/en/gps/additional/atmosphere.jpg)

The layer above the tropopause is called the **stratosphere**. It reaches an altitude of about 50 km. The name stratosphere comes from the Greek word *stratus* which means *layered*. The temperature in this layer increases with height, which makes it very stable with extremely low vertical wind velocity. There is very little water vapour in this region and therefore hardly any clouds. Ultra-violet (UV) radiation in this part of the atmosphere splits oxygen molecules to form ozone. The global and longtime average location of the ozone maximum is at about 25 km which is why this layer is known as the "ozone layer". In turn, the ability of ozone to absorb UV radiation leads to a temperature increase, a feedback process between the ozone and the thermodynamics. The filtering of UV radiation in the stratosphere is extremely important for life on Earth. Without the protection of stratospheric ozone, the UV irradiation at the surface would be much larger and life on Earth would not be possible in its current form. The top of the stratosphere is characterised by the temperature maximum which is at -3 °C in the climatological global average. It is called the **stratopause** above which little ozone is left to heat the atmosphere.

Adjoining the stratopause the next higher layer is called the **mesosphere**. It is between 50-80 km and characterised by decreasing temperature with altitude, due to the low air density and no ozone to absorb UV. The **mesopause** is located at about 80 km where the temperature stops to decrease.

The region above the mesopause is called the **thermosphere**. It extends from 80-800 km and stretches up to the frontier of interplanetary space. Temperature increases with altitude again because cosmic rays lead to ionisation. Air density is extremely low in this region and gases (e.g. nitrogen and oxygen) are photo-dissociated and partly ionised. The lower part of the thermosphere, from 80 to 550 km above the Earth's surface, is therefore also known as the **ionosphere**. This is the region of the atmosphere where the aurorae occur. Beyond the ionosphere, the upper part of the thermosphere, extending out to perhaps 10,000 km is the **exosphere** or outer thermosphere, which gradually merges into space. Air atoms and molecules are constantly escaping to space from the exosphere. In this region of the atmosphere, hydrogen and helium are the prime components and are only present at extremely low densities.

1.2 Dynamics of the Atmosphere

1.2.1 Meridional and Zonal Circulation

Explanation for why the surface winds on global scales blow from the east at subtropical latitudes and from the west in middle latitudes, and why the trade winds are steady from one day to the next, whereas the westerlies in midlatitudes are not, has been sought for since the pioneering studies of *Halley* [1676]. In 1735 George Hadley [*Hadley*, 1735] suggested that the intensity differences in the amount of sunshine between the equatorial region (up to 300 Wm^{-2}) and the polar regions (down to 100 Wm^{-2}) lead to energy and temperature contrasts which would create a thermal circulation in the form of a large convection cell over each hemisphere (Figure 1.2(a)). In the 1920s, a three-cell model was introduced with two active cells (Hadley cells) over the polar regions and the equatorial

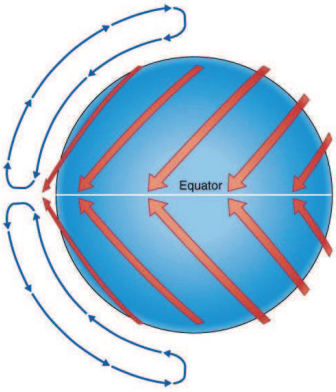

(a) Hadley circulation model (1735)

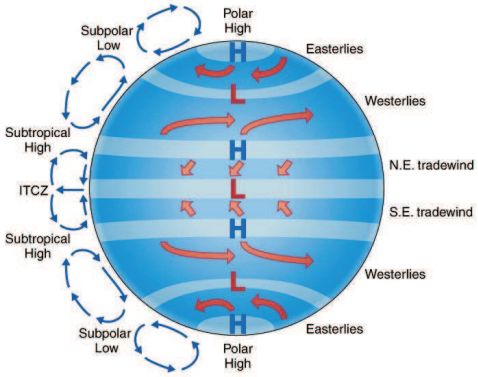

(b) Three-cell circulation model (1920s)

Figure 1.2: Schematics of Hadley circulation and the three-cell circulation models of the general circulation of the atmosphere

regions and one indirect cell (Ferrel cell) in between, over the midlatitudes (Figure 1.2(b)) [*Holton*, 1992]. The scientific breakthrough to understanding the general circulation in the atmosphere occurred in the middle of the 20th century with the discovery of baroclinic instability by *Eady* [1949] and *Charney* [1947] and the development of general circulation models.

Most atmospheric models of the general circulation are based on the primitive equations, which govern the evolution of large-scale atmospheric motion. They include the horizontal equation of motion as well as equations relating the vertical component of the motion to the time rates of change of the thermodynamic variables p, ρ and T [e.g. *Wallace and Hobbs*, 2006]. Starting with a stable and

stratified atmosphere, the first "action" of a general circulation model would be to cool the polar regions and warm the tropics in analogy to the equator-to-pole energy gradient in the real atmosphere. The temperature differences would lead to thermal expansion of the pressure surfaces in the tropical upper troposphere and to descent of the pressure surface over the polar regions. The sloping of the pressure surface results in an equator-to-pole pressure gradient which in turn causes a poleward flow above the surface. Due to the poleward flow in the upper troposphere, mass gets redistributed which causes the surface pressure at the poles to rise and at the equator to sink. This in turn causes a compensating equatorward flow at low levels. The next step in the model would be that the Coriolis force adds a westward component to the equatorward flow in the lower branch of the cell and an eastward component to the poleward flow in the upper branch of the cell. The flow becomes progressively more zonal (parallel to circles of constant latitude) until geostrophic balance between the meridional (parallel to circles of constant longitude) component of the Coriolis force and the pressure gradient force is achieved. Vertical wind shear between the surface and the upper levels strengthens the equator-to-pole temperature gradient. When the meridional temperature gradient in the model reaches a critical value, baroclinic instability creates a wave-like structure on the flow. Wave induced forces are essential for describing the real atmosphere in a general circulation model.

Waves dissipating in the stratosphere are responsible for driving the transport circulation in the meridional plane and influence the observed temperature distribution (Figure 1.3). This circulation is also known as the Brewer-Dobson circulation in honour of the work of *Brewer* [1949] and *Dobson* [1956]. It had been assumed that the temperature of the polar lower stratosphere is mainly controlled by the variation of the solar declination from the winter solstice to the summer solstice and by the distribution of radiatively active trace gases such as ozone, water and carbon dioxide [*Shine*, 1987]. However, during winter, the lower stratosphere was found to be considerably warmer than would be expected from a pure radiative calculation [*Fels*, 1982]. This additional warming is caused

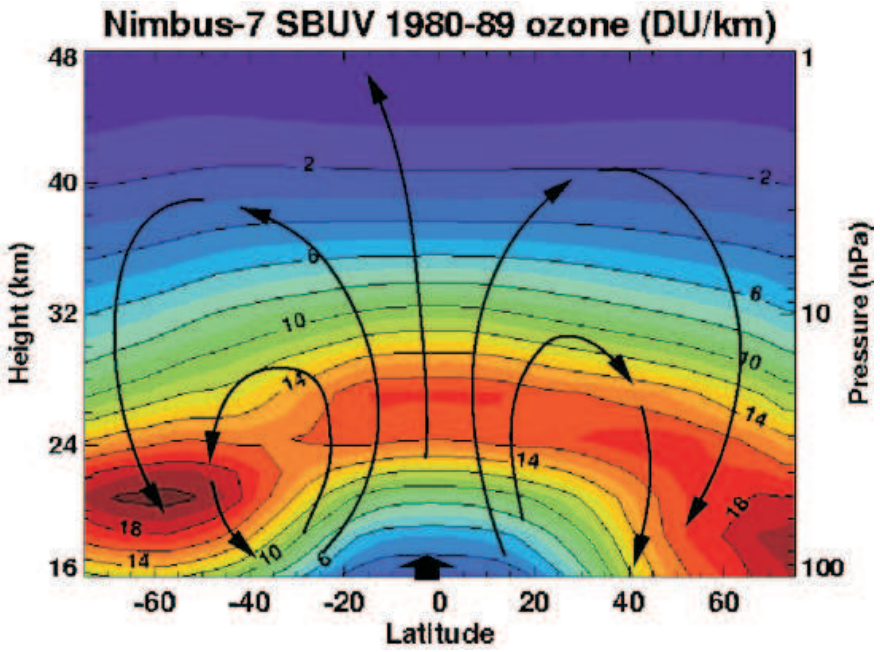

Figure 1.3: Dynamical aspects in the stratosphere: equatorial air masses ascend and move polewards (Brewer-Dobson circulation). Due to this circulation least ozone is found in the tropical stratosphere even though this is where most of it is produced (Source: http://www.ccpo.odu.edu/SEES/ozone/oz-class.htm).

by non-linear wave breaking or dissipation of waves and polar descent via the Brewer-Dobson circulation [*Andrews et al.*, 1987]. In addition, this circulation advects trace constituents meridionally and vertically and has a strong impact on the concentration of stratospheric ozone [*Holton and Alexander*, 2000]. Ozone is carried from the photochemical production region in the tropical upper stratosphere to the polar lower stratosphere, resulting in the steady accumulation of ozone in the polar lower stratosphere [*Chipperfield and Jones*, 1999].

The westward zonal flow caused primarily by wave breaking results in a poleward drift. Following the law of mass continuity, this meridional drift leads to upward motion in low latitudes and downward motion in high latitudes. Thus, the extratropical wave drag force acts as a "pump": it pulls air upward in the tropics and pushes air downward at high latitudes (Figure 1.4). The relationship of the stratospheric circulations to the wave from the troposphere was confirmed by *Haynes et al.* [1991] with the "downward control" principle. It states that

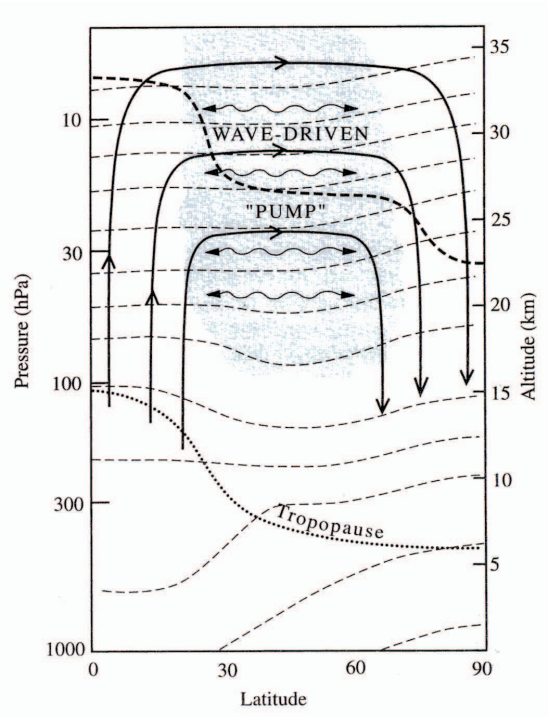

Figure 1.4: Schematic latitude-height cross section showing the wave-driven transport circulation (solid lines with arrows) of the winter stratosphere. Shading indicates the region of planetary wave-breaking ("surf-zone"). Light dashed lines are isentropes, dotted line indicates the tropopause. Wavy double-headed arrows indicate meridional mixing by wave-breaking. Heavy dashed line shows a constant mixing ratio surface for a long-lived tracer (Source: [*Holton and Alexander*, 2000]).

the circulation across an isentropic surface (surface of constant potential temperature) is controlled by the upward propagating waves that break at higher levels. It has been used for example by *Fusco and Salby* [1999] to investigate the coherence of the inter-annual variation of northern hemisphere midlatitude ozone with upwelling wave activity.

1.2.2 Polar Vortices

The stratospheric polar night jet stream forms during autumn at the boundary of adjacent air masses with significant differences in temperature, i.e. the polar region and the warmer air equatorwards [*Reid*, 2000]. Low temperatures over the polar regions are due to the absence of solar heating in winter and the warmer air

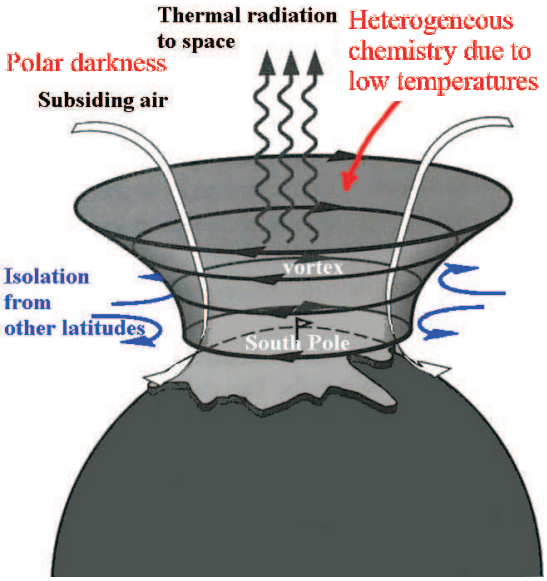

Figure 1.5: Schematic of the Antarctic polar vortex during polar darkness (modified from www.ldeo.columbia.edu)

equatorwards is due to the adiabatic warming caused by the descending branch of the Brewer-Dobson circulation [*WMO*, 2003]. The polar night jet is generally located close to the latitude separating night and day during the polar winter, and represents the boundary of the spinning vortex over the pole (Figure 1.5). The polar vortex itself represents the cyclonic low pressure system developing over the winter pole, resulting in circumpolar winds as described by the thermal wind equation. The Antarctic polar vortex persists throughout the winter until seasonal temperatures increase due to radiation and dynamics, causing a weakening of the polar vortex until a final warming event breaks the structure apart. In the Arctic however, sudden warming events due to stronger wave activity than in the southern hemisphere, can weaken or even dissipate the jet during polar winter.

The area of the vortex increases with altitude and the structure acts as a quasi-isolated containment vessel. Most of the air inside the polar vortex is trapped through the entire winter and often into spring, and temperature decreases to very low values (<180 K). At temperatures below 195 K polar stratospheric clouds start to form. On the surface of the cloud particles heterogeneous chemistry leads

to chlorine activation and when sunlight returns to the polar regions this leads to ozone destruction [*Solomon*, 1999, and Section 1.3.2-1.3.3].

Vertical transport leads to descent of tracers in and around the vortices, while mixing redistributes ozone and trace gases on isentropic levels. Large-scale mixing events lead to some exchange across the vortex edge [*WMO*, 2003]. *Manney et al.* [2003] examined how different meteorological analyses affect the amount of exchange between middle latitudes and the vortex. They found that overall the vortex remains well isolated in wintertime. Descent inside the polar vortex during winter, driven by the descending branch of the Brewer-Dobson circulation, builds up and maintains low stratospheric ozone at certain isentropic levels [*WMO*, 2003]. Current evidence suggests that the Arctic vortex is well mixed in the absence of intrusions of air from the vortex edge [*Richard et al.*, 2001], however, the Antarctic vortex is considered to be separated into two regions: a strongly mixed vortex core and a weakly mixed vortex collar extending to the vortex boundary [*Lee et al.*, 2001].

1.2.3 Planetary Waves

Planetary waves are large-scale motions in the ocean or atmosphere whose restoring force is the variation in Coriolis force with latitude (β-effect). In an inviscid barotropic fluid of constant depth, the planetary wave is an absolute vorticity conserving motion. They are also known as rotational waves or Rossby waves, as the waves were first identified in the atmosphere in 1939 by Carl-Gustaf Arvid Rossby [*Rossby*, 1939].

Rossby waves in the atmosphere are easy to observe as large-scale meanders of the jet stream. When these loops become very pronounced, they detach masses of cold, or warm air that can become cyclones and anticyclones that are responsible for day-to-day weather patterns at midlatitudes (Figure 1.6).

While the zonal phase propagation of gravity waves can be either eastward or westward, the phase propagation of Rossby waves can only be westward relative

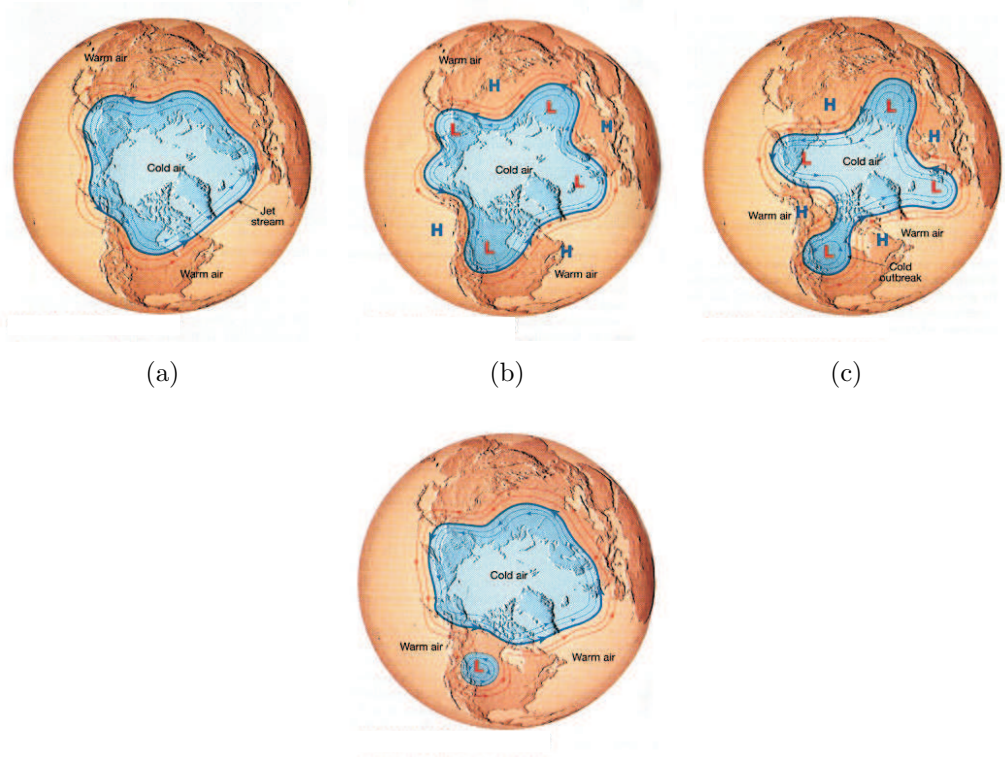

Figure 1.6: Schematics of formation of planetary waves in the northern hemisphere: (a) slightly undulating air motion around the North Pole, (b) meanders form in jet stream, (c) strong waves in upper air flow, and (d) return to gentle undulating motion.

to the mean flow [*Holton and Alexander*, 2000, and Appendix C]. Atmospheric waves are excited when air is disturbed from equilibrium, for example when air is displaced over elevated terrain or heated inside convection [*Salby*, 1996]. Different topography in the northern and southern hemispheres, and more land-sea contrasts in the northern hemisphere, leads to stronger planetary-scale wave activity than in the southern hemisphere. Synoptic-scale motions decay rapidly with height above the tropopause. Therefore, throughout most of the stratosphere, the primary motion systems are planetary in scale. Above the lowest layers of the stratosphere, the global-scale circulation is dominated by a mean flow that is eastward in the winter hemisphere and westward in the summer hemisphere. Planetary waves excited by orographic or thermal forcing in the troposphere cannot propagate into the westward wind regime of the summer

stratosphere (Charney-Drazin criterion). The Charney-Drazin criterion provides an approximate explanation for the absence of stationary planetary waves in the summer stratosphere and the dominance of waves of zonal wavenumbers 1 and 2 in the winter stratosphere, as described in more detail in Appendix C.

The summer stratosphere wave disturbances are therefore much weaker than in the winter stratosphere. In particular, in the summer hemisphere the flow is nearly parallel to latitude circles. In the winter hemisphere however, the flow is disturbed by planetary-scale waves of zonal wavenumbers 1 and 2 and departs significantly from zonal symmetry. This effect is much stronger in the northern hemisphere but with the unique splitting of the Antarctic polar vortex in 2002, its significance for the southern hemisphere was demonstrated (see also Section 2.1).

The planetary waves in the northern winter stratosphere can amplify dramatically over a short span of time leading to rapid deceleration of the mean zonal flow which can be accompanied by a sudden stratospheric warming in the polar region. In a major warming the temperature at the 10 hPa level ($\sim$ 31 km) may increase by as much as 60 °C in less than a week [*Holton and Alexander*, 2000]. Until 2002, such major warmings occurred only in the northern hemisphere, in frequencies less than two years. Warmings of a less intense nature (minor stratospheric warmings) occur throughout the winter in both hemispheres, and lead to episodic pulses in the meridional transport.

1.2.4 Quasi-Biennial Oscillation

Waves play an important role in driving the equatorial quasi-biennial and semi-annual oscillations (QBO and SAO) [*Holton and Alexander*, 2000] which in turn can affect the year-to-year fluctuations in Antarctic stratospheric ozone. The QBO is a quasi-periodic oscillation of the equatorial zonal wind between easterlies and westerlies in the tropical stratosphere with a mean period of approximately two years (Figure 1.7). The alternating wind regimes develop at the top of the stratosphere and propagate downwards at about one kilometre per month until they are dissipated at the tropical tropopause. The amplitude of the easterly

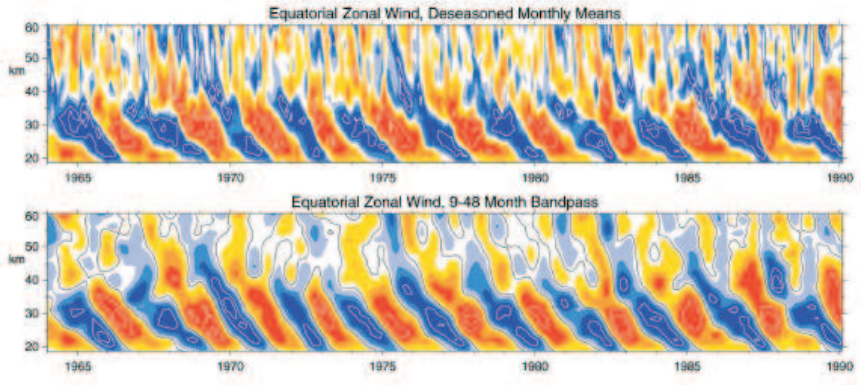

Figure 1.7: In the top panel time-height section of the monthly-mean zonal wind component, with the seasonal cycle removed, are displayed for 1964-1990. Red represents positive (westerly) winds [*Gray et al.*, 2001]. In the bottom panel the data are band-pass filtered to retain periods between 9 and 48 months (Source: *Baldwin et al.* [2001]).

phase is about twice as strong as that of the westerly phase.

The influence of the QBO on the polar atmosphere has been examined for example by *Garcia and Solomon* [1987] in the minimum vortex temperature at 200-50 hPa layer during October and *Lait et al.* [1989] in the South Pole temperature. *Newman and Randel* [1988] found a quasi-biennial modulation of the September-October wave 1 eddy heat flux in southern midlatitudes. During the west-phase QBO, the high-latitude southern stratosphere is slightly colder throughout the winter, planetary waves tend to propagate higher and more poleward, and the final warming occurs later. When the equatorial winds at 50 hPa are easterly, the northern polar vortex is more disturbed by waves, therefore it is warmer, and disruption of the vortex by sudden stratospheric warmings is more likely [*Baldwin and Dunkerton*, 1998]. This is caused by the propagation of quasi-stationary planetary-scale waves, which originate in the troposphere and propagate vertically and meridionally. The propagation and interaction with the mean flow depend on the latitude-height structure of the zonal mean wind, and in particular the position of the "zero-wind-line" which separates easterlies from westerlies [*O'Sullivan and Dunkerton*, 1995]. The phase of the QBO affects both

the position of the zero-wind-line and the structure of the zonal-mean wind field.

The influence of the QBO on the polar atmosphere has a similar magnitude in the northern and southern hemispheres but its timing and location are different [*Dunkerton and Baldwin*, 1992]. In the southern hemisphere the planetary wave amplitudes are relatively small and a major midwinter warming was only observed in 2002. The inter-annual variability of the wintertime southern vortex is smaller because the vortex is much stronger, colder, longer-lived and more quiescent than in the northern hemisphere due to less wave activity (see Section 1.2.3). During the west phase of the QBO the southern hemisphere vortex is slightly colder. The largest influence of the QBO in the southern hemisphere occurs during late spring (November). The time of the final warming in the southern hemisphere is comparable to the northern hemisphere where it occurs during January. However, the QBO in the southern hemisphere does not appear to modulate the strength of the high-latitude vortex during midwinter, as planetary waves do not significantly disrupt the vortex in the lower and middle stratosphere.

1.3 Stratospheric Ozone Depletion

1.3.1 Ozone Chemistry

Ozone is a trace gas and if the entire ozone in the total atmospheric column was brought to the ground at standard temperature and pressure, this compressed layer of ozone would be only three mm thick on average. However, stratospheric ozone is of great importance for life on Earth due to its ability to absorb UV-B and UV-C radiation. This protective shield has been threatened over the past 30 years because gases from anthropogenic sources (i.e. chlorofluorocarbons (CFCs)) have lead to anomalous stratospheric ozone loss in the atmosphere since the 1970s [*Solomon et al.*, 2005]. The strongest effects have been observed over the polar regions where in certain altitude levels all ozone is destroyed in spring time. Especially in the Antarctic this occurrence is known as the **ozone hole**. Fifteen percent of the ozone column is located in the upper stratosphere (above

∼30 km). Ozone loss in the stratospheric region affects global stratospheric temperatures and may impact the radiative balance in this region [*WMO*, 1999]. The thickness of the ozone layer is commonly expressed in Dobson units (DU), where 1 DU (1 DU=$2.69{\cdot}10^{16}$ molec/cm^2) is the thickness in hundredths of a millimetre that the total ozone column would occupy at standard temperature and pressure [*Wallace and Hobbs*, 2006]. It is named after G. M. B. Dobson who produced the first ozone spectrometer in 1923.

The main production of stratospheric ozone happens in tropical latitudes in two steps. The first step is photolysis of molecular oxygen which results in two highly reactive oxygen atoms. The second step is recombination of atomic and molecular oxygen to form ozone. In the schematic in Figure 1.8 the chemical reactions involved in ozone production are illustrated. Photochemical destruction of ozone is caused by photolysis of ozone molecules (Reaction 1.1) which again results in a highly reactive oxygen atom and an oxygen molecule. The oxygen atom can react with ozone to form two oxygen molecules (Reaction 1.2).

$$\mathrm{O_3} + h\nu \longrightarrow \mathrm{O} + \mathrm{O_2} \quad (\lambda < 320\ nm) \tag{1.1}$$

$$\mathrm{O} + \mathrm{O_3} \longrightarrow 2\ \mathrm{O_2} \tag{1.2}$$

$$Net:\ 2\ \mathrm{O_3} + h\nu \longrightarrow 3\ \mathrm{O_2} \tag{1.3}$$

where hν is the photon energy (h=$6.626{\cdot}10^{-34}$ is the Planck constant; ν is the frequency) and λ is the wavelength.

Chemical production and destruction of ozone as illustrated above are known as the **Chapman Cycle** after *Chapman* [1930]. Models based on these chemical reaction equations result in realistic global ozone distributions, however, the total amount of ozone is overestimated by a factor of two [*Kraus*, 2000]. The addition of the catalytic ozone destruction cycles lead to models which better capture the true extent of ozone depletion. Catalytic cycles are very effective in

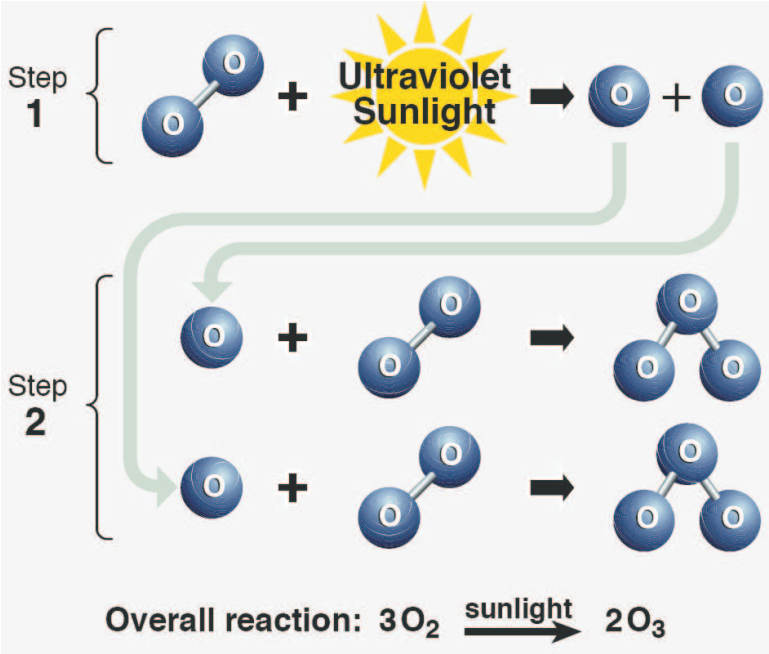

Figure 1.8: Ozone is naturally produced in the stratosphere in a two-step process. In the first step, ultraviolet sunlight breaks apart an oxygen molecule to form two separate oxygen atoms. In the second step, these atoms then undergo a binding collision with other oxygen molecules to form two ozone molecules. In the overall process, three oxygen molecules react to form two ozone molecules (Source: *WMO* [2003]).

destroying ozone and one catalyst can destroy several hundred ozone molecules before reaction with a different substance removes it from the cycle [*WMO*, 2003]. Different catalytic cycles happen with different radicals, e.g. hydroxide radical (OH), nitrogen oxides (NO_x), halogens (Cl, Br, ClO, BrO), etc. The importance of the different catalytic cycles depends on altitude, meteorological conditions and the concentration of the radicals which react with ozone [*WMO*, 1999]. The most important catalytic cycles in the upper stratosphere are those involving NO_x radicals, chlorine/bromine radicals, and OH radicals. All reactions can be summarised in Reaction 1.4, where X stands for the different radicals and selected examples are given in Appendix D.

$$\begin{aligned} X + O_3 &\longrightarrow XO + O_2 \\ O_3 + h\nu &\longrightarrow O_2 + O \\ XO + O &\longrightarrow X + O_2 \end{aligned}$$

$$Net: \ 2\ O_3 + h\nu \longrightarrow 3\ O_2 \tag{1.4}$$

Below 40 km the HO_x-catalysed loss of ozone is important [*Crutzen*, 1970], whereas at altitudes above 42-45 km loss of ozone is dominated by catalytic cycles involving OH radicals. The importance of the chlorine- and bromine-catalysed ozone loss cycles peaks at around 40 km in the gas-phase chemistry [*Molina and Rowland*, 1974]. Whereas bromine is found in lower concentrations than chlorine in the stratosphere, the effectiveness of bromine to destroy ozone is 60 times larger on a global average basis [*WMO*, 2007].

1.3.2 Polar Stratospheric Clouds

Polar stratospheric clouds (PSCs) were named by *McCormick et al.* [1982]. They are also known as nacreous clouds and can be observed in the stratosphere during polar winter between 12 and 25 km at temperatures < 195 K [*Solomon*, 1999]. In the Antarctic they are present from June to late September, in the Arctic they have been observed from about January until mid-March [*Saitoh et al.*, 2002]. PSCs play a critical role in stratospheric ozone depletion. First, on the surface of the cloud particles the unreactive chlorine reservoir species chlorine nitrate ($ClONO_2$) and hydrogen chloride (HCl) can be converted into reactive chlorine radicals, i.e. chlorine monoxide (ClO), and second because denitrification (temporarily removal of nitric acid (HNO_3) due to binding in PSC particles or irreversible removal due to sedimentation of those particles) slows the deactivation of chlorine.

PSC particles grow large enough and are numerous enough that cloud-like features can be observed from the ground under certain conditions, particularly when the

Figure 1.9: Polar stratospheric clouds as seen from Scott Base, Antarctica, 2003 (Photo courtesy of Rebecca Batchelor).

Sun is near the horizon. Figure 1.9 shows a picture of PSCs taken from Scott Base, Antarctica, in the winter of 2003.

PSC particles form at low polar temperatures when HNO_3 and sulfur-containing gases condense with water vapour. Ice particles form at even lower temperatures as displayed in Figure 1.10. The exact temperature for the formation of PSCs depends on pressure, abundance of trace gases (e.g. HNO_3, H_2O) and on the nature of the particles. In the present scientific understanding there are two main composition types of PSCs. Type I is further subdivided in Type Ia, containing nonspherical, crystalline particles, i.e. nitric acid trihydrate (NAT=$HNO_3(H_2O)_3$), and Type Ib, spherical, liquid particles, i.e. supercooled, ternary solution (STS=$H_2SO_4/HNO_3/H_2O$). Type II contains ice particles [*Kim et al.*, 2006, and references therein] and therefore these particles form only at temperatures below the ice frost point. The detection of the true composition of PSCs is still ongoing research.

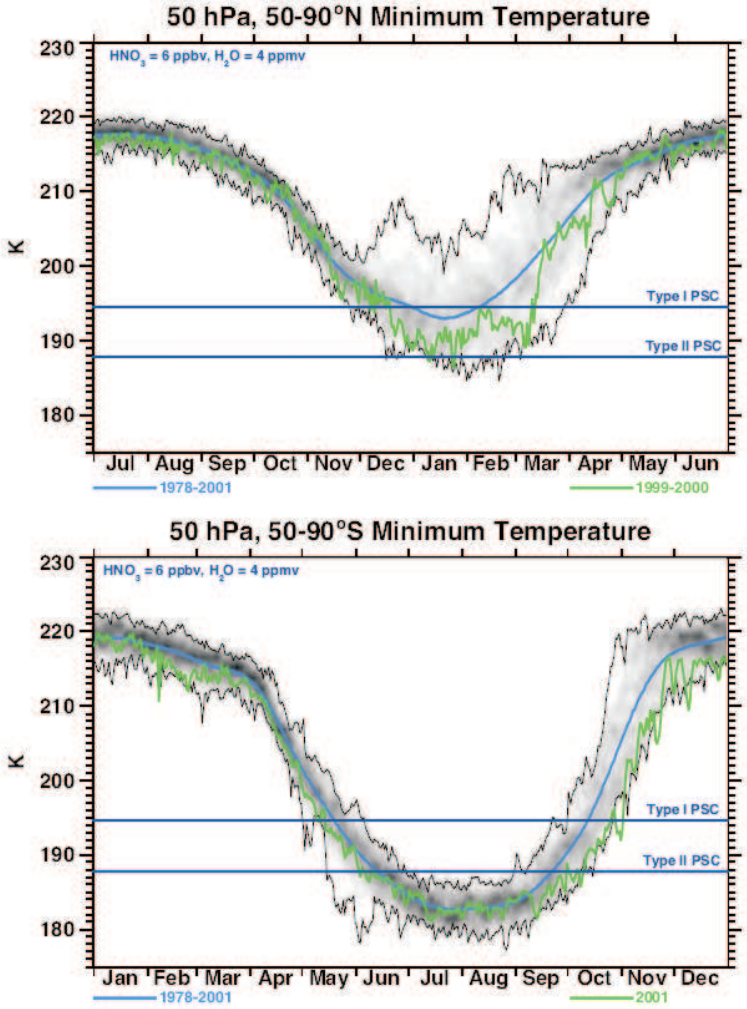

Figure 1.10: Time series showing distributions of 50 hPa minimum polar temperatures for 50-90N (top) and 50-90S (bottom). The blue line shows the 1978-2001 mean, and the thin black lines show the maximum–minimum values. Shading shows the density of observations, with heavy shading indicating a high probability and light shading indicating a low probability. The seasonal cycles are offset by six months so that the seasonal progression in each hemisphere is contrasted. Thresholds for PSC formation are indicated by the horizontal lines (Source: *WMO* [2003]).

1.3.3 Heterogeneous Chemistry

Gas-phase chemistry is not capable of explaining the dramatic stratospheric ozone depletion over the polar regions. Ordinarily, the CFCs which are released in the troposphere, reach the stratosphere where they form halogen reservoir species, i.e. HCl, $ClONO_2$, HBr, $BrONO_2$, HOBr, etc. Liberation of active chlorine is rather slow in the gas-phase and would not lead to the drastic ozone loss observed. However, heterogeneous reactions occurring on PSCs promote the conversion of the halogen reservoirs to photolytically active species (ClO, Cl) [e.g. *Solomon et al.*, 1986; *McElroy et al.*, 1986].

The first step of the process is the gaseous absorption of HCl by PSCs, followed by the heterogeneous reaction of $ClONO_2$ (gas-phase) with the particle (Reaction 1.5). All heterogeneous reactions (listed in detail in Appendix D.2) would be extremely slow in gas-phase [*Seinfeld and Pandis*, 1998].

$$ClONO_2^{(g)} + HCl^{(s)} \longrightarrow Cl_2^{(g)} + HNO_3^{(s)} \tag{1.5}$$

where (s) denotes a species on the ice and (g) a species in gas-phase. The resulting forms of chlorine/bromine (Cl_2, HOCl, ClBr) are photochemically labile states and with the return of sunlight to the polar regions they can be photolysed to Cl atoms. Free Cl atoms can then react with O_3. ClO can be removed from the catalytic cycle by reaction with NO_2 back into the reservoir species $ClONO_2$. However, due to denitrification NO_2 is not available and O atoms which could also complete the cycle are essentially absent in the polar stratosphere. Therefore ClO accumulates until the concentrations are sufficiently large for the catalytic cycle 1.7, known as the **Molina dimer cycle** [*Molina and Molina*, 1987], to become active (Cl_2O_2 being the dimer). This cycle is most effective towards the end of the winter inside the polar vortex at lower stratospheric levels when large amounts of ClO have been accumulated and sunlight causes photolysis.

$$\begin{aligned} \mathrm{ClO} + \mathrm{ClO} + M &\longrightarrow \mathrm{ClOOCl} + M \\ \mathrm{ClOOCl} + \mathrm{h}\nu &\longrightarrow \mathrm{Cl} + \mathrm{ClOO} \\ \mathrm{ClOO} + M &\longrightarrow \mathrm{Cl} + \mathrm{O_2} + M \\ 2[\mathrm{Cl} + \mathrm{O_3} &\longrightarrow \mathrm{ClO} + \mathrm{O_2}] \end{aligned} \tag{1.6}$$

$$Net: \ 2\ \mathrm{O_3} + \mathrm{h}\nu \longrightarrow 3\ \mathrm{O_2} \tag{1.7}$$

Bromine monoxide (BrO) contributes about 50 % of the total chemical loss rate of Arctic ozone [*Chipperfield and Pyle*, 1998]. Unlike ClO, the abundance of BrO is not strongly affected by heterogeneous chemistry because less than half of the available inorganic bromine is transferred into the inactive reservoir species, i.e. bromine nitrate ($BrNO_3$) and hydrogen bromide (HBr). Results in *WMO* [2003] suggest that the contribution of bromine to ozone loss in the polar regions has increased faster than the contribution of chlorine, and bromine will continue to increase for a longer period than chlorine. However, since ozone loss by this reaction cycle depends on ClO, it is expected that major declines in chlorine will dominate over the bromine abundance and lead to less total chemical ozone depletion in the polar regions.

In Figure 1.11 the schematic displays the time evolution of the polar stratospheric chlorine chemistry. PSCs provide the surface for the heterogeneous reactions. Sufficiently large PSC particles fall out of the stratosphere and carry the absorbed HNO_3 with them, thus causing denitrification of the stratosphere. Since the vertical transport within the Antarctic polar vortex as well as horizontal transport across the boundaries of the vortex is slower than the characteristic time for the ozone-depleting reactions, the local rate of ozone loss can be approximated as that of the rate-determining step in Reaction 1.7.

Towards the end of the winter, the polar air masses warm up through absorption of sunlight and the PSCs disappear. Evaporation of the PSCs releases the HNO_3,

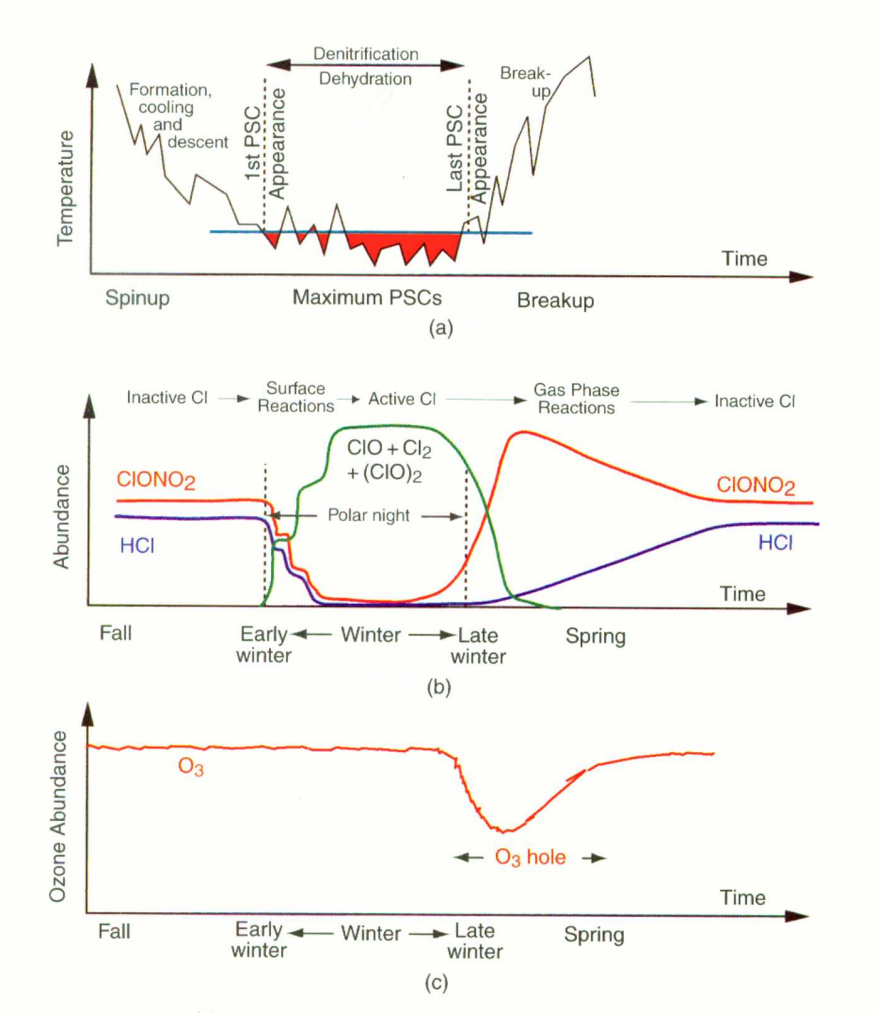

Figure 1.11: Illustration of the time evolution of the main processes associated with the evolution of the Antarctic ozone hole (Source: *Wallace and Hobbs* [2006]).

which reacts with OH to restore the gas-phase NO_x and ClO can react with NO_2 to its reservoir $ClONO_2$.

1.4 Thesis Outline

The research in this thesis is presented in three main parts in Chapters 2-4. The main focus is to examine the coupling of dynamics and chemistry in the Antarctic stratosphere by studying the inter- and intra-annual variability in Antarctic ozone depletion.

In Chapter 2 the main focus is to describe the year-to-year variability in ozone mass deficit over Antarctica. The long-term trend in the ozone depletion measure is controlled by chemistry and can be described with equivalent effective Antarctic stratospheric chlorine. Inter-annual variability is controlled by dynamics. The metrics for the dynamics in the Antarctic stratosphere in this chapter are the meteorological parameters of South Pole temperature and total wave power or eddy heat flux, respectively. Anomaly time series of ozone mass deficit are calculated by subtracting the long-term trend due to halogens in the stratosphere. A linear regression model is presented to derive Antarctic vortex mean ozone anomalies with South Pole temperature anomalies and wave activity anomalies as the basis functions. The coefficients derived with the linear regression model can be applied to temperature and wave activity outputs from chemistry-climate models to obtain estimates of how the Antarctic ozone hole might develop in the near future.

When expanding the studies to describe the intra-annual evolution of depleted ozone, an ozone measure sensitive to all processes involved is required. In Chapter 3, an improved version of the ozone mass deficit is presented. This new measure is defined relative to pre-ozone hole levels and it better represents the full extent of chemically depleted ozone. It can be shown that the old measure which was based on a constant level of 220 DU rather than a pre-ozone hole background omits large parts of the chemically depleted ozone. Comparison of the start day of ozone depletion and the day when sunlight first reaches areas with polar stratospheric clouds is performed as a quality check of the ozone measures. Vortex average total column ozone loss derived with the pre-ozone

hole background is validated by comparison with accumulated chemical ozone loss derived with a tracer-tracer correlation. In addition to a new ozone mass deficit measure, the same method was applied to derive a new measure of ozone hole area. The new measures represent chemically depleted ozone within the vortex except for dynamically highly active years. Criteria for identifying highly dynamically active years are presented.

The main focus of Chapter 4 is to investigate the intra-annual variability in Antarctic ozone depletion. The seasonal evolution of Antarctic ozone mass deficit is controlled by temperature, sunlight, halogen loading in the stratosphere, dynamical activity and saturation effects. Two semi-empirical models are presented connecting the physical processes of the Antarctic ozone hole. The first model describes the conversion of non-reactive chlorine reservoir species into reactive chlorine monoxide by taking the sunlit area of polar stratospheric clouds into account. Equivalent to ozone mass deficit, the total mass of activated chlorine with respect to pre-ozone hole activated chlorine levels is presented. This measure can be used to describe the rate of change of ozone mass deficit which is presented in the second semi-empirical model. In addition to ozone depletion due to activated chlorine, in-situ production and dynamical activity are considered in this second model. Predictive capabilities of the ozone model are tested for 2005 and 2006 and future work to predict inter- and intra-annual variability in Antarctic ozone depletion is outlined.

In Chapter 5 the research performed in this thesis is summarised and conclusions are presented for the three main parts as well as an overall conclusion. Possible extensions on the study as well as future application are outlined in this chapter.

Chapter 2

Inter-annual Variability in Antarctic Ozone Depletion Controlled by Planetary Waves and Polar Temperature*

The Antarctic ozone hole shows large inter-annual variability on top of the long-term trend. While the long-term trend is primarily controlled by emissions of human-produced ozone depleting substances, the year-to-year variability is mainly controlled by midlatitude planetary wave activity which in turn influences stratospheric temperatures. The dependence of Antarctic ozone depletion on midlatitude planetary wave activity and South Pole temperatures was examined from 1979-2005 using NCEP/NCAR reanalyses and total column ozone data. The annual severity of Antarctic ozone depletion was quantified using the seasonal mean of daily ozone mass deficit.

One of the most discussed scientific topics in recent years is the recovery of the Antarctic ozone hole. To better understand the effects of the dynamics of the atmosphere on the severity of Antarctic ozone depletion, separation of the dynamical effects from the long-term trend due to chemistry is necessary. In this chapter, the dependence of annual mean ozone mass deficit on halogens in the Antarctic stratosphere was removed to produce an ozone mass deficit anomaly time series. Equivalent effective Antarctic stratospheric chlorine was used as a

*This chapter is based on the publication Huck, P.E., McDonald, A.J., Bodeker, G.E. and Struthers, H., 2005. Interannual variability in Antarctic ozone depletion controlled by planetary waves and polar temperature. *Geophysical Research Letters*, 32(13): doi:10.1029/2005GL022943.

measure of the total concentration of ozone depleting substances in the Antarctic stratosphere. Similar to ozone mass deficit, anomaly time series for 100 hPa South Pole temperatures and 20 hPa midlatitude planetary wave activity at 60°S were calculated by removing the linear trend. Regression of the ozone mass deficit anomaly time series against temperature and planetary wave activity anomaly times series confirms that most of the inter-annual variability in Antarctic ozone depletion can be explained by variability in midlatitude planetary wave activity and South Pole temperatures.

To estimate how future changes in South Pole temperatures, midlatitude wave activity and stratospheric halogens will affect Antarctic ozone depletion, the regression model coefficients derived from the observational database were applied to temperature and planetary wave activity anomaly values from chemistry-climate model runs (1960-2050). This chapter is based on the analyses published in *Huck et al.* [2005] and has been updated and extended.

2.1 Introduction

Ozone abundance and variability in the polar stratosphere is controlled by atmospheric dynamics and chemistry. While chemistry explains most of the long-term trend in polar stratospheric ozone, the inter-annual differences are primarily driven by transport and dynamical variability of the atmosphere. Strong correlations between ozone and various meteorological parameters have been analysed in the past, for example tropopause hight [*Schubert and Muntenau*, 1988; *Steinbrecht*, 1998], lower stratospheric temperature [*Randel and Cobb*, 1994], potential vorticity [*Allaart et al.*, 1993], and planetary wave activity [*Fusco and Salby*, 1999]. Previous analyses based on measurements [*Bodeker and Scourfield*, 1995] and modelling [*Shindell et al.*, 1997] have shown that inter-annual differences in the severity of Antarctic ozone depletion are anti-correlated with southern hemisphere midlatitude planetary wave activity.

There are a number of mechanisms whereby changes in wave activity affect the

Antarctic stratosphere. Waves may affect the total column ozone distribution directly through meridional and vertical transport of ozone. Irreversible mixing associated with wave-breaking episodes leads to a permanent exchange of air between latitudes [*Austin and Butchart*, 1992]. During the winter, heat transport induced by upward propagating planetary waves [*Schoeberl and Hartmann*, 1991] warms the vortex which reduces the occurrence of polar stratospheric clouds (PSCs), a key prerequisite for the heterogeneous chemistry that depletes ozone. Reversible transport, for example displacement of the vortex off the pole (wave 1), or elongation of the vortex (wave 2) perturbs the polar photochemistry [*Solomon et al.*, 1993] and allows photochemical ozone destruction to occur earlier than would be the case without large disturbances to the circumpolar flow. Variations in wave forcing influence the strength of the diabatic descent and the frequency and amplitude of vortex displacements which may facilitate mixing with midlatitude air. Planetary waves can also change the size of the Antarctic vortex, influence the isolation of the vortex from midlatitudes, and affect the longevity of the polar vortex [*Strahan*, 2002, and Section 2.2].

A good example of midlatitude planetary wave perturbation of the Antarctic ozone hole was the wave induced major stratospheric warming in 2002, which split the polar vortex and thus the ozone hole into two parts (Figure 2.1) [*Hoppel et al.*, 2003; *Sinnhuber et al.*, 2003]. Major warmings result from planetary waves propagating up from the troposphere, decelerating the polar night jet and deforming and/or splitting the vortex. They cause the stratospheric zonal circulation to reverse its direction which leads to dramatic changes in polar temperatures and therefore in polar chemistry. The zonal mean wind reversal can be best identified as a reversal from westerly to easterly at 10 hPa and the zonal mean temperature increase is best identified at 10 hPa poleward of 60° [*Julian*, 1967; *Labitzke*, 1968].

Before the September 2002 major stratospheric warming in the southern hemisphere, it was thought that this phenomenon did not occur in the southern hemisphere where tropospheric-forced planetary wave activity is much weaker than in the northern hemisphere [*WMO*, 1985]. The Arctic polar vortex is regularly

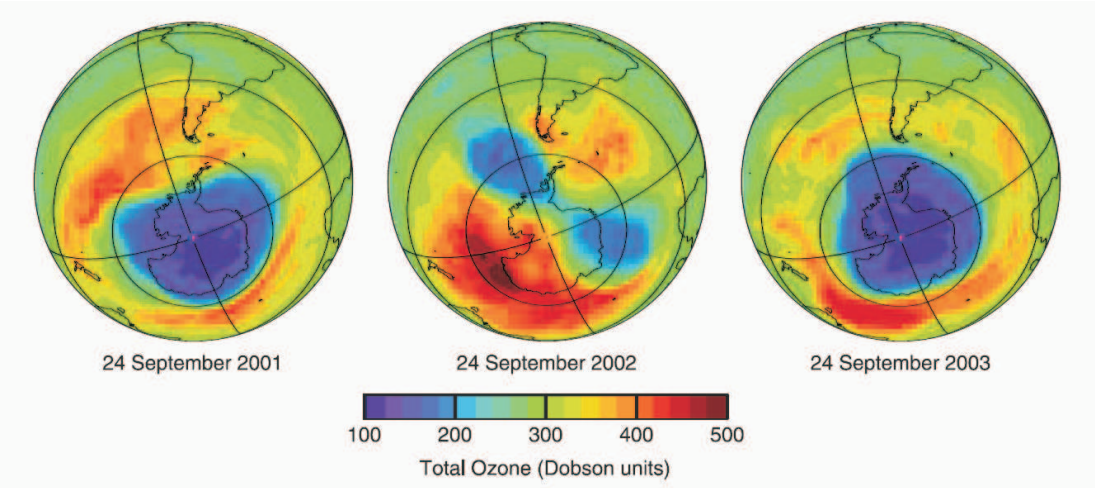

Figure 2.1: Comparison of a *normal* ozone hole, e.g. 2001 and 2003 in the left and right panel, respectively, and the unusual vortex split up in 2002 in middle panel (Source: *WMO* [2007]).

disturbed by planetary wave events and major stratospheric warmings occur every two to three years on average. The reasons for a less disturbed Antarctic polar vortex are less orographic forcing, weaker longitudinal land-sea contrasts in the southern hemisphere, and the presence of the cold elevated Antarctic continent at the pole, resulting in reduced planetary wave activity [*WMO*, 2007].

Temperature records show that there has not been another major Antarctic stratospheric warming since the records started in 1940 [*Roscoe et al.*, 2005; *Naujokat and Roscoe*, 2005]. This unprecedented event in 2002 resulted in the smallest ozone hole observed since 1988 [*Newman and Nash*, 2005]. During the week of September 24, 2002, the polar vortex size near 70 hPa decreased from 25 to 16 million km^2, the area below the threshold temperature for PSC type I formation decreased from 10 to 1 million km^2, and the ozone hole area decreased from 18 to 3 million km^2.

There are a number of metrics which can be used to quantify the severity of Antarctic ozone depletion which are presented in more detail in Section 3.1. In summary, most often ozone hole area, [*Newman et al.*, 2004; *Alvarez-Madrigal and Pérez-Peraza*, 2005] or ozone minima over Antarctica [*WMO*, 2003] are used.

However, ozone hole area and ozone minima, show little growth over the 1990s and are therefore relatively insensitive to future changes in stratospheric halogen loading [*Newman et al.*, 2004; *WMO*, 2003]. In contrast, ozone mass deficit [*Uchino et al.*, 1999], which combines the effects of changes in ozone hole area and depth, almost doubled during the 1990s and is therefore expected to be more sensitive to future changes in stratospheric halogen loading than ozone hole area [*Bodeker et al.*, 2005]. Therefore, ozone mass deficit is used as the metric for the severity of Antarctic ozone depletion in this thesis. Inter-annual variability in ozone hole area is affected primarily by variability in the vortex collar (55°S-75°S) temperature [*Newman et al.*, 2004]. In this chapter, the combined effects of polar temperatures and midlatitude planetary wave activity on ozone mass deficit is examined. It should be noted that the wave driving also affects polar temperatures and that the two influences are coupled.

Furthermore, models suggest that there is a delay between anomalies in planetary wave activity and anomalous Antarctic ozone depletion so that mid-winter planetary wave activity could be used to forecast Antarctic ozone hole severity [*Shindell et al.*, 1997]. In this chapter, Antarctic vortex averages of ozone mass deficit, midlatitude planetary wave activity, and polar temperature anomalies are used to investigate time lags between the measures and to find the most suitable measure when expanding these studies to intra-annual variability in Antarctic ozone depletion (see Chapter 4).

A summary of the theory which describes how planetary wave activity affects Antarctic stratospheric ozone depletion is presented in Section 2.2. To investigate the dependence of ozone mass deficit on polar temperatures and midlatitude planetary wave activity, ozone mass deficit anomalies are regressed against temperature anomalies and wave activity anomalies as detailed in Section 2.3. The correlations and relationships derived from the regression are presented in Section 2.4 together with an estimate of the future evolution of Antarctic ozone depletion based on predictions of polar temperatures and wave activity. The results are discussed and conclusions are drawn in Section 2.5.

2.2 Background

This section describes how planetary wave effects influence polar temperatures and ozone depletion. The general aspects are outlined in Sections 1.2.1 and 1.2.3 and in Section 2.1. In summary, waves cause meridional heat and momentum fluxes and induce an additional mean meridional circulation. Temperature changes caused by the wave induced heat fluxes are compensated for by diabatic heating/cooling as a result of the vertical motion due to the waves. Deviation of the wave induced meridional motion due to the Coriolis force compensates for the acceleration of the background flow due to the momentum fluxes of the waves.

To anticipate how the zonal mean flow responds to a specific eddy heat flux or eddy momentum flux, or in turn to investigate the physical properties of waves controlling these eddy fluxes it is convenient to examine the Eulerian mean-flow equations in their alternative form (transformed Eulerian mean equations, Equations 3.5.2(a)-3.5.2(e) in *Andrews et al.* [1987]). This set of equations defines the Eliassen-Palm (EP) flux **F**:

$$F_\phi = \rho_0 \; a \; \cos\phi \; \left(\frac{\partial \overline{u}}{\partial z} \overline{v'T'} / \frac{\partial \overline{T}}{\partial z} - \overline{v'u'} \right) \tag{2.1}$$

$$F_z = \rho_0 \; a \; \cos\phi \; \left(\left(f - \frac{1}{\mathrm{a} \; \cos\phi} \frac{\partial (\overline{u} \; \cos\phi)}{\partial \phi} \right) \; \overline{v'T'} / \frac{\partial \overline{T}}{\partial z} - \overline{w'u'} \right) \tag{2.2}$$

where ϕ is the latitude, ρ_0 is basic density ($\rho_0 = \mathrm{p}_s/\mathrm{RT}$), a is the mean radius for the distance from any point in the atmosphere to the centre of the Earth, u, v and w are the zonal, meridional and vertical wind components, respectively, z stands for longitude, T is temperature, whereby the overbar over a certain parameter denotes the zonal mean and primed quantities denote departure from the zonal mean.

Divergence of the EP flux describes the impact of waves on the background circulation. For linear, stationary and conservative waves the background flow does not change (Charney-Drazin Nonacceleration Theorem, see Appendix C)

and the divergence of the EP flux is zero ($\nabla \cdot \mathbf{F} = 0$). For transient dissipative waves however, the background flow gets accelerated or decelerated, i.e. in case of a divergence ($\nabla \cdot \mathbf{F} > 0$) acceleration to the east and in case of convergence ($\nabla \cdot \mathbf{F} < 0$) acceleration to the west.

Under the quasi-geostrophic approximation, the meridional component of the EP vector is proportional to the zonally averaged momentum flux ($\overline{u'v'}$, Equation 2.3) and the vertical component of the EP vector is proportional to the zonally averaged eddy heat flux ($\overline{v'T'}$, Equation 2.4). Planetary wave energy entering the lower stratosphere can therefore be specified by the eddy heat flux ($\overline{v'T'}$).

$$F_\phi = -\rho_0 \; a \; \cos\phi \; \overline{u'v'} \tag{2.3}$$

$$F_z = \rho_0 \; a \; \cos\phi \; f \frac{\overline{v'T'}}{\partial \overline{T}/\partial z} \tag{2.4}$$

Wave driving affects the advection of ozone via the residual circulation. Strong wave driving decelerates the polar jet, weakening the mixing barrier at the vortex edge and allowing poleward transport of lower latitude ozone-rich air [*Newman et al.*, 2001; *Randel*, 1993; *Fritz and Soules*, 1972]. *Fusco and Salby* [1999] also suggested that variations in planetary wave activity entering the lower stratosphere are coherent with tendencies in column ozone.

The overall patterns of correlation between eddy heat flux and the ozone tendency are similar between northern and southern hemispheres, showing a latitudinal see-saw with negative correlations in the tropics and positive correlations at high latitudes, and a movement of the positive correlations to polar latitudes in spring. For locations with a strong correlation between ozone tendency and eddy heat flux it is possible to estimate ozone tendencies in the absence of wave forcing. Comparison of this "zero wave forcing" provides an empirical estimate of the net wave driven circulation effects on column ozone [*Randel et al.*, 2002]. In addition, the 100 hPa eddy heat flux averaged over 45-75°N has been found to be highly correlated with the 50 hPa polar temperatures averaged over 60-90°N

for a 45-day time period after the eddy heat flux period (r=0.95) [*Newman et al.*, 2001]. This excellent correlation allows an estimation of polar temperatures in the absence of dynamics ($\overline{v'T'} = 0$), similar to the estimation of the net wave driven circulation effects on column ozone. Significant correlations between the total ozone perturbation and the temperature perturbation in the lower stratosphere have been found as well [*Wirth*, 1993].

Most studies on the effects of planetary waves on stratospheric ozone have been performed for the Arctic. In general, effects of wave activity on ozone depletion are more pronounced in the northern hemisphere and data availability is also better there. One example are the unusual features of the 1996-1997 northern hemisphere spring polar vortex. The vortex was found to be very strong, cold, and symmetric, and therefore similar to the Antarctic spring vortex. This year provides an excellent example of the impact of the dynamics on the chemistry of the stratosphere [*Coy et al.*, 1997]. The strong wave driving in 1998-1999 was another example of how unusually high levels of ozone were transported into the Arctic vortex and how vortex temperatures were driven above the threshold for PSC formation. The high levels of Arctic ozone in the 1999 winter were not found to be a result of low chlorine loading but of unusually strong horizontal transport and mixing. The opposite effect occurred the following winter when weak wave driving led to a strong barrier to mixing and to lower polar temperatures which allowed the formation of PSCs and in turn the activation of ozone destroying molecules [*Strahan*, 2002].

Numerical experiments using a three-dimensional model have examined the relationship between the meteorological conditions and polar ozone chemistry including dynamics and tracer transport, diabatic heating, photochemistry, heterogenous chemistry and chlorine reservoir species. The modelled ozone amounts over the polar region show considerable sensitivity to planetary wave forcing: small forcing leads to substantial ozone depletion, whereas with the largest forcing little ozone depletion occurred [*Austin and Butchart*, 1992].

Mixing and induced meridional circulation due to planetary wave breaking in-

creases the seasonal variation of total column ozone. In southern midlatitudes the variability is increased by about 10 % and in the northern hemisphere by about 20 % [*Nathan et al.*, 2000]. Planetary wave-breaking effects are significant in the midlatitude stratosphere during winter. In the southern hemisphere, wave effects of zonal wavenumber 1 play an important role for stratospheric ozone depletion, whereas wave 1 and wave 2 have been found to be significant during northern hemisphere winters [*Randel*, 1987].

Maximum wave activity in the northern hemisphere occurs during November-March, lagged approximately one month compared to the maximum of the ozone tendency at 40-50°N [*Randel et al.*, 2002]. In the southern hemisphere positive ozone tendency during May-September coincides with elevated wave activity, but the strong wave fluxes in southern hemisphere spring (October-November) occur when the ozone tendency is small or negative, suggesting that photochemistry dominates over dynamical effects for midlatitude ozone at that time [*Randel et al.*, 2002].

2.3 Methods

Global ozone fields from version 2.6 of the NIWA combined total column ozone database [*Bodeker et al.*, 2005] were used to calculate daily ozone mass deficits [*Bodeker and Scourfield*, 1995]. To relate the results to those from previous studies [*Newman and Nash*, 2005], and to compare the attributes of different measures of Antarctic ozone depletion, daily measures of ozone hole area were derived from the same database. For both measures a threshold of $O_3 < 220$ Dobson Units (DU; $1\,\mathrm{DU} = 2.69 \times 10^{16}$ molecules/cm^2) south of 40°S was used. The ozone mass deficit (OMD) in kg within a given Total Ozone Mapping Spectrometer (TOMS) cell (1.25° longitude × 1° latitude) is given by:

$$\mathrm{OMD} = (220\,\mathrm{DU} - x) \times 2.11 \times 10^{-5} \times A \tag{2.5}$$

where x is the total column ozone in DU and A is the area in m^2 of the TOMS cell.

In Chapter 3 an improved version of OMD is introduced that better represents the intra-annual variability in ozone depletion. However, in this chapter the standard definition for OMD has been retained since it represents inter-annual variability in ozone loss well. The OMD values were summed to produce daily OMDs, which were then averaged over the Antarctic vortex period (AVP, 18 July to 30 November) to produce annual OMD values. The primary driver of long-term changes in OMD is changes in halogen loading of the stratosphere. Therefore AVP mean OMD values were first regressed against equivalent effective Antarctic stratospheric chlorine (EEASC) and replaced with their regression residuals to produce an anomaly time series independent of stratospheric chlorine and bromine concentrations.

The EEASC is the Antarctic version of the equivalent effective stratospheric chlorine (EESC), and while the analyses in *Huck et al.* [2005] were performed with EESC, they have now been updated with EEASC. EESC is a measure of ozone depleting substances. The abundances of the ozone depleting substances are estimated from ground-based measurements of halocarbons. Furthermore, assumptions about transit times and the effectiveness in depleting ozone of each halocarbon in the stratosphere is taken into account when calculating the EESC and EEASC, respectively. EESC is calculated as in equation 2.6 [*Daniel et al.*, 1995] with EESC data obtained from the European Environment Agency web page at http://dataservice.eea.eu.int/dataservice/.

$$EESC = \left(\sum_{Cl_y} n_x Cl_{trop}^{t-3} \frac{FC_x}{FC_{CFC-11}} + \sum_{Br_y} n_x \alpha Br_{trop}^{t-3} \frac{FC_x}{FC_{CFC-11}} \right) FC_{CFC-11}, \tag{2.6}$$

where $t-3$ indicates a three year time lag for the transport of the ozone depleting substances from the surface to the stratosphere, Cl_y and Br_y are the chlorine- and bromine-containing halocarbon concentrations, n_x is the number of chlorine or bromine atoms in each halocarbon x, $\frac{FC_x}{FC_{CFC-11}}$ is the fractional release of chlorine (or bromine), FC_{CFC-11} is the absolute fractional release of CFC-11 and α is

an efficiency factor accounting for the increased chemical ability of a bromine atom to destroy ozone compared to a chlorine atom. The global average for α is 60 [*WMO*, 2007]. Fractional release values as listed in Table 2.1 were used to calculate EESC and an absolute release value for CFC-11 of 0.9 was assumed for the calculation. The individual species concentrations can be obtained from Table 11-5 in *WMO* [1999].

Different scenarios were considered when calculating the EESC. Some of the scenarios are displayed in Figure 2.2, including the baseline scenario which was used in this study. The baseline scenario is the "best-guess" scenario following the Beijing Amendments from 1999 [*WMO*, 2003]. For the "zero emissions" scenario anthropogenic emission of all ozone depleting substances was set to zero from 2003 onwards. The "maximum" scenario assumes the maximum emission allowed under the Montreal Protocol, for the "zero production" scenario production of all ozone depleting substances was set to zero from 2003 onwards but emissions continue based on the amount of unemitted reserves. The "continued production" scenario assumes a constant production of ozone depleting substances with the rate from 1999. In addition, the different development of EESC for different protocols is displayed in the same figure.

EESC has some limitations when applied to the Antarctic stratosphere and therefore *Newman et al.* [2006] developed the EEASC, an Antarctic equivalent to EESC, by considering a 6 year transit time from the troposphere to the stratosphere [*Waugh and Hall*, 2002], species-specific half lives and an age of air spectrum. The time series of EESC and EEASC are compared in Figure 2.3. It can be seen that considering a mean age-of-air spectrum of 6 years as has been done for the EEASC, higher overall values of the ozone depleting substances in the stratosphere are observed. In addition, the EEASC also peaks about six years later (2001), compared to the maximum of EESC in 1995.

Theoretically, ozone loss rates depend on the square of the ClO concentration [*Salawitch et al.*, 1993]. However, complete destruction of ozone within the polar lower stratosphere [*Kröger et al.*, 2003] causes saturation of the ozone destruction

Ozone Depleting Substance	Chemical Formula	Number of Cl or Br Atoms	Relative Fractional Release Factor
Carbon tetrachloride	CCl_4	4	1.06
CFC-11	CCl_3F	3	1
CFC-12	CCl_2F_2	2	0.6
CFC-113	CCl_2FCClF_2	3	0.75
CFC-114	$CClF_2CClF_2$	2	0.35
CFC-115	$CClF_2CF_3$	1	0.35
H-1211	$CBrClF_2$	1	1.10
H-1301	$CBrF_3$	1	0.8
H-2402	$CBrF_2CBrF_2$	2	0.95
HCFC-141b	CH_3CCl_2F	2	0.72
HCFC-142b	CH_3CClF_2	1	0.36
HCFC-22	$CHClF_2$	1	0.35
Methyl bromide	CH_3Br	1	1.08
Methyl chloride	CH_3Cl	1	0.8
Methyl chloroform	CH_3CCl_3	3	1.08
H-1202	CBr_2F_2	2	0.9

Table 2.1: Ozone depleting substances and their fractional release values.

chemistry and hence a lower than second order dependence on ClO [*Jiang et al.*, 1996]. Therefore OMD anomalies (OMD′) were calculated as:

$$\mathrm{OMD}' = \mathrm{OMD} - \left(a \times \mathrm{EEASC}^2 + b \times \mathrm{EEASC} + c\right) \tag{2.7}$$

Using the coefficients from this equation to model OMD, it was found that EEASC describes about 80% of the variance in OMD. The same equation was used to derive ozone hole area (OHA) anomaly values. This high correlation is to be expected because of the importance of chlorine and bromine in driving polar ozone depletion [*Solomon*, 1999, and references therein].

Two different measures for daily polar stratospheric temperatures were extracted from the NCEP/NCAR reanalyses, viz.: the primary measure of South Pole temperatures at 100 hPa and a secondary measure of zonal mean temperature between 55°S and 75°S equivalent latitude [*Butchart and Remsberg*, 1986], on the 450 K isentropic surface. Several pressure levels for the stratospheric South Pole

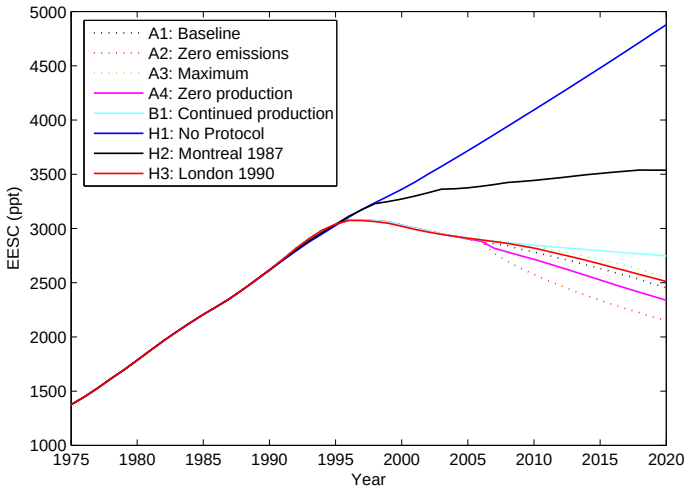

Figure 2.2: Different scenarios for future emission of ozone depleting substances as listed in the legend. See text for discussion of the different scenarios.

temperature were considered, and the values at the 100 hPa level were found to produce the highest correlation with the OMD anomaly time series. *Newman et al.* [2004] calculated collar temperatures at 50 hPa between 55°S and 75°S geographical latitude. Calculation of zonal mean temperature by geographical latitude when the vortex is distorted away from zonal symmetry, blurs the steep meridional temperature gradient. Therefore collar temperatures were calculated by equivalent latitude. Daily temperature anomalies were calculated by subtracting the mean annual cycle (1979-2005), and were then averaged over the Antarctic vortex period to provide annual temperature anomalies.

Two different measures of daily planetary wave activity were also derived from the NCEP/NCAR reanalyses. The first is wave power calculated by applying a discrete Fourier transform to the geopotential heights at 60°S and 20 hPa and then taking the root sum of squares of the amplitudes of the first 6 wave modes. Planetary wave energy entering the lower stratosphere can also be specified by the vertical component of the Eliassen-Palm flux [*Fusco and Salby*, 1999]. Within the quasi-geostrophic approximation, this can be approximated as the zonally averaged eddy heat flux, $\overline{v'T'}$ [*Andrews et al.*, 1987], as described in more detail

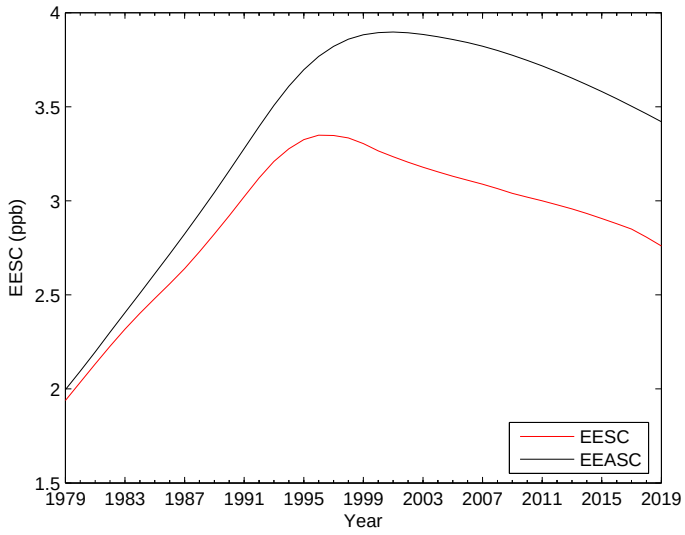

Figure 2.3: Comparison of EESC and the Antarctic equivalent EEASC in colours as indicated in the legend.

in Section 2.2. The second measure was therefore the eddy heat flux calculated at 60°S and 20 hPa. Similar to the polar temperature data, daily wave power and eddy heat flux anomalies were calculated by subtracting the mean annual cycle (1979-2005), and were then averaged over the Antarctic vortex period to provide annual planetary wave activity anomalies.

A linear least squares regression model was used to relate OMD anomalies and OHA anomalies to temperature and wave activity anomalies, noting that two different measures for temperature and for wave activity are used. The variance explained by the four resultant regression models for each ozone measure provides an indication of which anomaly time series provide the best predictor of the inter-annual variability in the severity of Antarctic ozone depletion. Assuming that the linear dependencies between OMD, temperature, and wave activity anomalies will not change in the future, the regression coefficients from this empirical model can be applied to temperature and wave activity anomaly time series extracted from a global climate model or from a chemistry-climate model. This provides an indication of how future trends and inter-annual variability in temperature and/or wave activity anomalies may affect the future evolution of Antarctic ozone depletion

(more discussion in Section 2.4). The advantage of this empirical approach over the estimation of ozone values directly from the chemistry-climate models is that temperature biases in the models are avoided. To this end, anomaly times series of temperature and wave activity were extracted from 28 chemistry-climate model runs and used as basis functions in the statistical model derived above.

2.4 Results and Discussion

The observed ozone mass deficits averaged over the Antarctic vortex period are shown together with the EEASC in Figure 2.4(a). While the long-term evolution of the OMD follows the halogen loading, there is higher frequency year-to-year variability where years with anomalously high wave activity (1988 and 2002; *Newman et al.* [1990]; *Newman and Nash* [2005]) show weak Antarctic ozone depletion, and years with suppressed wave activity (1987; *Newman et al.* [1990]) show severe ozone depletion. The OMD peaks in 1995, which better coincided with the peak of EESC than with the peak of EEASC (see Section 2.3). However, the OMD in recent years was anomalously low due to exceptionally warm temperatures in the past few years [*Labitzke and Kunze*, 2005] and therefore the low OMD values in recent years are unlikely to be caused by reductions in the halogen loading of the stratosphere.

While the differences in variance explained by the four regression models tested were not large, the model using South Pole temperature anomalies and eddy heat flux anomalies was found to be the best and, unless otherwise stated, it is the results from this model that are reported below. In an earlier study [*Newman et al.*, 2004], vortex collar temperatures were found to strongly modulate inter-annual variability in OHA. In this study, regression of OMD anomalies against each of the two temperature anomaly series alone (ignoring the wave activity) suggested that South Pole temperature anomalies are a better predictor of inter-annual variability in OMD than are collar temperatures. Furthermore, it was found that temperature anomalies (from South Pole or vortex collar tempera-

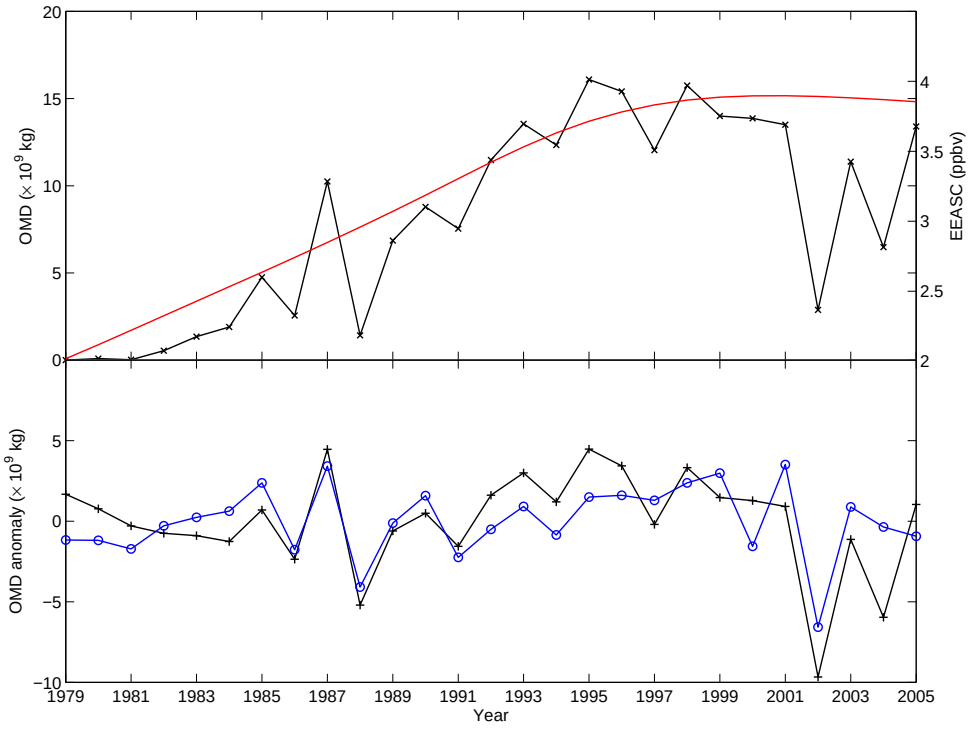

Figure 2.4: a) Antarctic vortex period mean OMD plotted against the left ordinate (black line with crosses) and EEASC plotted against the right ordinate (red). b) Measurement-based OMD anomalies (black line with plus signs) and OMD anomalies from the regression model (blue line with circles).

tures) can explain more of the inter-annual variability in OMD than eddy heat flux anomalies. However, the results in this chapter indicate that addition of the eddy heat flux anomaly time series to the temperature anomaly time series as an explanatory variable produces the best model for explaining inter-annual variability in OMD. The measured and regression modelled OMD anomaly values are plotted in Figure 2.4b. The good agreement (r=0.73) between the two time series, and in particular the ability of the simple statistical model to capture the anomalous 2002 ozone hole (see Section 2.1), confirms that most of the inter-annual variability in Antarctic ozone depletion can be explained by polar temperature anomalies and midlatitude eddy heat flux anomalies. Closer examination of the 2000 ozone hole reveals that the polar vortex was strongly distorted during

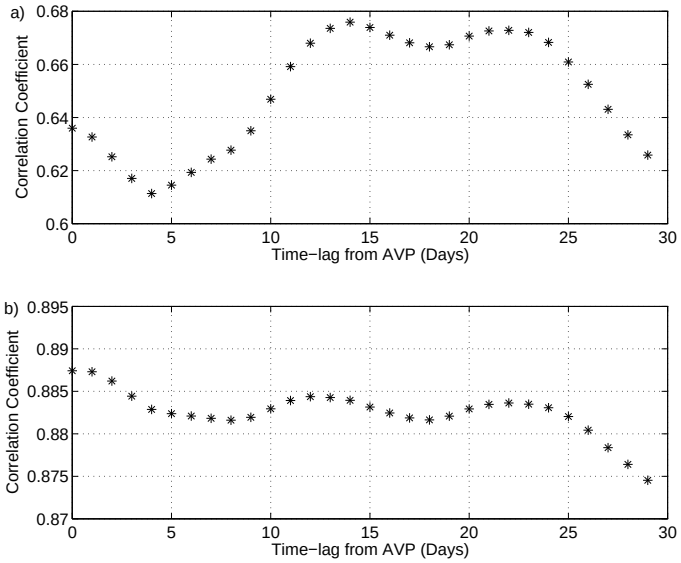

Figure 2.5: a) Correlation coefficients (r values) for OMD anomalies correlated against eddy heat flux anomalies for lags of 0-30 days applied to the period over which the daily eddy heat flux anomalies were averaged. b) Correlation coefficients (r values) for OMD anomalies correlated against eddy heat flux and temperature anomalies for lags of 0-30 days applied to the period over which the daily eddy heat flux anomalies were averaged.

August and September. This could be a reason why the model underestimates the ozone depletion for this year. Similar effects can be observed in 2004 [*Hoppel et al.*, 2005].

Comparison of correlations between measured and regression modelled OMD and OHA anomalies indicate that South Pole temperature anomalies are a better predictor of OMD anomalies compared to collar temperature anomalies as a predictor of OHA anomalies, if temperature alone is used as the explanatory variable. Furthermore, if both meteorological variables are used as predictors, then eddy heat flux and temperature anomaly time series are better predictors of inter-annual variability in OHA than eddy heat flux and collar temperature anomalies, but that eddy heat flux and South Pole temperature anomalies explain more of the variance in OMD than eddy heat flux and South Pole temperature anomalies explain in OHA.

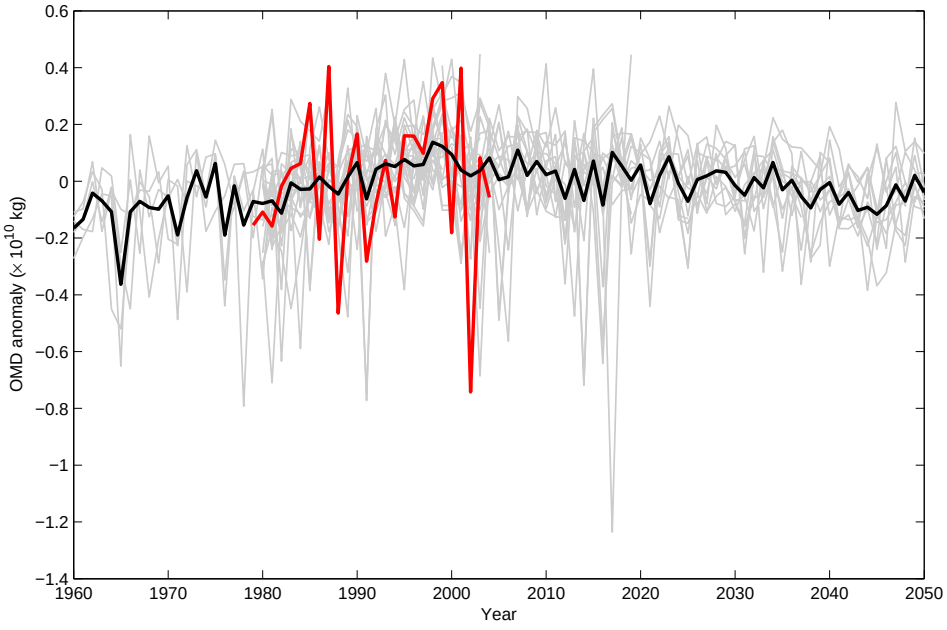

Figure 2.6: Measurement-based OMD anomalies (red line; 1979-2003) compared with OMD anomalies derived by applying the regression model to temperature and wave activity anomalies calculated from 28 CCM run outputs (grey lines). The thick black line is the ensemble mean of the CCM outputs.

So far, in this chapter annual mean values were calculated over the 136 day period from 18 July to 30 November. This however ignores any intra-seasonal temporal lags between dynamical drivers and their effect on ozone depletion, i.e. anomalous wave activity is expected to influence ozone depletion with some time lag [*Shindell et al.*, 1997; *Newman et al.*, 2004]. To test whether such lags need to be considered, the variance in OMD explained by the regression model was calculated with increasing time lags (0-30 days) applied to the period over which temperatures and eddy heat fluxes were averaged. Correlation coefficients (r values) for the regression model with only eddy heat flux anomalies as the explanatory variable, and with lags applied to the eddy heat flux anomalies averaging period, are shown in Figure 2.5a. Lag 1 shows the correlation coefficient between unlagged OMD anomalies and eddy heat flux anomalies averaged over 17 July to 29 November, those at 2 are for values averaged over 16 July to 28 November etc. The highest

correlation is found for a lag of two weeks (a similar result was found if wave power anomalies were used as the measure of wave activity). Therefore, if only wave activity is to be used as a predictor of variability in Antarctic ozone depletion, a lag of 2 weeks applied to the wave activity metric provides the highest correlation. If temperature alone is used as the predictor the highest correlation is achieved with zero lag. If both eddy heat flux and temperature anomalies are used as explanatory variables, with lags applied only to the eddy heat flux time series, then again the highest correlation is achieved with zero lag (Figure 2.5b) since the temperature dominates the eddy heat flux in explaining the inter-annual variability in the ozone depletion (as detailed above).

Using chemistry-climate models (CCMs) to investigate whether recovery of Antarctic ozone is likely to be delayed or accelerated by climate change is complicated by the fact that there is significant disagreement between different models [*WMO*, 2003]. Temperature biases within CCMs, and their parameterisations dependent on temperature, for example PSC formation processes, result in inaccurate representation of the Antarctic ozone hole. However, by using only the year-to-year temperature and wave activity anomalies from a CCM run as the explanatory variables in this regression model, many of these uncertainties are avoided. For example, by removing the effect of temperature biases in the CCMs from the ozone measure, OMD from different CCMs and/or observations become more comparable. To this end time series of wave power and South Pole temperature were extracted from 28 CCM runs from 13 different models accessible through the Chemistry-Climate Model Validation (CCMVal) webpage (Source: http://www.pa.op.dlr.de/CCMVal/). The CCMs involved in this study are listed in Table 2.2 together with references where more information about each model can be found. Different forcings were applied: 1) REF 1, core time period 1980 to 2000, reproducing the past, 2) REF 2, core time period 1980-2025, making predictions without natural forcings, and 3) SCN 2, equivalent to REF 2 but including natural forcings. More details about the forcings are listed in Table 2.3.

Anomaly values of the temperature and heat flux time series of the 28 CCM runs were calculated by subtracting the model-dependent average from the 100 hPa South Pole temperatures and 100 hPa heat fluxes at 60 °S. Annual mean anomalies of the data sets were calculated by averaging the monthly anomalies from July-November. The regression model coefficients for ozone mass deficit anomalies derived above, were then applied to the annual mean anomalies of all CCM runs to indicate how future changes in OMD may be driven by future trends in stratospheric temperature and planetary wave activity anomalies, which in turn are likely to be affected by climate change [*Butchart and Scaife*, 2001]. The resultant OMD anomaly time series from the CCM runs are compared with those derived from the measurements in Figure 2.6. The ensemble mean for all CCM runs is displayed as well as the spread of all the OMD anomaly time series.

Overall the model derived OMD anomaly time series show similar results with inter-annual variability of the same magnitude as the observations. However, when comparing single model runs, some show higher inter-annual variability than the measurements and than other models. This is not surprising since it is well-known that there are models, for example UMETRAC [*Austin et al.*, 2003], that display excessive year-to-year variability over the Antarctic. From the REF2 model runs, which do not include natural forcings, there is some indication from Figure 2.6 that after 2020 less extreme events (like 2002) are to be expected in the OMD anomalies.

Model	**Group**	**Reference**
AMTRAC	GFDL USA	*Austin et al.* [2007] *Austin and Wilson* [2006]
CCSRNIES	NIES Tokyo, Japan	*Akiyoshi et al.* [2004] *Kurokawa et al.* [2005]
CMAM	MSC University of Toronto and York University Canada	*Beagley et al.* [1997] *de Grandpre et al.* [2000]
E39C	DLR Oberpfaffenhofen Germany	*Dameris et al.* [2005] *Dameris et al.* [2006]
GEOSCCM	NASA/GSFC USA	*Bloom et al.* [2005] *Stolarski et al.* [2006]
LMDZrepro	IPSL France	*Lefevre et al.* [1994] (chemistry part)
MAECHAM4CHEM	MPI Mainz MPI Hamburg Germany	*Manzini et al.* [2003] *Steil et al.* [2003]
MRI	MRI Tsukuba, Japan	*Shibata and Deushi* [2005] *Shibata et al.* [2005]
SOCOL	PMOD/WRC and ETHZ Switzerland	*Egorova et al.* [2005] *Rozanov et al.* [2005]
ULAQ	University of L'Aquila Italy	*Pitari et al.* [2002]
UMETRAC	UK Met Office UK	*Austin* [2002] *Austin and Butchart* [2003] *Struthers et al.* [2004]
UMSLIMCAT	University of Leeds UK	*Tian and Chipperfield* [2005]
WACCM	NCAR USA	*Garcia et al.* [2007]

Table 2.2: Thirteen CCMs participating in CCMVal. Variability in ozone depletion for these models were calculated by applying regression model coefficients derived from observations. Source: http://www.pa.op.dlr.de/CCMVal/CCMVal_ ParticipatingCCMs.html

Scenario	Period	Trace Gases	Halogens	SSTs	Aerosol	Solar Var.	QBO
REF 1	1980-2004 (1960-2004)	OBS GHG used for WMO/UNEP 2002 runs. Extended until 2004	OBS used for WMO/UNEP 2002 runs.	OBS HadISST1	OBS Surface Area Density data (SAD)	OBS MAVER data set, observed flux	OBS or internally generated
REF 2	1980-2025 (-2050)	OBS + A1B(medium)	OBS + Ab scenario from WMO/UNEP 2002	Modeled SSTs	Constant SADs (1999 background aerosol for entire period)	Not included average solar flux for the entire REF2 period	
SCN 2	1980-2025	OBS + A1B(medium)	OBS + Ab scenario from WMO/UNEP 2002	Modeled SSTs (same as in REF2)	Constant SADs (1999 background aerosol for entire period)	OBS in past and repeating in future	OBS repeating in future or internally generated

Table 2.3: Three different forcings on CCM runs as applied to the 27 model runs compared in this section. Source: http://www.pa.op.dlr.de/CCMVal/Forcings/CCMVal_ Forcings.html

To further investigate the inter-annual variability between the model runs, the variability over the same time periods, for the same models and with the same forcings applied to the CCM runs was considered. In Figure 2.7 the standard deviation of the OMD anomaly time series of the CCM runs and the observations are displayed in a bar graph. To allow a direct comparison of the variability for the different scenarios and time periods, the standard deviation for all three model groups and the observations was calculated. The model groups are REF1 (including natural forcings) from 1980-1999, REF2 (no natural forcings) from 1980-1999, and REF2 (no natural forcings) from 2000-2019. To calculate the standard deviation of the three model groups, only models that are represented in all model groups were considered. The standard deviation of the OMD anomaly time series of the observations was calculated for 1980-1999. All three model groups show on average less variability than the observations. Highest variability in the models is seen for the REF1 scenario and least variability is seen in the REF2 scenario over the first time period. From this analysis, the conclusion can be drawn that natural forcings lead to 20.5 % more variability in the inter-annual variability of Antarctic ozone depletion. Comparison of the REF2 scenario over the two different periods indicates an increase in variability from the past to the future of about 12.7 %, when no natural forcings are considered.

2.5 Conclusions

The analysis presented above confirms that halogen loading in the stratosphere is the primary driver of the severity of Antarctic ozone depletion. Furthermore, year-to-year variability on top of this secular change is driven primarily by inter-annual variability in temperatures, particularly those deep within the vortex, for example South Pole temperatures. These temperatures in turn are affected by midlatitude planetary wave activity, and addition of wave activity as an explanatory variable provides the most powerful model of inter-annual variability in Antarctic ozone depletion. The preliminary investigations of time lags indicate that planetary wave activity is likely to be preferable to temperatures if these dy-

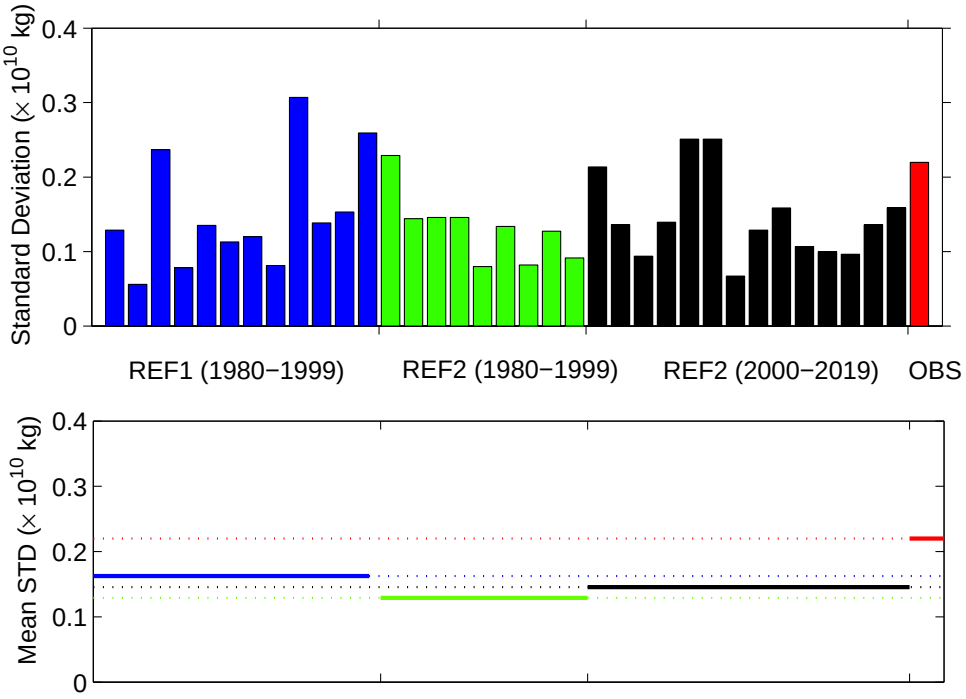

Figure 2.7: In the bar diagram the standard deviation of the OMD anomaly time series as a measure of variability of the CCM runs and the observations is displayed. Additionally, in the lower panel the lines indicate the standard deviation for the same models of the three model groups (REF1 from 1980-1999 (blue), REF2 from 1980-1999 (green), and REF2 from 2000-2019 (black)) and the standard deviation of the OMD anomaly time series of the observations. The standard deviation of the OMD anomaly time series of the observations is displayed from 1980-1999 (red).

namical variables are to be used to provide intra-seasonal forecasts of the severity of Antarctic ozone depletion (see Chapter 4). Application of the regression model derived here to output from 28 chemistry-climate model runs suggests that inter-annual variability in ozone over the Antarctic may increase in the future and less extreme events are to be expected when excluding natural forcings.

Chapter 3

An Improved Measure of Ozone Depletion in the Antarctic Stratosphere*

Ozone mass deficit (OMD) is a commonly used index to quantify Antarctic ozone depletion. However, as currently defined, this measure is not robust with respect to reflecting chemical ozone loss within the Antarctic vortex. Therefore, in this chapter, a new definition of OMD is developed. The 220 Dobson Unit based value currently used as the threshold for ozone depletion has been replaced with a new ozone background representative of pre-ozone hole conditions. Secondly, the new OMD measure is based on ozone measurements within the dynamical vortex. A simpler method is also proposed whereby calculation of the vortex edge is avoided by using the average latitude of the vortex edge (62°S) as the limiting spatial contour. An indication of the errors in OMD introduced when using this simpler approach is provided. By comparing vortex average total ozone loss (defined using the new background and limiting contour) with partial column accumulated chemical ozone loss calculated with a tracer-tracer correlation method for 1992-2004 and in more detail for 1996 and 2003, it is shown that the new OMD measure is representative of chemical ozone loss within the vortex. In addition, the new criteria have been applied to the calculation of ozone hole area (OHA). The sensitivity of the new measures to uncertainties in the background have been quantified. The new ozone loss measures under-estimate chemical ozone loss in highly dynamically disturbed years (2002 and 2004) and criteria for identifying

*This chapter is based on the publication Huck, P. E., Tilmes, S., Bodeker, G. E., Randel W. J., McDonald, A. J., and Nakajima, H., 2006. An improved measure of ozone depletion in the Antarctic stratosphere. *Journal of Geophysical Research*, 112(D11104): doi:10.1029/2006JD007860.

these years are presented. These new definitions of OMD and OHA should aid chemistry-climate model intercomparisons since they would be based on modelled pre-ozone hole backgrounds and would therefore be less sensitive to ozone biases.

3.1 Introduction

Ozone destruction over Antarctica has been of scientific interest since the discovery of the ozone hole in 1985 (see Chapter 1). Three metrics (minimum total column ozone, ozone hole area (OHA) and ozone mass deficit (OMD)) which can be used to quantify the severity of Antarctic ozone depletion were already listed in Section 2.1 and are now presented in more detail.

Initially the severity of Antarctic ozone depletion was quantified using minimum total column ozone values over Antarctica. However, later studies [*Stolarski et al.*, 1990] showed that in some years (e.g. 1987 and 1989) while minimum ozone values were similar, the development of the ozone hole area was quite different. OHA, introduced by *Stolarski et al.* [1990], and defined as the area within the 220 Dobson Unit (DU) contour, has become another standard measure of the severity of Antarctic ozone depletion. More recently, the third measure, OMD, that combines the size and depth of the ozone hole has been used [*Uchino et al.*, 1999]. This metric is calculated by integrating air masses depleted in ozone over latitudes poleward of 40°S. In this case air masses depleted in ozone are identified as those with less than 220 DU of total column ozone. This threshold has been generally acknowledged because it is lower than all pre-ozone hole values (before 1980) and the 220 DU contour lies in the region of steep ozone gradients surrounding the ozone hole. All three measures mentioned above have been used to describe and study inter- and intra-annual variations in Antarctic ozone depletion [*WMO*, 2003].

However, the annual minimum value in total column ozone over Antarctica is largely insensitive to reversible dynamical disturbances of the vortex edge and has shown little change through the 1990s during the annual Antarctic vortex

period (18 July-30 November) [*WMO*, 2003]. The minimum appears usually in late September or early October and has remained essentially unchanged at about 100 DU since 1993 after the considerable decrease during the 1980s and early 1990s. Equivalent effective Antarctic stratospheric chlorine (EEASC), a measure of the concentration of ozone depleting substances in the Antarctic stratosphere (see Section 2.1), peaks in 2001 [*Newman et al.*, 2006]. The insensitivity of annual minimum ozone values to changing EEASC suggests that its use in detecting a response of Antarctic ozone depletion to reductions in ozone depleting substances is limited. Similar saturation effects are observed in OHA, however, it is more sensitive to changes in the vortex collar region than minimum total ozone. The spring-time OHA increased rapidly during the 1980s and more gradually during the 1990s [*WMO*, 2003] while EEASC steadily increased. From 1995 to 2005 the OHA also shows a lack of response to EEASC [*Newman et al.*, 2006]. Unlike minimum total column ozone and OHA averaged over the Antarctic vortex period, the OMD averaged over the same time period shows significant growth during the 1990s, as discussed in *Bodeker et al.* [2005], and greater sensitivity to recent changes in EEASC.

As was shown in Chapter 2, the long-term trend in ozone depletion is mainly controlled by chemical processes and the inter-annual variability can be explained by fluctuations of temperatures and planetary wave activity. However, when expanding these studies to intra-annual variability, more detailed chemical and dynamical processes need to be considered (see also Chapter 1) which can be neglected when averaging over the Antarctic vortex period. In particular, the start date and the rate of ozone destruction depend on temperatures and on sunlight reaching areas which contain polar stratospheric clouds. Furthermore, ozone depletion is controlled indirectly by planetary wave activity displacing air masses out of the polar darkness and therefore causing earlier ozone depletion in some regions [*Solomon et al.*, 1993; *Austin and Butchart*, 2003, and Section 2.1]. By transporting heat, waves directly affect polar temperatures and therefore the occurrence of polar stratospheric clouds (PSCs) which control chlorine activation

and therefore ozone destruction [*Schoeberl and Hartmann*, 1991, and Chapter 1]. To quantify intra-annual variability in ozone depletion a measure sensitive to all of these processes is necessary.

If the OMD and OHA definitions are based on a 220 DU threshold, as was done in *Huck et al.* [2005] and earlier studies, the identified onset of ozone depletion occurs well after sunlight returns to the polar regions, which is inconsistent with accepted theory of polar ozone depletion chemistry (i.e. that ozone depletion commences with the return of sunlight to regions containing PSCs) and with observations of chemical ozone loss within the vortex. The 220 DU-based measures do not capture the full deviation from pre-ozone hole conditions (see Figure 3.1; figure details presented in Section 3.2.1). This suggests that the first step towards improving the OMD and OHA metrics is to define a background value that describes the column ozone for pre-ozone hole conditions. Since the 220 DU contour has previously provided the unperturbed background ozone as well as the limiting contour for the Antarctic vortex, calculation of a new contour for defining the region within which ozone depletion is considered becomes necessary when using a pre-ozone hole background. However, it should be noted that the OHA is not always exactly equal to the area within the inner vortex edge.

To test whether these new parameters for OMD and OHA calculation are likely to lead to more representative measures of Antarctic ozone depletion, vortex average total column ozone loss is derived using the pre-ozone hole background. This measure is compared with the accumulated chemical loss in partial column ozone derived using tracer-tracer correlations for Halogen Occultation Experiment (HALOE) and Improved Limb Atmospheric Spectrometer (ILAS) data. While the HALOE comparisons show the utility of the new measures in tracking spring-time ozone loss, the comparisons with ILAS show how the new measures are able to track the winter-time ozone depletion.

With the tracer-tracer correlation method the impact of dynamical changes on ozone within the analysed layer are separated from the chemical ozone loss [*Proffitt et al.*, 1990; *Müller et al.*, 2001]. It can be shown that the magnitude of ozone

loss in the new measure, especially in winter, is due to chemical ozone loss.

The approach used to calculate the pre-ozone hole background and the two spatial integration limits considered are introduced in Section 3.2.1. In Section 3.2.2 the application of the pre-ozone hole background and the new spatial integration limits to OMD and OHA is described. In Section 3.2.3 the new method is tested by investigating whether these changes result in better tracking of Antarctic chemical ozone loss calculated with more complex techniques such as the tracer-tracer correlation method. The results are presented in Section 3.3, in particular OMD in Section 3.3.1 and the chemical ozone loss in Section 3.3.2. The results are summarised and conclusions are drawn in Section 3.4.

3.2 Methods

3.2.1 Derivation of Pre-Ozone Hole Background

To estimate the pre-ozone hole mean annual cycle in total column ozone over Antarctica (where pre-ozone hole means prior to 1980 in general agreement [*WMO*, 2007]), coefficients from a regression model applied to ozone in an equivalent latitude coordinate were used to construct the stationary part of the annual cycle within the Antarctic polar vortex [*Bodeker et al.*, 2001]. This mean annual cycle is compared with vortex average daily total column ozone from the NIWA combined total column ozone database for 1979, 1980 and 1981 in Figure 3.1, which shows the consistency of this background with pre-ozone hole conditions in observations. In addition, using data for 2003 as an example, the red area in Figure 3.1 shows the ozone deficit below the pre-ozone hole background that would be excluded from a 220 DU-based ozone hole metric. The winter/spring decrease in the pre-ozone hole background results from the cold polar trough region south of 70°S where planetary wave activity is weak [*Chandra and McPeters*, 1986]. A function of the form:

$$\mathrm{O_3} = A_0 + \sum_{i=1}^{4} \left[A_{2\times i-1} \sin\left(2i\pi\frac{d}{366}\right) + A_{2\times i} \cos\left(2i\pi\frac{d}{366}\right) \right]$$

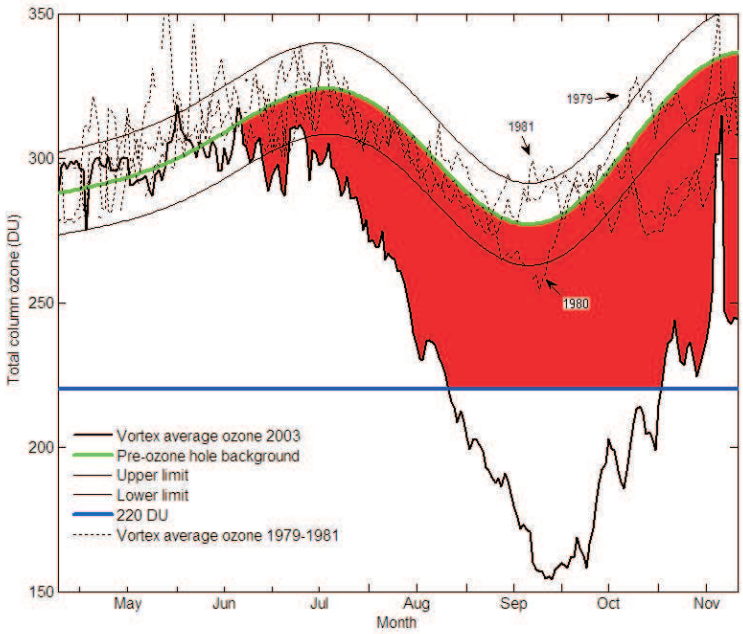

Figure 3.1: The pre-ozone hole mean annual cycle within the Antarctic vortex (green line) and its three σ uncertainty (thin black lines) is displayed together with the 1979-1981 (dotted lines) and 2003 vortex mean ozone (thick black line) from the NIWA combined total column ozone database (see text). The 220 DU threshold, commonly used in calculations of OMD and OHA, is shown with a blue line. The red area indicates ozone loss that would not be incorporated in an ozone depletion index based on a 220 DU threshold.

was fitted to this mean annual cycle, where d is the day number of the year. The coefficients A_0 to A_8 are listed in Table 3.1 and can be used to reconstruct the pre-ozone hole background shown as the greeen curve in Figure 3.1. If this method is used for calculations based on chemistry-climate model output, the method described in Appendix 1 of *Eyring et al.* [2006] can be used to construct the pre-ozone hole background.

Coeff	A_0	A_1	A_2	A_3	A_4	A_5	A_6	A_7	A_8
Value	302.2	-9.522	2.753	-8.708	17.8	-11.07	-4.121	1.518	-2.250

Table 3.1: Regression model coefficients to calculate the pre-ozone hole background.

To test the sensitivity of the new measures to the pre-ozone hole background, a three σ envelope around the green curve in Figure 3.1 was calculated from 100 000 Monte Carlo calculations of the background using the parameter uncertainties provided by the regression model [*Bodeker et al.*, 2001]. The upper and lower limits for the pre-ozone hole background are displayed in Figure 3.1. The resultant uncertainties in the OMD and OHA measures are indicated in the figures below.

Ideally the Antarctic ozone depletion index should be sensitive only to ozone depletion that occurs within the Antarctic vortex. Therefore, the primary approach is to use the inner vortex edge, derived using the method developed by *Nash et al.* [1996], to define the region over which the ozone loss is calculated (the spatial integration limit). NCEP/NCAR reanalyses isentropic potential vorticity (PV) values were transformed into equivalent latitude coordinates. The vortex edge is located at the steepest PV gradient constraint by the maximum of the total wind speed. The inner and outer edge of the polar vortex are defined by the maximum and minimum in the second derivative of PV with respect to equivalent latitude (for more details see http://www.pa.op.dlr.de/CCMVal/HowToCalculateEqlat.pdf). The inner vortex edge is used in these studies to avoid counting any mixed air in the vortex boundary region which would affect the value of ozone depletion. However, this also means that any ozone depletion occurring in the vortex collar region will not be accounted for and therefore a slight under-estimation of depleted ozone mass and ozone hole area would occur. The vortex edge has been calculated for an altitude range between approximately 17-25 km at potential temperature levels of 450, 550 and 650 K. An ozone measurement is flagged as being inside the vortex if the equivalent latitude at that location is poleward of the equivalent latitude of the inner vortex edge at any of the 3 levels. It should be noted that the vortex edge might be shifted or twisted at altitudes above 650 K and therefore does not match the derived vortex edge between 450-650 K. This effect could possibly occur at the end of winter or during a disturbed vortex (e.g. in 2002 [*Newman and Nash*, 2005]). The entire ozone column would be affected and it could result

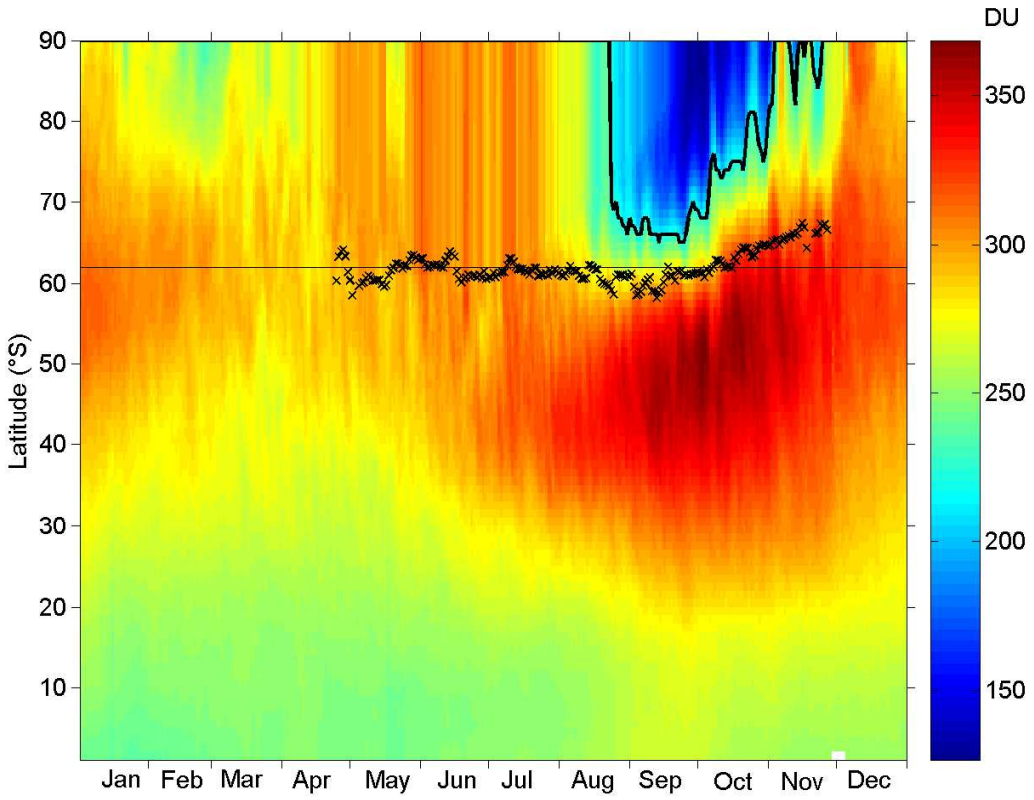

Figure 3.2: Zonal mean total column ozone over the southern hemisphere in 2003 shown as the contour plot as indicated by the colour scale on the right, together with the different spatial integration limits used in this and previous studies, i.e. the inner vortex edge (black crosses), the mean location of the vortex edge at 62°S (thin black line) and the 220 DU contour (thick black line).

in an under-estimation of OMD and OHA.

Given the additional complexity associated with calculating the vortex edge, and to ensure the utility of this method, an additional spatial integration limit of 62°S, the average latitude of the Antarctic vortex edge [*Bodeker et al.*, 2002], is considered. Hereafter, quantities calculated based on the vortex edge are denoted with a *vortex* subscript while those based on the 62°S limit are denoted with a *62S* subscript. In Figure 3.2 the limiting contours, including the 220 DU contour, are displayed on top of a latitude-time ozone distribution for 2003. It is obvious that when using the 220 DU contour as the spatial integration limit instead of

the actual inner vortex edge (thick black line and crosses in Figure 3.2) the area of ozone depletion is restricted to within the polar vortex. However, it also omits much of the vortex region, particularly early in the season.

3.2.2 Ozone Mass Deficit and Ozone Hole Area

In theory, ozone depletion begins as soon as sunlight reaches areas of polar stratospheric clouds, activates chlorine, and initiates heterogenous ozone depleting reactions (Section 1.3). These processes continue until solar radiation and dynamics warm the polar region to temperatures above the threshold for PSC existence. Activated chlorine then returns to inactive reservoir species. The warming of the polar regions also causes a weakening of the polar vortex until the final warming event breaks the structure apart. From theory it is therefore expected that the start of the ozone hole should coincide with the day when sunlight first reaches PSC areas. This date has been calculated and compared to the date when the OMD and OHA first become non-zero, as discussed in more detail in Section 3.3.1.

In addition to calculating the daily OMD using the method described in Chapter 2, OMD_{vortex} and OMD_{62S} have been calculated by replacing the 220 DU threshold with the pre-ozone hole background as in Figure 3.1. Daily values of these indices were calculated from the NIWA combined total column ozone database [*Bodeker et al.*, 2005] from 1979 to 2004. Through the period when a vortex edge can be defined, ozone measurements within the vortex that fall below the background add to the OMD_{vortex} total while measurements above the background are subtracted from the OMD_{vortex} total. The same approach is used when calculating OMD_{62S} using values poleward of 62°S. The NIWA combined database has also been used to calculate daily OHA_{vortex} and OHA_{62S} by adding the area of each cell with an ozone value below the pre-ozone hole background to a daily total if it is within the spatial integration limit and subtracting the area of each cell with an ozone value above the background. OMD and OHA values have only been calculated during the Antarctic vortex season and are considered

to be zero outside that period. Because the date when sunlight first illuminates PSC regions occurs after the date when the dynamical vortex is first defined, this restriction does not affect the start date of OMD and OHA. Shortly after the vortex forms, in the absence of other drivers of ozone variability, the OMD and OHA values should be zero. However, the derived pre-ozone hole background does not account for year-to-year ozone fluctuations caused by various transport processes, for example the quasi-biennial oscillation (see Section 1.2.4), solar cycle and volcanic eruptions. This results in OMD and OHA values that are occasionally non-zero during this period. To correct for this artifact, the average May value for OMD and OHA for each year has been subtracted from the data. Averaged over 26 years (1979-2004) the OMD is corrected by 1.5 % of the annual maximum value and the OHA by 5.6 %.

3.2.3 Comparison with Tracer-Tracer Correlation Derived Chemical Ozone Loss

To test whether the newly defined OMD measure better tracks chemical ozone loss within the Antarctic vortex, spatially averaged ozone loss over the two regions defined above, was compared with ozone loss within the vortex calculated with a tracer-tracer correlation method performed by S. Tilmes [*Tilmes et al.*, 2006b]. These two methods for calculating Antarctic ozone depletion are therefore completely independent. Daily vortex average total column ozone loss was calculated for 1992-2004 by subtracting the measured ozone column from the pre-ozone hole background. Chemical ozone loss was derived with the tracer-tracer correlation method for 1992-2004. This method requires measurements of an ozone profile and simultaneous measurements of a passive tracer which can be used to track the diabatic descent of air parcels within the vortex. HALOE measurements were used for 1992-2004 while ILAS V6.0 and ILAS-II V1.4 measurements were used for more detailed comparisons in 1996 and 2003, respectively. For the accumulated ozone loss derived from HALOE data, CH_4 and/or HF were used as the passive tracer while for the accumulated ozone loss derived from ILAS-II, N_2O was used as the passive tracer. HALOE provided discontinuous measurements of O_3, CH_4

and HF inside the polar vortex [*Russell III et al.*, 1993] which have been averaged over periods between 1 and 20 days and result in one to four data points per year. ILAS provided daily measurements of O_3 and N_2O inside the polar vortex from 30 October to 13 December 1996 [*Suzuki et al.*, 1995; *Sasano et al.*, 1999] and ILAS-II from 2 April to 24 October 2003 [*Nakajima et al.*, 2006; *Nakajima*, 2006]. While HALOE provides more years for comparison of the tracer-tracer method with the total column ozone loss derived here (1992-2004), ILAS and ILAS-II provide better temporal coverage during the years for which data are available (1996 and 2003).

For the tracer-tracer correlation method an early winter reference function is derived for chemically unperturbed conditions in an established vortex. Deviations from this reference function are used to identify chemical ozone loss. This reference function was calculated using O_3 and N_2O measurements in June from ILAS and ILAS-II. The relationship between ozone and N_2O does not change within the confined borders of the polar vortex unless ozone reacts chemically. Accumulated chemical ozone loss was calculated by integrating the tracer-tracer correlation derived ozone loss profiles between 350 K and 550 K for HALOE and between 350 K and 600 K for ILAS and ILAS-II. These altitude ranges have been identified as the region where the halogen-catalysed polar ozone loss takes place [*Tilmes et al.*, 2006a]. Therefore the integrated values represent the total amount of chemically destroyed ozone in the polar vortex. Mixing of air from outside to inside the vortex could potentially result in an under-estimation of chemical ozone loss [*Müller et al.*, 2005].

3.3 Results

3.3.1 Ozone Mass Deficit and Ozone Hole Area

The OMD_{vortex} and OMD_{62S} measures, calculated as described in Section 3.2.2, are compared with each other, and with the OMD based on the 220 DU threshold, for 2003 in Figure 3.3. While the 220 DU-based OMD starts about two months

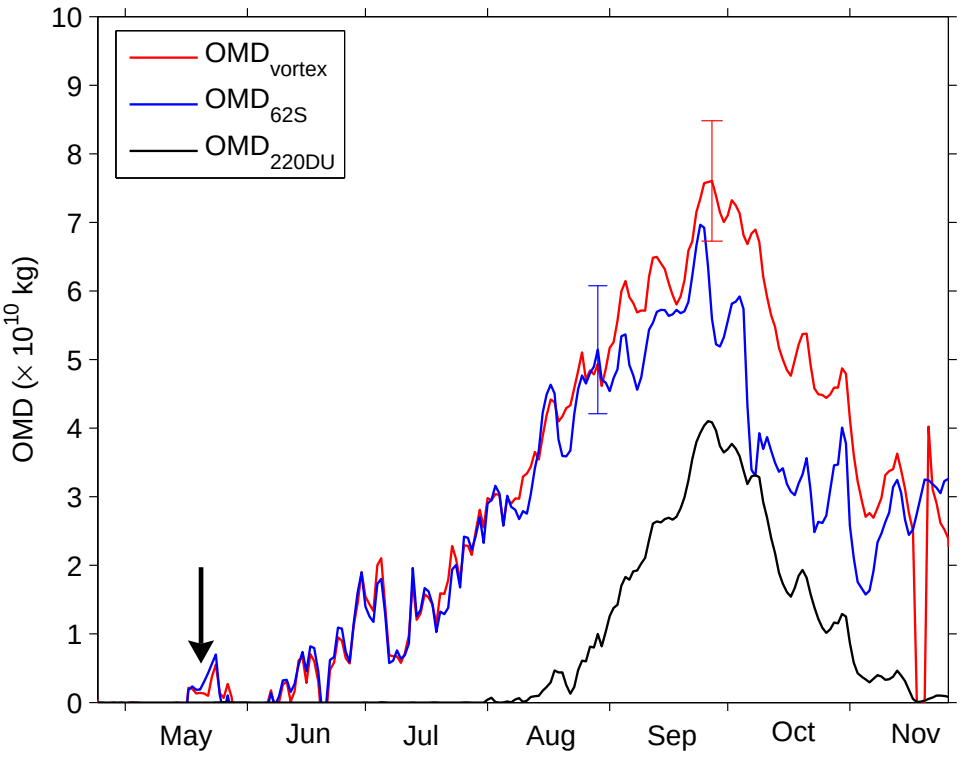

Figure 3.3: Daily values of OMD_{vortex} (red line), OMD_{62S} (blue line) and OMD_{220DU} (black line) for 2003. The arrow early in the period shows the first day of sunlight on PSC areas in 2003. The two error bars on the OMD_{vortex} and OMD_{62S} curves indicate the uncertainties on these measures, resulting from uncertainty in the pre-ozone hole background (see Figure 1), which are similar throughout the season.

later than both new measures, the seasonal start date of the new OMDs is now very close to the date when sunlight first illuminates PSC areas (i.e. 21 May 2003) which is consistent with observations and theory. As defined, OMD_{vortex} terminates at the same time as the vortex breaks up (the time when no edge can be found using the criterion of *Nash et al.* [1996]) while OMD_{62S} remains positive to the end of the year. Both new measures for OMD track each other closely until shortly after the seasonal maximum after which OMD_{62S} displays lower values compared to OMD_{vortex}. Overall, considering the years 1979-2004 (not all shown), more depleted ozone mass is accounted for in the new OMD measures compared to the 220 DU-based OMD. This confirms that it is likely that the

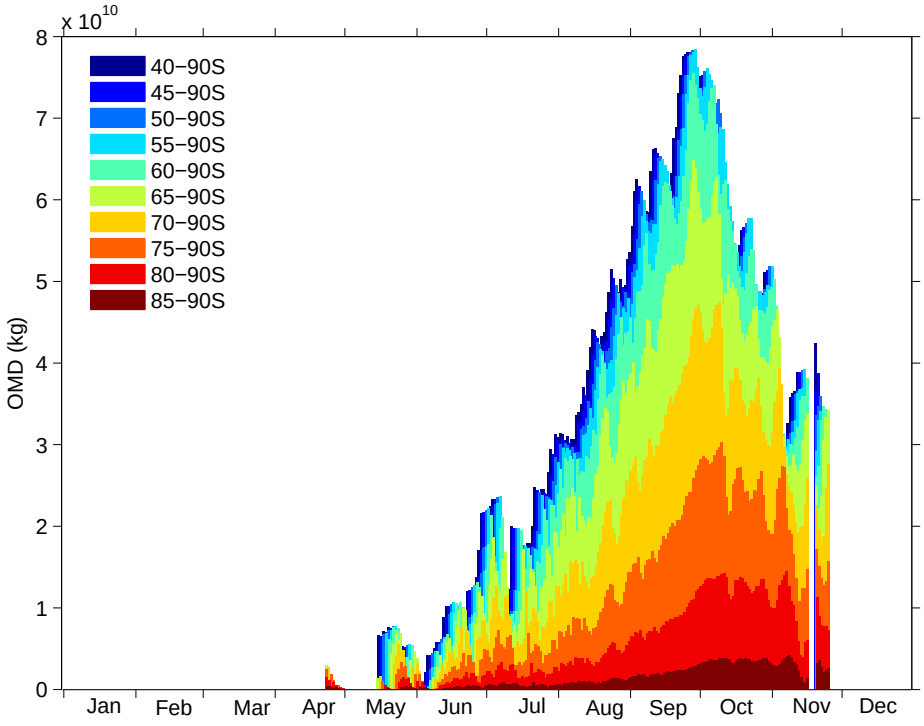

Figure 3.4: Contributions to OMD_{vortex} in different latitude bands as listed in the legend for 2003.

220 DU-based OMD omits some of the depleted ozone mass, as suggested by Figure 3.1.

In Figure 3.4 contributions to OMD_{vortex} from different latitude bands are displayed. The latitude bands start at the South Pole and increase equatorwards by 5 degrees until 40°S is reached. Largest contributions of ozone depleted mass comes from the region between 60-80°S. Contributions from the vortex edge region are comparatively small. The percentage contribution of each latitude band of 5°

Lat	40-45°	45-50°	50-55°	55-60°	60-65°
%	1.1 %	0.5 %	1.3 %	5.2 %	13.9 %
Lat	65-70°	70-75°	75-80°	80-85°	85-90°
%	21.3 %	21.9 %	18.1 %	12.1 %	4.6 %

Table 3.2: The percentage contribution of each latitude band to the total amount of OMD.

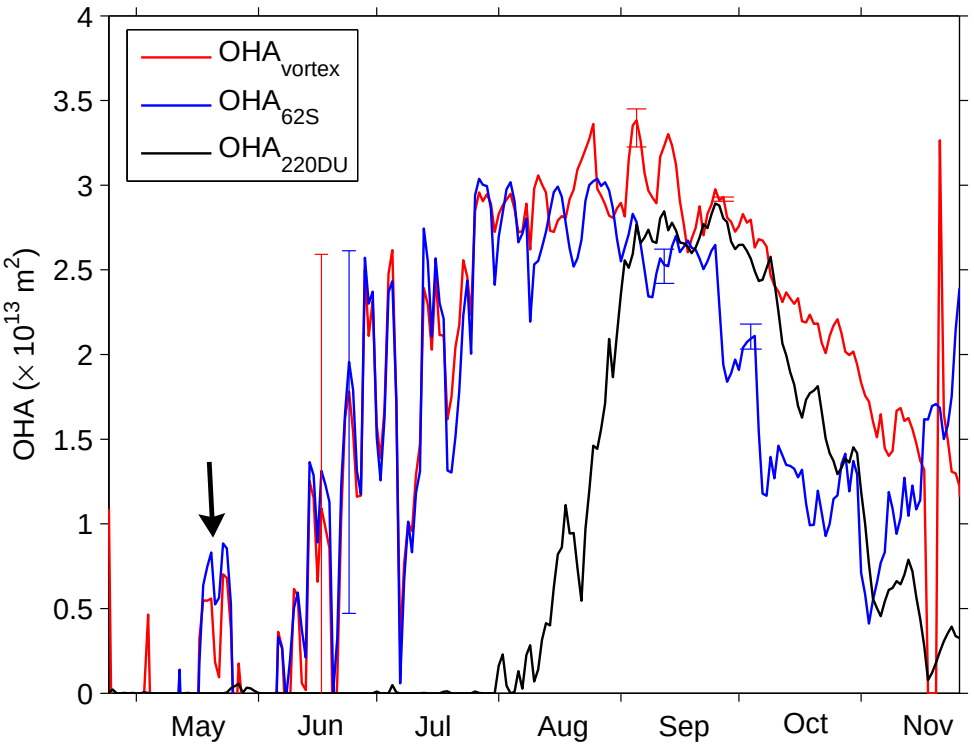

Figure 3.5: Daily values of OHA$_{vortex}$ (red line), OHA$_{62S}$ (blue line) and OHA$_{220DU}$ (black line) for 2003. The arrow early in the period shows the first day of sunlight on PSC areas in 2003. The error bars on the OHA$_{vortex}$ and OHA$_{62S}$ curves indicate the uncertainties on these measures, resulting from uncertainty in the pre-ozone hole background (see Figure 3.1), which decrease throughout the season: by June the error is more than 1×10^{13} m^2 whereas by August-September it is only 0.05×10^{13} m^2.

width is listed in Table 3.2. The rate of change of OMD with time in OMD$_{vortex}$ is increasing from late August until end of September which can be seen in most of the layers, indicating rapid ozone destruction with increasing illumination of the vortex.

Comparison of the OHA measures (OHA$_{vortex}$, OHA$_{62S}$, and OHA based on the 220 DU threshold) for 2003 (Figure 3.5), indicates similar results as for OMD. The seasonal evolution of the two new measures, i.e. OHA$_{vortex}$ and OHA$_{62S}$, shows an earlier start compared to the original OHA. All three measures show similar values after the maximum of the 220 DU-based OHA is reached. Because

Period	**OMD$_{62S}$ vs. OMD$_{vortex}$**	**OHA$_{62S}$ vs. OHA$_{vortex}$**
June	62.9 %	17.9 %
July	10.6 %	07.8 %
August	-4.7 %	-4.2 %
September	-27.1 %	-16.1 %
October	-37.4 %	-38.1 %
November	-29.9 %	-33.0 %

Table 3.3: The percentage error in OMD and OHA when calculating these quantities poleward of 62°S rather than poleward of the inner vortex edge.

the seasonal start date for the new OHA measures is similar to that for when sunlight first reaches PSC areas (and earlier than if the 220 DU contour is used), the new measures are considered to be a better measure of the OHA than the method using the 220 DU contour.

Use of 62°S as the spatial integration limit rather than the vortex edge introduces errors in the values of OMD$_{62S}$ and OHA$_{62S}$ compared to the *vortex* measures which in this case are considered the "true" values. Calendar month averages of these errors over 26 years are summarised in Table 3.3. Early in the winter (June-July), when ozone depletion occurs predominantly in the vortex edge regions where sunlight reaches areas of PSCs and therefore the relative contribution from the vortex edge region is larger than later in the year, OMD$_{62S}$ and OHA$_{62S}$ show greater values than OMD$_{vortex}$ and OHA$_{vortex}$. Later in the season (August-November) OMD$_{62S}$ and OHA$_{62S}$ result in smaller values than OMD$_{vortex}$ and OHA$_{vortex}$. This might indicate that the average location of the inner vortex edge might be slightly polewards of 62°S early in the season and slightly equatorwards later in the season. The best agreement for the OMD and OHA measures, respectively, is in August where the magnitude of the *62S*-measures is about 95 % of the *vortex*-measures.

3.3.2 Vortex Average Chemical Ozone Loss

Two measures for vortex average chemical ozone loss have been derived as described in Section 3.2. The two measures are 1) the total column ozone loss derived by subtracting a pre-ozone hole background from column ozone measurements within the vortex, and 2) the accumulated chemical ozone loss derived with the tracer-tracer correlation method. Unlike the tracer-tracer correlation method which is specific to chemical ozone loss, the total column ozone loss method considers the combination of chemical ozone loss and dynamical resupply. The two methods are compared, from 1992 to 2004, in Figure 3.6. To reduce uncertainties in the accumulated chemical ozone loss, up to 20 profiles inside the vortex have been averaged for each data point. Due to the orbit of the HALOE instrument this results in 1 to 4 data points per year. Except for 2002 and 2004 (unusually dynamically perturbed years - see below) the two methods show excellent agreement, well within the 1σ uncertainties on the HALOE based ozone loss and the uncertainty resulting from the pre-ozone hole background envelopes. In dynamically perturbed years, the vortex average total column ozone loss (and by inference the new OMD metric) is reduced as a result of dynamical resupply of ozone to the vortex i.e. it does not accurately reflect the pure chemical depletion of ozone. Dynamically perturbed years can be identified using the following indicators:

1. when the September average temperature at 65°S and 50 hPa exceeds 210 K, and/or

2. when the standard deviation on daily September zonal mean zonal winds at 60°S and 50 hPa exceeds $10\,\mathrm{m\,s^{-1}}$, and/or

3. when the standard deviation on September average total wave power at 60°S and 20 hPa, derived from geopotential height fields, exceeds 300 m.

The two methods (subtraction of the pre-ozone hole background from vortex average total column ozone and the tracer-tracer correlation method) provide

very similar measures of Antarctic ozone loss in spite of the fact that they cover different altitude ranges (suggesting that ozone loss above or below the region diagnosed with the tracer-tracer correlation method is negligible) and that the tracer-tracer correlation measurement samples only a few locations within the vortex (suggesting that the air within the core of the vortex is well mixed). The large discrepancy in 2002 is not surprising since in that year a mid-winter major warming [*Hoppel et al.*, 2003; *Sinnhuber et al.*, 2003] caused a significant influx of ozone-rich air into the vortex (more details on the unusual dynamics in the 2002 Southern Hemisphere winter are presented in Section 2.1). The under-estimation of the ozone loss in 2002 and 2004 using the total column ozone loss method suggests that dynamical resupply of ozone to the Antarctic vortex may have become more prevalent in recent years. While no major stratospheric warming was observed in 2004, vortex minimum temperatures were higher than in the previous decade, and winter-time PSC frequencies were significantly lower than in the previous decade [*Hoppel et al.*, 2005]. Furthermore, our analysis of wave powers in geopotential height fields from 1979 to 2004, showed that the standard deviation on September wave powers of wavenumber 5 were anomalously high in 2004.

In Figure 3.7 the relationship between the two different vortex ozone depletion measures is displayed as a scatter diagram. Except for 2002 and 2004, the two ozone loss measures are correlated with a correlation coefficient of r=0.6 at 99.9 % significance (when 2002 and 2004 are excluded), with the total column ozone loss method showing smaller ozone loss as expected since it considers both the effects of chemical loss and dynamical resupply.

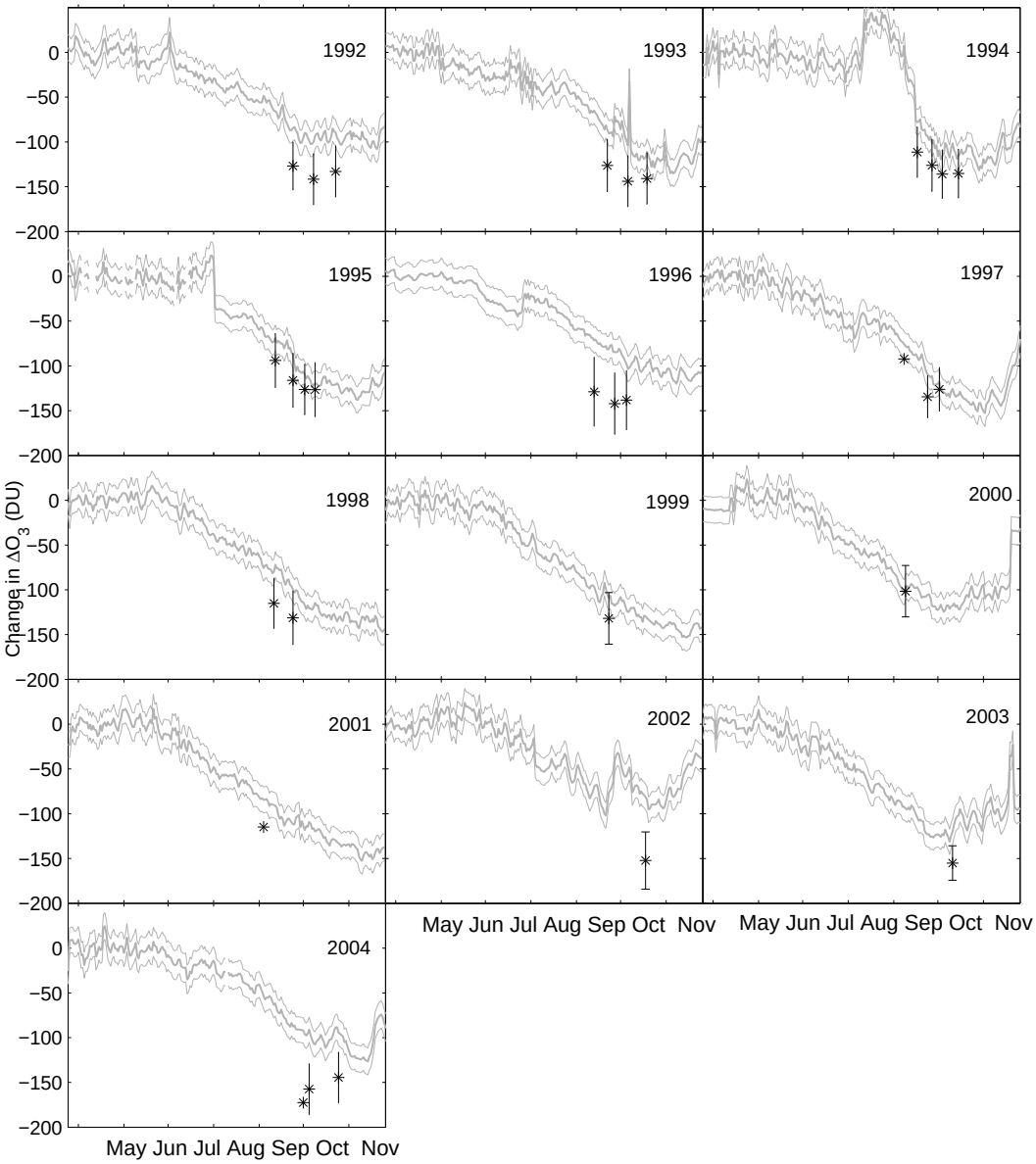

Figure 3.6: HALOE chemical ozone loss (black stars) compared to vortex average total column ozone loss (thick grey line) for 1992-2004. Uncertainties in calculating the accumulated chemical ozone loss (error bars on black stars) result from the estimation of the reference function as well as averaging over the profiles inside the vortex, whereas the uncertainties in calculating the vortex average ozone loss have been estimated with the uncertainties on the pre-ozone hole background (thin grey lines).

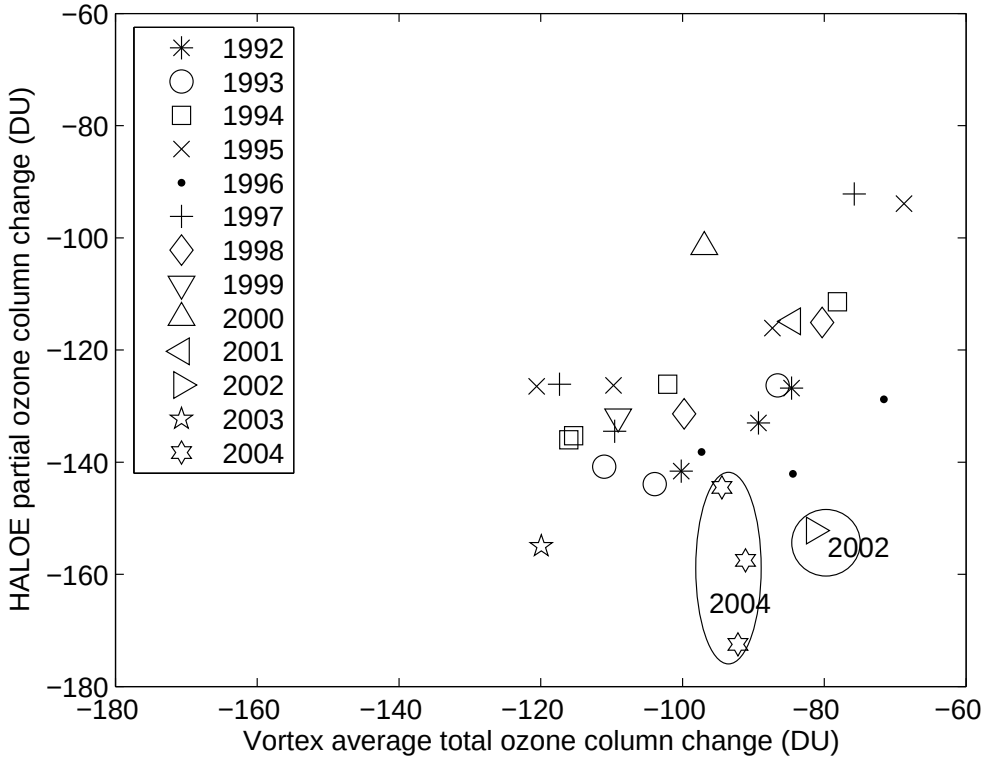

Figure 3.7: Comparison of vortex average chemical ozone losses derived with two different methods for 1992-2004. Different symbols stand for different years.

A day-by-day comparison of total column ozone loss and accumulated chemical ozone loss for 30 October to 13 December 1996 and 1 June to 20 October 2003 is displayed in Figure 3.8 and Figure 3.9, respectively. The accumulated chemical ozone loss for these periods is based on ILAS and ILAS-II observations [e.g. *Tilmes et al.*, 2006a]. In this comparison, two different total column ozone loss time series, resulting from integration over the two regions described in Section 3.2.1 are considered. In 1996 ILAS data are only available for late in the season. Good agreement between the accumulated chemical ozone loss and the total column ozone loss are observed when averaging the total column ozone loss within the vortex boundaries (Figure 3.8). From 6 December 1996 onwards larger deviations occur. As was the case for OMD_{vortex} and OMD_{62S} (Figure 3.3), the ozone loss integrated within the vortex is greater than that integrated poleward of 62°S from

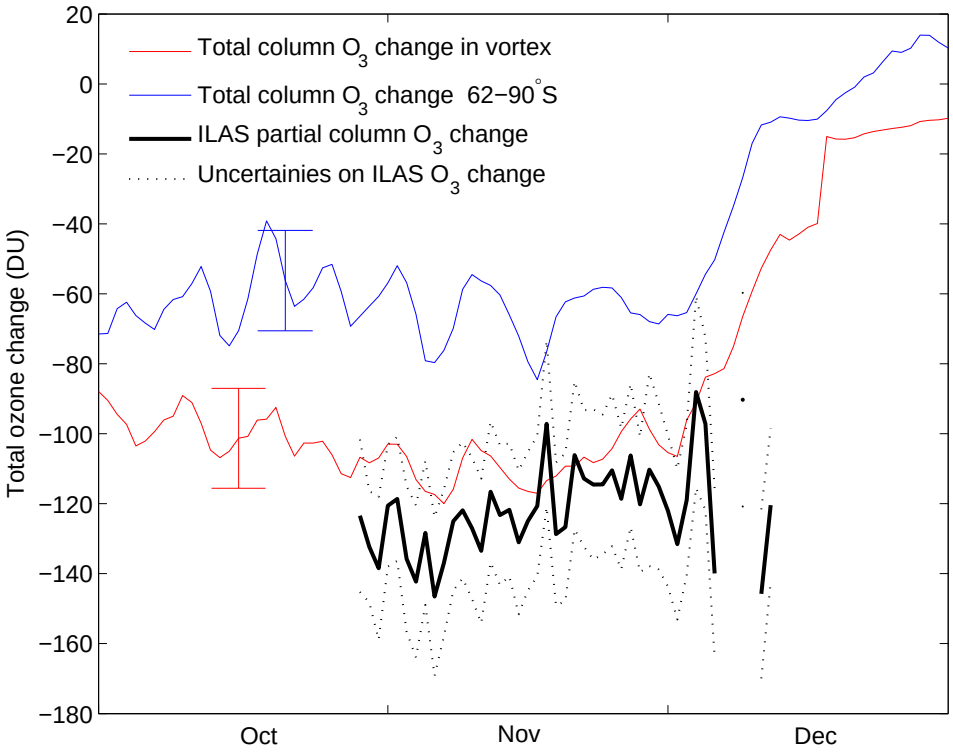

Figure 3.8: Chemical ozone loss derived with tracer-tracer-correlations and total column ozone loss derived with the new method are displayed for October to December 1996 (Black line: ILAS ozone loss; dotted lines: uncertainties on ILAS ozone loss; red line: total column ozone loss (inside vortex); blue line: total column ozone loss (poleward of 62 °S)). Two single error bars on the vortex average total column ozone loss lines indicate the uncertainties on these measures.

October onwards.

In 2003 ILAS-II data are available for the whole Antarctic vortex period. High correlations between accumulated chemical ozone loss and vortex average total column ozone loss are observed from the start of the ozone hole until the minimum is reached (Figure 3.9). The day-to-day variability of accumulated chemical ozone loss and total column ozone loss (both within the vortex and poleward of 62°S) are similar. Comparing the accumulated chemical ozone loss and the vortex average total column ozone loss, some deviation occurs after the minimum value is

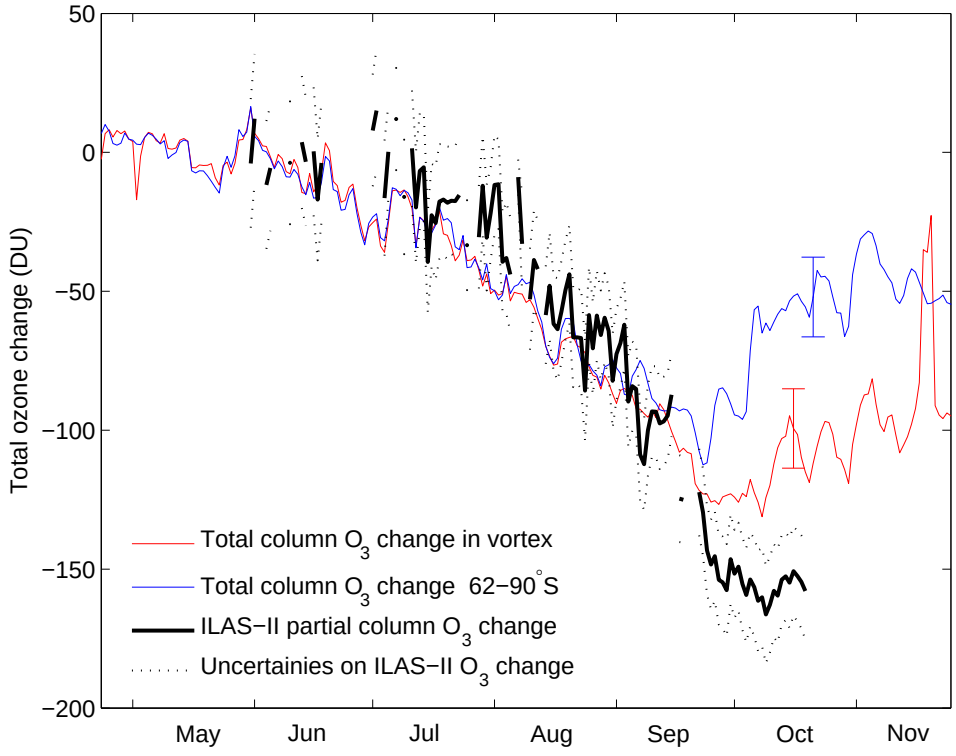

Figure 3.9: Chemical ozone loss derived with tracer-tracer-correlations and total column ozone loss for 2003 (Black line: ILAS-II ozone loss; dotted lines: uncertainties on ILAS-II ozone loss; red line: total column ozone loss (inside vortex); blue line: total column ozone loss (poleward of 62 °S)). Two single error bars on the vortex average total column ozone loss lines indicate the uncertainties on these measures.

reached whereas the average poleward of 62°S starts deviating at the beginning of September and shows greater deviations. Therefore, if ozone loss only until early September is considered, ozone loss poleward of 62°S (the simpler diagnostic) provides the same accuracy as ozone loss within the vortex. Vortex average total column ozone loss reaches its minimum at about 20 DU higher than the accumulated chemical ozone loss. The date when the minimum is reached is in both cases around 9 October 2003. The differences could be due to the different altitude ranges considered by the two measures, filaments from lower latitudes intruding into the vortex and/or mixing of ozone-rich air from the top of the

vortex. Since the tracer-tracer correlation requires an impenetrable vortex edge, filaments from lower latitudes and mixing of ozone-rich air from the top of the vortex are not accounted for. In Figure 3.2 it can be seen that there is a slight increase in total ozone in the vortex core after about 4 October 2003. This increase is most probably due to mixing of polar air masses with ozone-rich air from lower latitudes at high altitudes.

3.4 Discussion and Conclusions

New definitions for the Antarctic OMD and Antarctic OHA have been presented and discussed above. The algorithm used to calculate these indices retains some of the simplicity of earlier methods (for example those that use 220 DU as both the unperturbed background and spatial integration limit) but has the advantage of better representing the chemical ozone loss within the vortex. This was demonstrated by comparing total column ozone loss, calculated using the pre-ozone hole background and spatial integration limits used for the new OMD and OHA indices, with accumulated chemical ozone loss from the more complex tracer-tracer correlation technique. Except for unusually dynamically perturbed years the two methods showed good agreement. Diagnostics for identifying such years are presented. As noted above, because the total column ozone loss method (which uses the same assumptions as for the OHA and OMD calculations) does not distinguish between chemical and dynamical induced changes in ozone, the newly proposed Antarctic ozone depletion indices will only be representative of chemical depletion of ozone in years when dynamical contributions to ozone variability within the vortex are small. However, even in unusually dynamically perturbed years, the new measures provide improved metrics (compared to 220 DU-based metrics) of the severity of Antarctic ozone depletion and for impact studies of ozone depletion on the biosphere, since the 220 DU-based metrics omit large parts of ozone depletion (Figure 3.1).

The new methods for calculating OMD and OHA require total column ozone fields

and, only for the option that uses the vortex edge, potential vorticity fields. Total column ozone fields are more readily available than the ozone and passive tracer profiles required for the tracer-tracer correlation method, and therefore accurate measures of Antarctic ozone depletion can be obtained over longer time periods. Thus the recommendation is that the former method for calculating OMD should be replaced with the new method that integrates depleted ozone mass poleward of the inner vortex edge from a pre-ozone hole background derived with the regression coefficients listed in Table 3.1. However, this method is somewhat more complicated than the former method in that it requires calculation of the dynamical vortex edge. It has been shown that for the seasonal average, the contribution from the vortex edge region is relatively small (Table 3.2). The resultant errors in the OMD (and OHA), when integrating poleward of 62°S (the average latitude of the vortex edge) and therefore avoiding the additional complication of calculating the dynamical vortex edge, are listed in Table 3.3.

Figure 3.10 is an updated version of Figure 2.4 showing the inter-annual variability and long-term trend in OMD_{vortex} compared to that based on the 220 DU threshold. While the long-term trend follows the chlorine and bromine loading of the stratosphere, strong inter-annual variability is seen over the years (see Chapter 2 for more details). Deviation of the OMD trend from the halogen loading in the stratosphere in more recent years is likely to be due to anomalously high temperatures in those years and is unlikely to be attributed to changes in ozone depleting substances. The differences in magnitude between the two OMD measures shows again that large amounts of ozone depleted air masses are omitted when using the 220 DU threshold.

The new OHA defined over regions within the vortex and where ozone is below the pre-ozone hole background has also shown an improvement when compared with the OHA defined within the 220 DU contour. In particular, the new version of OHA (and the new version of OMD) shows closer correspondence with the timing of the return of sunlight to the vortex and the onset of ozone depletion.

A further advantage of using the pre-ozone hole background is that the effect of

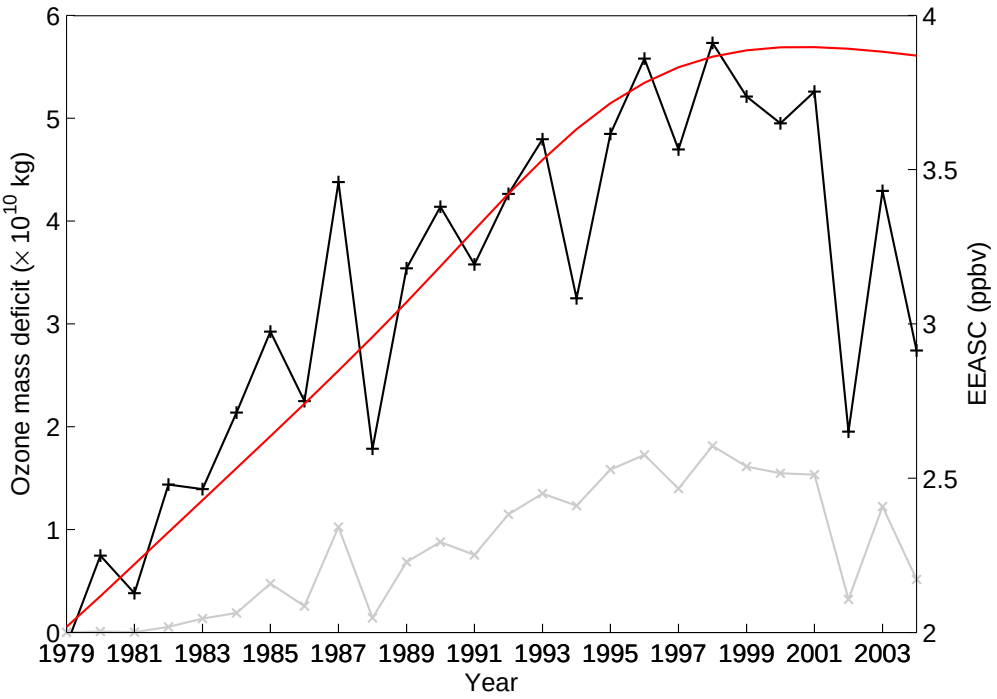

Figure 3.10: Comparison of the new (black line) and 220 DU-based (grey line) ozone mass deficits averaged over the Antarctic vortex period (18 July-30 November) for each year from 1979 to 2004. EEASC (red line) is plotted against the right ordinate. Both ozone mass deficit measures are plotted on the same scale and the EEASC scale has been selected so that the EEASC overlays best with the new OMD.

the annually repeating cycle in dynamics on ozone is better captured than when a constant background is used. This leads to better separation of the effects of chemistry and dynamics in a specific year from ozone changes driven by the long-term background meridional transport that has affected Antarctic ozone over climatological time periods. However, inter-annual variability due to the quasi-biennial oscillation, solar cycle or volcanic eruptions is not currently included in the pre-ozone hole background. To correct for these effects, an offset, derived in May when the vortex has formed but before ozone depletion has started, is subtracted from the Antarctic ozone loss measures.

These new definitions of OHA and OMD should also aid chemistry-climate model intercomparisons. The new measures will be less sensitive to ozone bias since the

pre-ozone hole background from which the OMD and OHA are calculated, will be specific to each model and will result in some cancellation of any ozone bias.

Chapter 4

Semi-Empirical Models for Chlorine Activation and Ozone Depletion in the Antarctic Stratosphere*

Intra-seasonal variability in Antarctic ozone depletion is controlled by a variety of meteorological and chemical processes. Theoretical understanding of the role of the processes involved and their interaction is used to derive empirical models for the processes of chlorine activation and ozone depletion in the Antarctic stratosphere. Beside the obvious factor of the quantity of halogens in the stratosphere, activation of chlorine (conversion of non-reactive chlorine species into reactive chlorine monoxide) depends on the occurrence of PSCs (prerequisite of heterogeneous chemistry and denitrification of the stratosphere), and on the amount of sunlight on PSC particles. Rapid deactivation of chlorine monoxide occurs when the returning sunlight warms the polar regions enough for PSCs to evaporate, leading to renitrification of the stratosphere and chemical reactions which transform active chlorine back into its reservoir species. The rate of change of chlorine in the Antarctic stratosphere is described by deriving a differential equation for activated equivalent effective Antarctic stratospheric chlorine ($EEASC_a$). The model was regressed against chlorine monoxide data from UARS Microwave Limb Sounder measurements. The derived model coefficients were then applied to seven pressure levels in the range of 250-30 hPa, the region where most of the PSCs occur. A pre-ozone hole $EEASC_a$ climatology for each level was calculated by

*This chapter will be submitted for publication as Huck, P.E., G.E. Bodeker, M.L. Santee and A.J. McDonald, Semi-empirical models for chlorine activation and ozone depletion in the Antarctic stratosphere, *Journal of Geophysical Research*.

fitting a combination of sine and cosine terms to the average of $EEASC_a$ from 1979-1981. After subtracting the pre-ozone hole values, the total volume and in turn the total mass of activated chlorine was calculated. This measure was then used to describe the rate of change of the total mass of depleted ozone, OMD, in a second differential equation.

This model can be used to describe and study intra- and inter-annual variability in Antarctic ozone depletion. Together with the model for $EEASC_a$ the mass of depleted ozone can be estimated into the future. EEASC values are available until 2100 [*Newman et al.*, 2006] and as long as temperature forecasts can be obtained, the volume of polar stratospheric clouds can be estimated, which in turn can be used to predict the intra-seasonal evolution of Antarctic ozone depletion.

4.1 Introduction

To describe the intra-annual variability in ozone depletion the interaction of gas-phase chemistry, heterogeneous chemistry, transport and circulation has to be examined. Details of the chemistry and dynamics involved have been presented in Chapter 1. In summary, the annual cycle of Antarctic stratospheric ozone depletion begins in June with the onset of the Antarctic winter. The temperature gradient between the dark polar regions and the sunlit regions at lower latitudes leads to the formation of the polar vortex. Temperatures within the polar vortex decrease to very low values. Below the threshold temperature of 195 K aerosol particles can start to form PSCs. Heterogeneous chemistry acts to free reactive chlorine from its reservoirs on these cloud particles. Denitrification and dehydration of the stratosphere begins due to binding of nitric acid (HNO_3) and water (H_2O) in cloud particles and sedimentation of those particles. Catalytic ozone destruction begins at the end of May/beginning of June. In August minimum temperatures are reached in the Antarctic stratosphere. First sunlight returns to the South Pole in September and catalytic ozone destruction now occurs over the entire polar region. Lowest ozone levels are observed in October. In late

winter, warming of the vortex causes PSCs to disappear. Renitrification of the stratosphere binds reactive chlorine back into its reservoir species. The final warming event usually happens some time in November and the polar vortex breaks apart. Transport of ozone-rich air from midlatitudes to polar latitudes replenishes the Antarctic ozone hole.

Stratospheric chemical ozone loss at high latitudes is regulated by the extent and temporal evolution of active chlorine [e.g. *WMO*, 1999]. Most of the active chlorine in the stratosphere is present as chlorine monoxide (ClO) [*Solomon et al.*, 2006]. Inter-annual variability in the ClO cycle is driven by dynamical parameters, such as the stability of the polar vortex and/or temperature. ClO has been found to be in an elevated state for 4-5 months in the southern hemisphere (May-October) [*Santee et al.*, 2003]. At a potential temperature level of 465 K ($\sim$17-18 km) low temperatures occur also in the vortex edge region and uniform mixing of ClO can be observed over the entire sunlit region of the vortex [*Santee et al.*, 2003]. ClO is present in very small abundances during darkness due to formation of the chlorine dimer (ClOOCl) [*Douglass et al.*, 1993] and can therefore only be observed in the sunlit portions of the vortex.

The symmetric chlorine dioxide (OClO) provides an indicator for stratospheric chlorine activation as demonstrated by *Wagner et al.* [2001] for data from the Global Monitoring Experiment (GOME). GOME spectra of OClO were analysed for both hemispheres from 1995-1999. From these analyses it was found that the Arctic chlorine activation has a duration from a few days to about 3 months and varies considerably in magnitude for different years caused by the seasonal variation in stratospheric temperature. In the southern hemisphere, temporal evolution and magnitude of OClO were found to be similar for all years observed and show excellent anti-correlation with the stratospheric temperatures over Antarctica.

The rate of the heterogeneous chemical reactions and therefore chlorine activation is determined by the PSC particle type. In particular, the rate of the heterogeneous chemical reaction is proportional to the product of the reaction probability

and the surface area density [*Kim et al.*, 2006]. Denitrification and dehydration of the Antarctic stratosphere during the existence of PSCs prevents most of the activated chlorine from returning to its unreactive reservoirs (more details in Section 1.3.2 and 1.3.3). However, with sunlight warming the polar regions later in the season, PSCs evaporate, releasing HNO_3 and H_2O, and deactivation of ClO happens rapidly. In the Arctic, OClO has been observed to drop steeply to values around the detection limit within approximately 5 days after the final PSC [*Wagner et al.*, 2002], and ClO has been observed to persist for 1-2 weeks after PSCs have last been detected [*Rodriguez*, 1993]. The seasonal pattern of ClO is therefore expected to show an increase of ClO with increasing sunlight reaching areas of PSCs. After reaching a maximum of activation of the chlorine present in the stratosphere, the ClO pattern remains constant until PSCs evaporate which leads to a steep decline in the ClO abundance.

Regarding ozone depletion, in addition to chlorine chemistry, bromine chemistry has to be discussed (see Section 1.3.1). On a molecule-for-molecule basis bromine is more efficient in destroying ozone than chlorine. However, the largest contribution to ozone depletion in the Antarctic stratosphere is due to the ClO+ClO and ClO+BrO cycles and bromine would be very inefficient in the absence of reactive chlorine [*Chipperfield and Pyle*, 1998]. In addition, bromine reservoirs are less stable than chlorine reservoirs and conversion of the reservoir species to reactive forms is less dependent on heterogeneous chemistry. Therefore, chlorine is the driving halogen for ozone destruction and the seasonal evolution of ClO provides a good estimate of the ozone destroying potential [*WMO*, 2003, and Section 1.3.3].

Modelling and predicting the ozone evolution with CCMs still shows large discrepancies in model-to-model and/or model-to-observation intercomparisons. *Eyring et al.* [2006] detected several possible sources which lead to non-representative ozone distributions. Overall they found that the southern hemisphere winter/spring showed largest differences in the intercomparison. The problem of the southern hemisphere lower stratosphere cold bias ("cold-pole") remains and

the vortex break-up occurs later than observed. In addition, the transport of trace gases (including ozone and ozone depleting substances) is not accurately represented. In this thesis, a semi-empirical model is derived which is fitted to 20 years of observations and can be used to forecast the intra-annual evolution of Antarctic stratospheric ozone depletion. These forecasts can also be used for comparison with CCM outputs. The regression coefficients capture key sensitivities in the observations. These sensitivities can also be calculated for CCMs and comparison of the two sets of coefficients may provide new insights into potential sources of differences in CCM projections of Antarctic ozone depletion.

The rate of change of Antarctic stratospheric ozone is controlled by the amount of ClO available [*Solomon*, 1999; *Wallace and Hobbs*, 2006]. More ClO leads to faster catalytic ozone destruction unless there are no ozone molecules left to destroy, which leads to saturation in ozone depletion. In this chapter, two differential equations are derived: 1) a differential equation to describe the time rate of change of activated chlorine, represented as the activated part of equivalent effective Antarctic stratospheric chlorine (d(EEASC_a)/dt), and 2) a differential equation to describe the rate of change of ozone mass deficit as derived in Chapter 3 (d(OMD)/dt). In the first differential equation, a production term and a loss term for chlorine activation are incorporated. The data have been fitted to ClO measurements from MLS [*Santee et al.*, 2003] to allow representative coefficients to be determined. The second differential equation considers the dependence of the rate of change of ozone on activated chlorine, in-situ production and dynamical activity. Dynamical effects on the intra-annual variability of ozone depletion are also indirectly taken into account in the ClO measure, which depends on how much of the vortex was pushed into sunlight, especially early in the season. The coefficients were derived by fitting the model to 20 years of OMD measurements. All quantities in this chapter are used to describe the rate of change of ozone depletion in the total column. Therefore, processes with different effects on multiple levels were summarised into how they affect the entire column of air.

Modelling of the rate of change of activated chlorine is introduced in Section 4.2.1, and in Section 4.2.2 derivation of the differential equation for the rate of change of ozone mass deficit is discussed in detail. Results of the chlorine activation model are summarised in Section 4.3.1 and of the ozone model in Section 4.3.2, respectively. The predictive capability of the derived models is tested for 2005 and 2006 in Section 4.4 and conclusions are drawn in Section 4.5.

4.2 Methods

4.2.1 Modelling Activation and Deactivation of Chlorine

The rate of change of activated equivalent effective Antarctic stratospheric chlorine ($EEASC_a$) is described with a differential equation consisting of two main terms, 1) production/activation term, and 2) loss/deactivation term (Equation 4.1). The production of activated chlorine is controlled by the amount of unactivated equivalent effective Antarctic stratospheric chlorine (i.e. EEASC-$EEASC_a$), and by the amount of sun hours on polar stratospheric clouds. In case of a full activation of the total amount of EEASC available, the production term becomes zero. The term including sunlight on PSC area indirectly takes dynamical disturbances into account, viz. dynamical disturbances leading to temperature changes are reflected in the occurrence of PSCs, and multiplication of PSC area with the number of hours of sunlight on this area takes into account that vortex distortion, elongation or displacement away from the pole, results in some parts of the vortex, and therefore PSCs, reaching sunlight sooner than others. The loss term describes the deactivation of $EEASC_a$ back into EEASC. This occurs as long as HNO_3 is available and therefore depends on how much HNO_3 is bound in PSC particles. It also accounts for the rapid deactivation of ClO when temperatures rise and PSCs fully disappear.

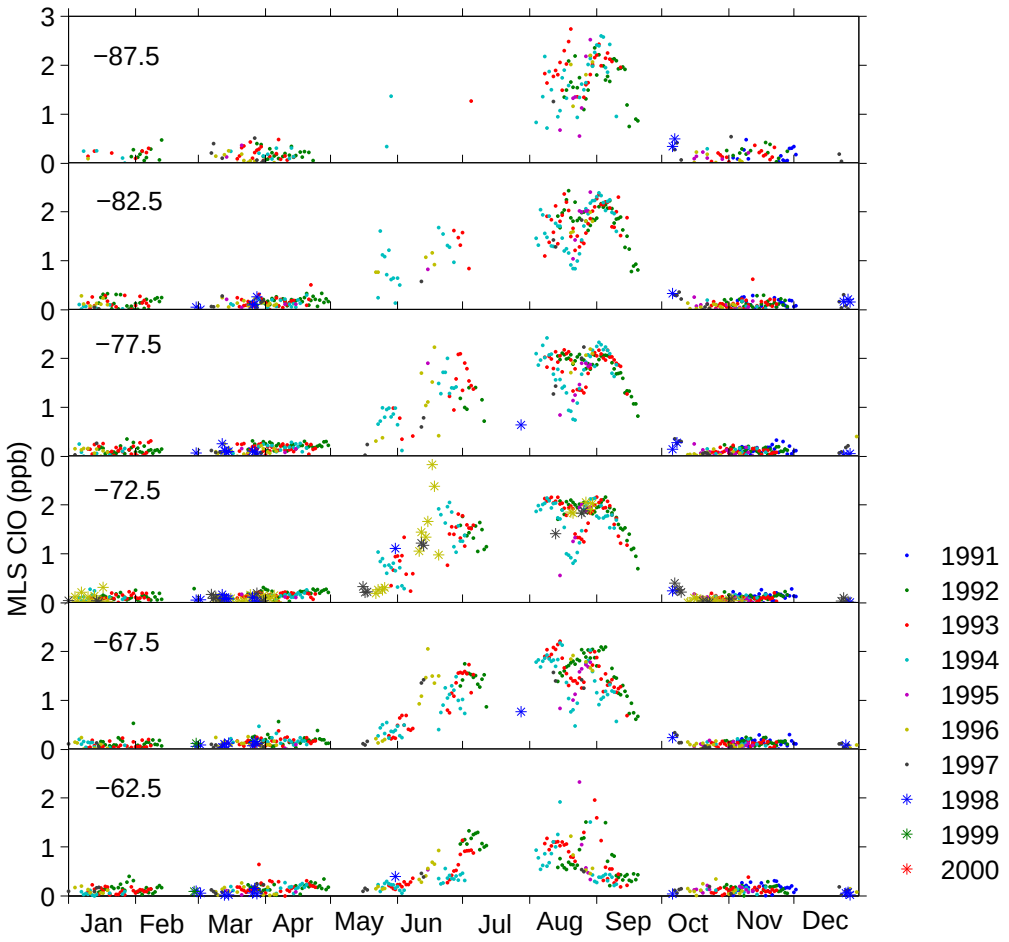

Figure 4.1: Time series of MLS ClO for different 5° equivalent latitude bands at 520 K. Different colours indicate different years (1991-2000) as labelled in legend.

The rate of change of EEASC was calculated as:

$$\frac{d\,(\mathrm{EEASC}_a)}{d\mathrm{t}} = \underbrace{\alpha \cdot (\mathrm{EEASC} - \mathrm{EEASC}_a) \cdot \mathrm{A}_{PSC} \cdot \mathrm{SUNHOUR}}_{Production} - \underbrace{\gamma \cdot \mathrm{EEASC}_a \cdot \left(1 - \frac{\mathrm{A}_{PSC}}{\mathrm{A}_{60S}}\right)}_{Loss} \tag{4.1}$$

where α and γ are the coefficients to be derived, EEASC-EEASC$_a$ is the amount of unactivated chlorine, A$_{PSC}$ is PSC area and A$_{60S}$ is the area poleward of 60°S, the largest possible area covered with PSCs.

To determine the proportionality constants α and γ, the model was regressed against five years of chlorine monoxide (ClO) data measured by the Microwave Limb Sounder (MLS) onboard the Upper Atmosphere Research Satellite [*Santee et al.*, 2003]. MLS ClO time series for the Antarctic region at 520 K were extracted for 1991-2000 (Figure 4.1). Peak values are observed in August followed by relatively constant values until early to mid-September. Due to sparse data in some years, only 1992-1996 data were used to fit the model. The fourth order Runge-Kutta method was chosen as the numerical method to solve the differential equation [*Boyce and DiPrima*, 2001]. The method is known to be relatively simple and robust and is considered to be the standard algorithm to solve differential equations. The fourth order Runge-Kutta method uses information from four points to move through one time step. The coefficients α and γ were derived by fitting the outputs from the differential equation to the ClO data for 1992-1996 with a non-linear least squares fit using the interior reflective Newton method [*Coleman and Li*, 1996, 1994]. This fitting method finds a minimum to the sum of squares of the functions. It is known for its efficient use of data and is commonly used to solve non-linear problems [*Press et al.*, 1997]. PSC area used in the model was derived from NCEP/NCAR temperature fields. The temperature fields are available on 17 pressure levels (1000-10 hPa) on a 2.5 degrees longitude by 2.5 degrees latitude grid. The threshold temperature for the formation of PSC type I of 195 K (Section 1.3.2) was used to define areas of PSC occurrence. The closest pressure level for PSC area to the 520 K theta level of the ClO data is 50 hPa. Especially in regions of steep ClO gradients this might lead to uncertainties in the modelled ClO. However, for this study, the MLS ClO data at 520 K were the only ClO measurements available. For future work, this model could be better fit to ClO observations on a range of pressure levels.

The derived model coefficients (α and γ) were then applied to seven pressure levels in the range of 250-30 hPa, the region where most of the PSCs occur [*Solomon*, 1999], to determine the amount of activated chlorine on each of those levels for the years 1979-2004. As indicated above, the MLS ClO data at 520 K were the only

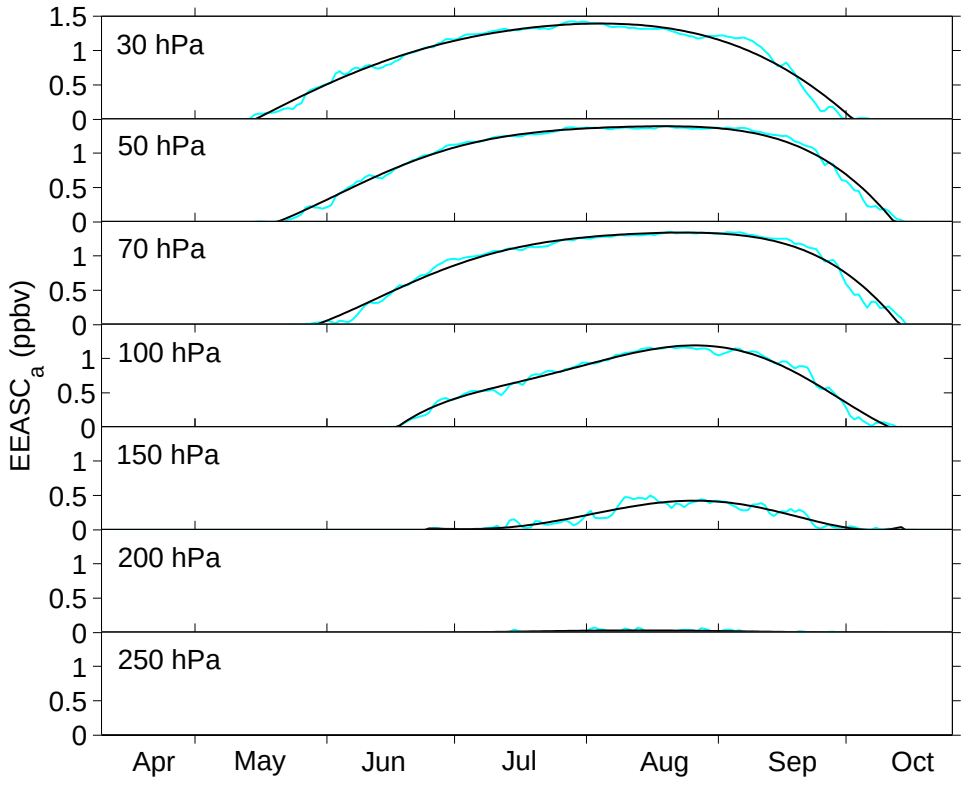

Figure 4.2: Pre-ozone hole EEASC$_a$ for pressure levels from 250-30hPa as indicated. The light blue line indicates the average for 1979-1981 and the black line is the fit to the data. See text for calculation of pre-ozone hole EEASC$_a$.

measurements available for this study and the assumption is made here that the derived coefficients α and γ are not altitude dependent which might lead to some uncertainty in the derived measure. Furthermore, to be consistent with the definition of the ozone measure, the measure of activated chlorine is defined as the total mass of activated chlorine relative to pre-ozone hole conditions (MAC). *Solomon et al.* [2005] showed that there was halogen depletion of Antarctic stratospheric ozone before 1980, however, due to the small amount of depleted ozone in those years, it is generally agreed that years before 1980 are considered pre-ozone hole [*WMO*, 2007]. In Chapter 3, the ozone depletion measure was defined relative to the pre-ozone hole background, therefore, the measure for activated chlorine is defined relative to pre-ozone hole chlorine activation in this chapter. Thus, a

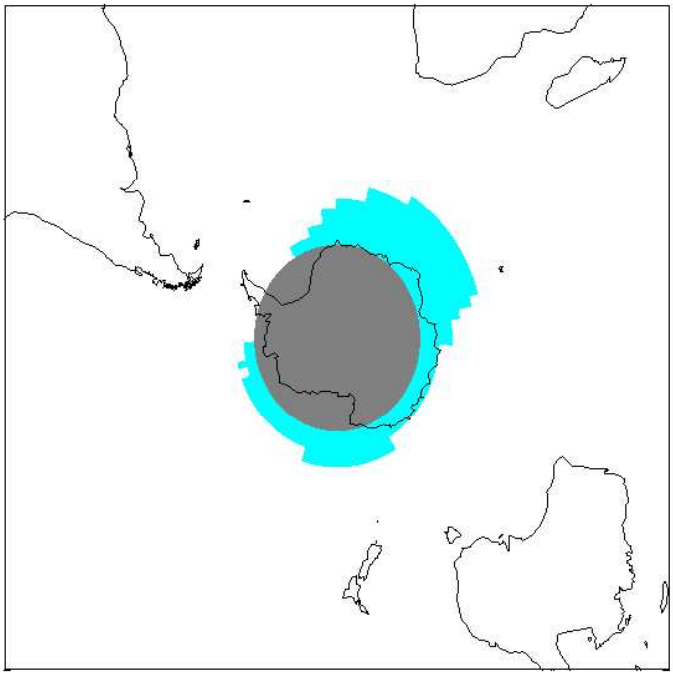

Figure 4.3: Schematic of the area over which activated chlorine is homogeneously distributed (light blue). The grey area indicates the area of polar darkness, and white is outside the polar vortex. This is an example for 18 July 2003.

pre-ozone hole $EEASC_a$ climatology for each level was calculated by fitting a six term Fourier expansion to the calender day average of $EEASC_a$ from 1979-1981 (Figure 4.2). The pre-ozone hole values were subtracted from the $EEASC_a$ data for each level and each year. MAC was determined by calculating the mass of activated chlorine for each of the layers centred around each of the seven pressure levels and integrating over all the layers. The area on each level over which chlorine is activated has been calculated as the sunlit area within the Antarctic vortex edge (see schematic in Figure 4.3) since within the sunlit portions of the Antarctic polar vortex homogeneous distribution of activated chlorine can be assumed [*Santee et al.*, 2003]. Calculation of the dynamical inner vortex edge is described in Section 3.2.1.

4.2.2 Modelling the Rate of Change of Ozone Mass Deficit

MAC as derived in Section 4.2.1 was used in a model for the rate of change of OMD (Equation 4.2). Since part of the activated chlorine is stored in the Cl_2O_2 dimer (see Section 1.3.3 and 4.1) the efficiency of chlorine destroying ozone molecules is less than quadratic [*Jiang et al.*, 1996] despite the dominance of the quadratic dependence on ClO in the Molina-Molina catalytic cycle (see Appendix D.1). This efficiency of chlorine to destroy ozone molecules is captured in the coefficient B in the differential equation below.

$$\frac{d\,(\mathrm{OMD})}{d\mathrm{t}} = \underbrace{A \cdot \mathrm{MAC}^{B} \cdot \overbrace{(1-\mathrm{R})}^{Saturation}}_{Ozone\ \ Destruction} - \underbrace{C \cdot \mathrm{OMD} \cdot \beta}_{In-Situ\ \ Production} - \underbrace{D \cdot \overline{v'T'}}_{Dynamics}, \tag{4.2}$$

where A, B, C, and D are the coefficients to be derived, MAC is the total mass of activated chlorine, R is OMD/OMD_{150} where OMD_{150} is the value that OMD would have if the total column ozone everywhere inside the vortex was 150 DU, β determines the amount of sunlight available for in-situ production of ozone (see also Equation 4.3), and $\overline{v'T'}$ is the eddy heat flux determining the influence of dynamical activity on the rate of change of Antarctic stratospheric ozone depletion.

In addition to the relationship between MAC and OMD, saturation in ozone depletion has to be taken into account (see Section 3.1). Minimum ozone levels within the vortex can reach values below 100 DU [*WMO*, 2003]. However, these are local events and for the vortex average quantity, an average threshold of 150 DU has been estimated [*Bodeker et al.*, 2002]. This threshold includes ozone from the troposphere and from layers in the stratosphere or above, where no ozone will be depleted. OMD_{150} was therefore calculated as the mass of depleted ozone within the Antarctic polar vortex if everywhere inside the vortex the total column ozone value was 150 DU. This is the estimated maximum amount of ozone that can be depleted within the polar vortex. The saturation term accounts for the amount of ozone that can be depleted (OMD_{150}-OMD), normalised by OMD_{150}.

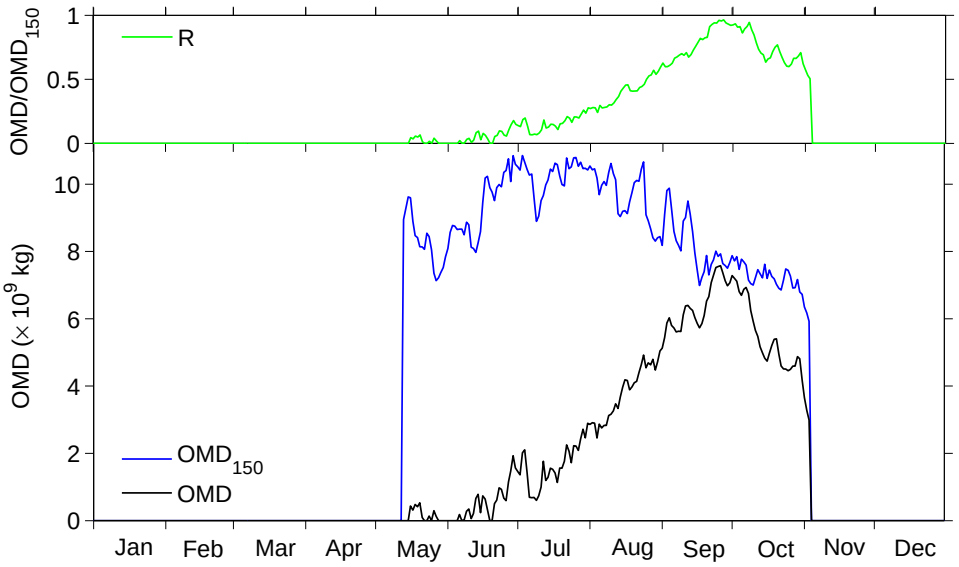

Figure 4.4: Saturation term R (green) in the upper panel and its two components, OMD (black) and OMD_{150} (blue) in the lower panel for 2003.

The closer the total column ozone value gets to 150 DU the stronger (closer to 1) the saturation term R gets, which can be seen in Figure 4.4. The lower panel of Figure 4.4 shows that the threshold of 150 DU is sensible because years with extensive ozone depletion (e.g. 2003) reach values very close to the assigned threshold. However, the threshold is not exceeded at any time.

The second term in the differential equation (see Equation 4.2) describes the decrease of OMD due to in-situ production of ozone. The effect of in-situ production is estimated by taking the amount of sunlight available to produce ozone via the Chapman cycle into account (see Section 1.3.1). Daily solar zenith angles (SZAs) at 12:00 local time were calculated on a 2.5 degrees longitude by 2.5 degrees latitude grid. The amount of in-situ production of ozone in the Antarctic stratosphere was estimated by taking the cosine of the solar zenith angle, the transmittance due to absorption by the ozone layer and the area within the polar vortex into account (Equation 4.3) and multiplying by the amount of depleted ozone. The cosine of the solar zenith angle describes the direct spectral irradiance on a horizontal surface. The term for the transmittance due to absorption by the

ozone layer was modified from the Lambert-Beer law [*Brasseur and Solomon*, 1984], by relating the absorption coefficient to the effective cross section.

$$\beta = cos\,(\mathrm{SZA}) \cdot e^{\frac{-k_\lambda}{cos(\mathrm{SZA})}} \cdot \mathrm{A_v}, \tag{4.3}$$

where k_λ=0.9·10^{-17} cm^2 is the absorption cross-section for ozone at λ=242 nm [*Brasseur and Solomon*, 1984], SZA is the solar zenith angle and A_v the area within the polar vortex.

Excellent agreement between the eddy heat flux and the rate of change in ozone has been found in earlier studies [*Randel et al.*, 2002]. Therefore, the eddy heat flux was chosen as a measure of how dynamical activity influences the rate of change in ozone depletion. Daily eddy heat fluxes were calculated by zonally averaging the product of temperature and meridional wind speed anomaly time series at 60°S. Temperature and wind fields were extracted from the NCEP/NCAR database. With the eddy heat flux ($\overline{v'T'}$) wave induced mixing of ozone into the vortex across the vortex edge or wave induced changes to inter-annual variability in diabatic descent are taken into account. These effects are expected to be small in years with average dynamical activity, however, as shown in Chapter 3, they are not negligible. The eddy heat flux is defined negative in the southern hemisphere. *Randel et al.* [2002] found that more (negative) eddy heat flux leads to an increase in the rate of change in ozone. Therefore, an increase in the (negative) eddy heat flux leads to a decrease in the rate of change in OMD.

A fourth order Runge-Kutta method was used as the numerical approximation method to solve the differential equation (Equation 4.2) equivalent to Section 4.2.1. The coefficients A, B, C, and D were derived by fitting the differential equation to OMD data with a non-linear least squares fit (see also Section 4.2.1) to 20 years of data. First, this fit was performed on each year separately to gain an overview of the variability of the coefficients. Secondly, the fit was performed on all years together to derive one set of coefficients that can be applied to any year. The time span chosen for this study is from 1980-2004. Data for calculating

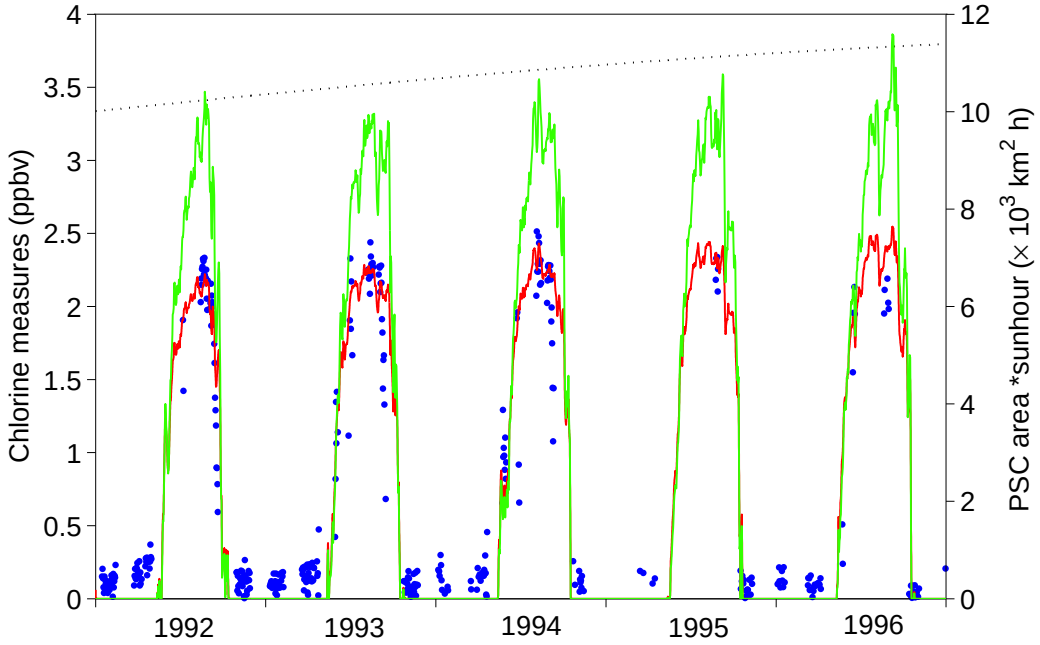

Figure 4.5: Model fit (red) to MLS ClO data (blue) in comparison with EEASC (dashed black)and PSC area times sunhours (green).

the new ozone mass deficit were available from 1979-2004 and 1979 was excluded since it was used as the reference year for the pre-ozone hole measures. From these data (1980-2004), years with dynamical activity above average (1988, 2002 and 2004; see Chapter 3 for identification of highly dynamical active years) were excluded since they are not representative for most of the years. In addition, the years 1994 and 1995 are excluded because of gaps in the observational database.

4.3 Results and Discussion

4.3.1 Activated Chlorine

The activated chlorine ($EEASC_a$) has been derived as described in Section 4.2.1. The regression model output for the coefficients derived with the non-linear least squares fit is compared to the MLS ClO observations, EEASC and PSC area times hours of sunlight for 1992-1996 in Figure 4.5. There is excellent agreement between the model and the observations for the period during which the polar

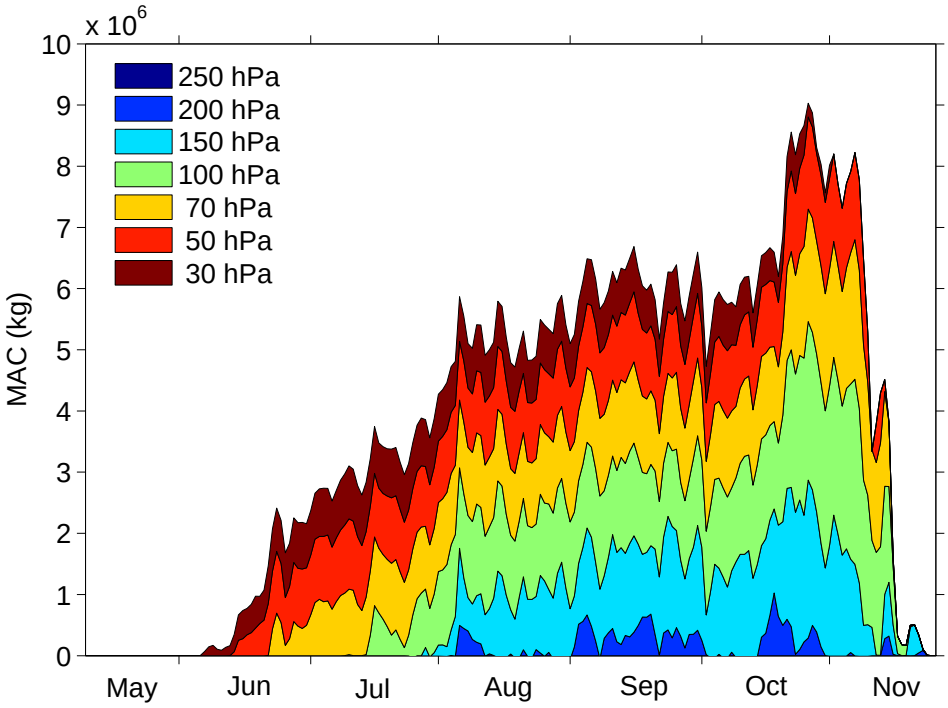

Figure 4.6: Contribution to MAC from each of the seven pressure levels in 2003. Level of centre of the layers is indicated in the legend.

vortex edge is well defined [*Nash et al.*, 1996]. The model captures the seasonal pattern of ClO including all major features, i.e. the fast increase in ClO at the beginning of the season and the rapid decline after deactivation begins. The standard deviation of the residual between measurement and model at the points where measurements are available is 0.26 ppbv. Deviations between model and measurements are also due to the fact that there might be some rapid variations in the observations which are not captured in the model and which are most likely local variations. Note that the MLS ClO shows some deviations from zero before and after the period of chlorine activation. The gas phase photochemical theory predicts 10 ppt of ClO [*Solomon*, 1999] which is not captured in the model since it only accounts for elevated ClO levels due to heterogeneous chemistry plus there is an unexplained positive bias in the night-time MLS ClO. Over the five years the absolute maximum in the activated chlorine appears around three days earlier in the modelled values compared to the observations. Some differences

Level	250 hPa	200 hPa	150 hPa	100 hPa	70 hPa	50 hPa	30 hPa
%	0 %	2.2 %	16.5 %	23.8 %	23.5 %	21.1 %	12.9 %

Table 4.1: The percentage contribution of each layer, centred at each of the pressure levels, to the total amount of MAC in 2003.

could be due to the fact that sparse data are available during the time of the maximum in the observations. The magnitude of the maximum over the five years is underestimated by the model by an average of 0.036 ppbv which is only 1.5 % of the average maximum. Since the EEASC did not change considerably over the period from 1992-1996, the maximum values over these years are of similar magnitude. In addition, in these five years, little inter-annual variability was observed in all measures displayed in Figure 4.5. The derived coefficients reach a value of α=1.14 and γ=9.40. Note that in the figure it can also be seen that the maximum of ClO is lower than the EEASC level which is not surprising since EEASC combines chlorine and bromine species. However, for the activation, only chlorine is considered because bromine activation is not as dependent on heterogeneous chemistry since bromine reservoir species are less stable than chlorine reservoirs. In addition, bromine would be very inefficient in destroying ozone without chlorine, as described in more detail in Section 4.1.

The derived coefficients α and γ were then applied to PSC areas at seven pressure levels (250-30 hPa) as described in detail in Section 4.2.1. In Figure 4.6 the contribution of each layer to the total mass of activated chlorine is shown for 2003. The layers are centred at the pressure levels indicated in the legend of the figure. The percentage contribution of each layer to the total MAC in 2003 is listed in Table 4.1. The largest contribution to the total mass of activated chlorine comes from the layers around the 150 hPa and 70 hPa levels. There is no contribution from the 250 hPa level since there were no PSCs at that level in 2003 (and most other years). Some uncertainties for these quantities might occur due to the fact that the parameters α and γ were derived for one pressure level and then applied to the full altitude range, as discussed in Section 4.2.1.

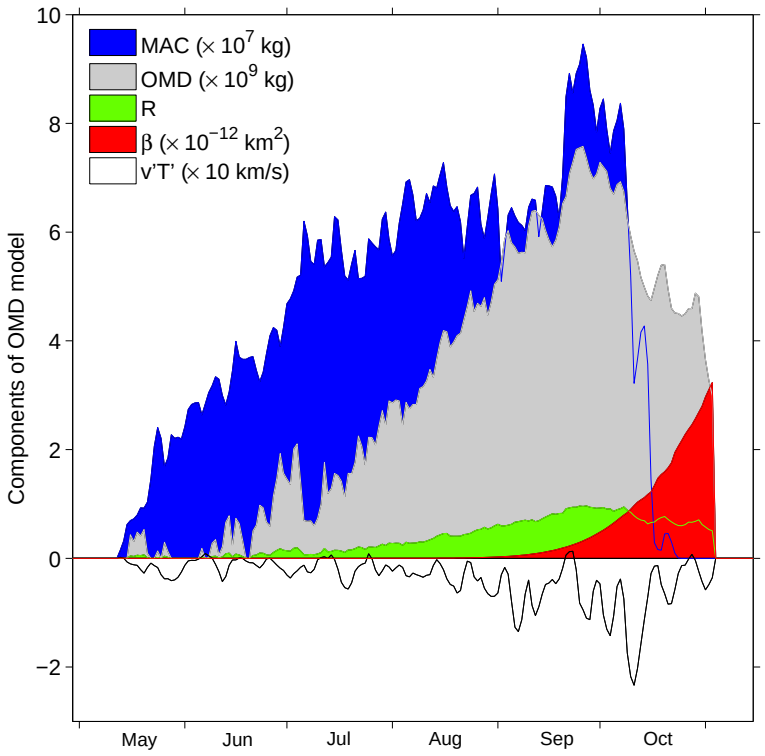

Figure 4.7: Components of the OMD model for 2003: total mass of activated chlorine (MAC), saturation factor R (R=OMD/OMD$_{150}$), ozone mass deficit (OMD) from observations, efficiency of in-situ production (β) and eddy heat flux (EHF) in colours as indicated in legend. The measures are scaled to the same magnitude.

4.3.2 Ozone Mass Deficit

The components for the OMD model are displayed in Figure 4.7. By definition OMD cannot be determined before the Antarctic polar vortex is formed (see Chapter 3). Therefore all components that are used to describe the rate of change in OMD are set to zero before the formation of the polar vortex. It can be seen that the largest contribution of MAC to the rate of change of OMD is from about May until September. Saturation effects (R), as defined above, slowly increase until the maximum is reached in September. The term for in-situ production begins in late August and increases rapidly during the end of the season. In this model, in-situ production of ozone is assumed to account for much of the decrease

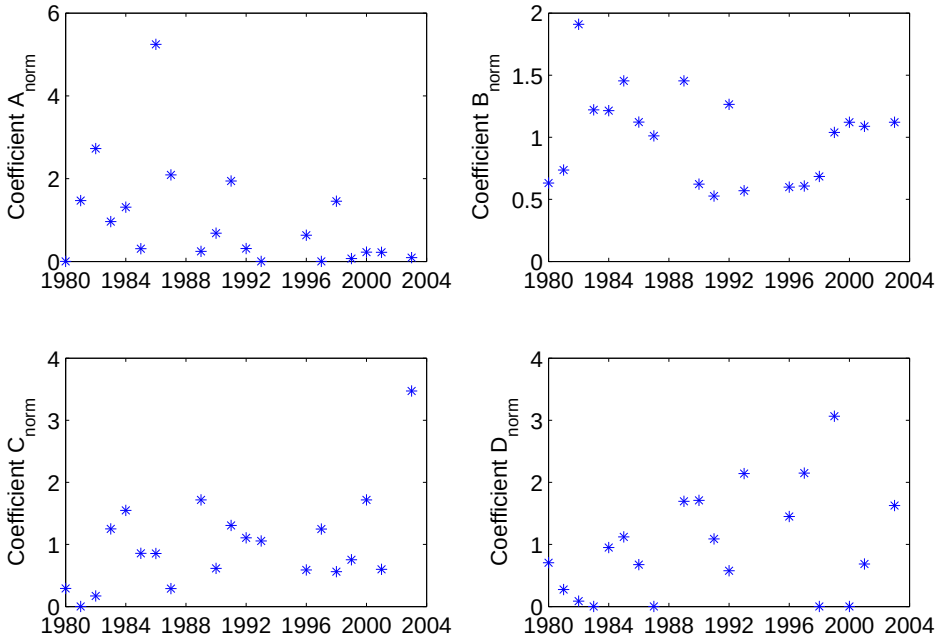

Figure 4.8: Normalised coefficients for the OMD model as in Equation 4.2. See discussion in text.

in OMD late in the season. However, other factors that also contribute to the decrease in OMD late in the season might have to be taken into account, for example mixing of ozone-rich air from the top of the vortex or in highly active years also through the vortex edge. The dynamical activity term has an effect throughout the season which increases from about September and maximises in October. It should be noted that dynamical activity leads to opposing effects, depending on the strength of the eddy heat flux. A certain amount of wave activity merely distorts the vortex, exposing some of the vortex interior to sunlight which leads to more ozone depletion. This happens particularly early in the season. Stronger wave activity, however, can mix in ozone-rich air from lower latitudes and can replenish some of the polar ozone. An additional term would have to be included in the model to account for that.

The resulting coefficients for model fits to each of the 20 years of OMD data separately were normalised by their mean value and are displayed in Figure 4.8.

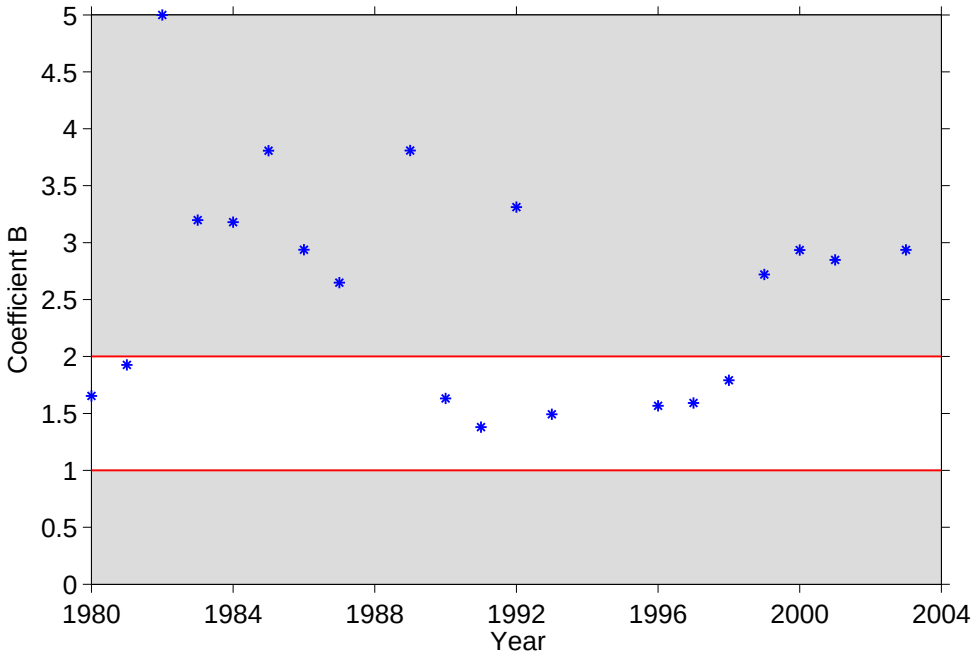

Figure 4.9: Coefficient B for the OMD model. The white area between the red lines in the plot indicate the boundaries between which coefficient B is expected to fall.

Some variability is observed in the coefficients, and the standard deviation of the normalised coefficients is σ_{A_n}=1.28, σ_{B_n}=0.37, σ_{C_n}=0.77, and σ_{D_n}=0.87. Coefficients A and B seem to be more variable in the earlier years, whereas coefficients C and D show more variability towards the later years. However, to move forward with this model, it is necessary to assume that this level of variability is acceptable in order to use one set of coefficients for all years. Coefficient B is expected to have a value between 1 and 2 (see Section 4.2.2). In Figure 4.9 the red lines indicate the boundaries within which coefficient B is expected to fall. It can be seen that the values from the model lie above the expected range for a few years. However, it falls within the expected range for almost half of the years considered. It should be noted that there are two effects that decrease the relationship of ozone depletion and chlorine monoxide to less then quadratic: 1) part of the chlorine is stored in the Cl_2O_2 dimer, and 2) ozone that was already destroyed is no longer available for reaction. The first effect is meant to be described in the coefficient B and the second in coefficient A. However, identifiability problems for these

coefficients might occur, which would explain why B does not always fall in its expected range.

Contributions of the different terms in the model are displayed in Figure 4.10 for 2003 together with the OMD observations for this year. The observations are displayed as grey area and all contributions are summed to the total fit in the red line. It can be seen that the fit closely follows the seasonal evolution of OMD. The maximum is slightly underestimated and short-term variations, presumably resulting from dynamical intrusions of ozone-rich air, are not well represented in the model. The only term in the model which shows some short-term variability is the D-term, however, its contribution is not as large. The contribution of the AB-term together with the D-term are responsible for the increase in OMD, whereas the C-term accounts for the decrease, as expected. Furthermore, the output from the single terms of the model suggests that dynamical activity has a strong influence on OMD very early in the season. From July onwards, the chemical contribution dominates the dynamical contribution until the beginning of October, where the chemical depletion reaches saturation.

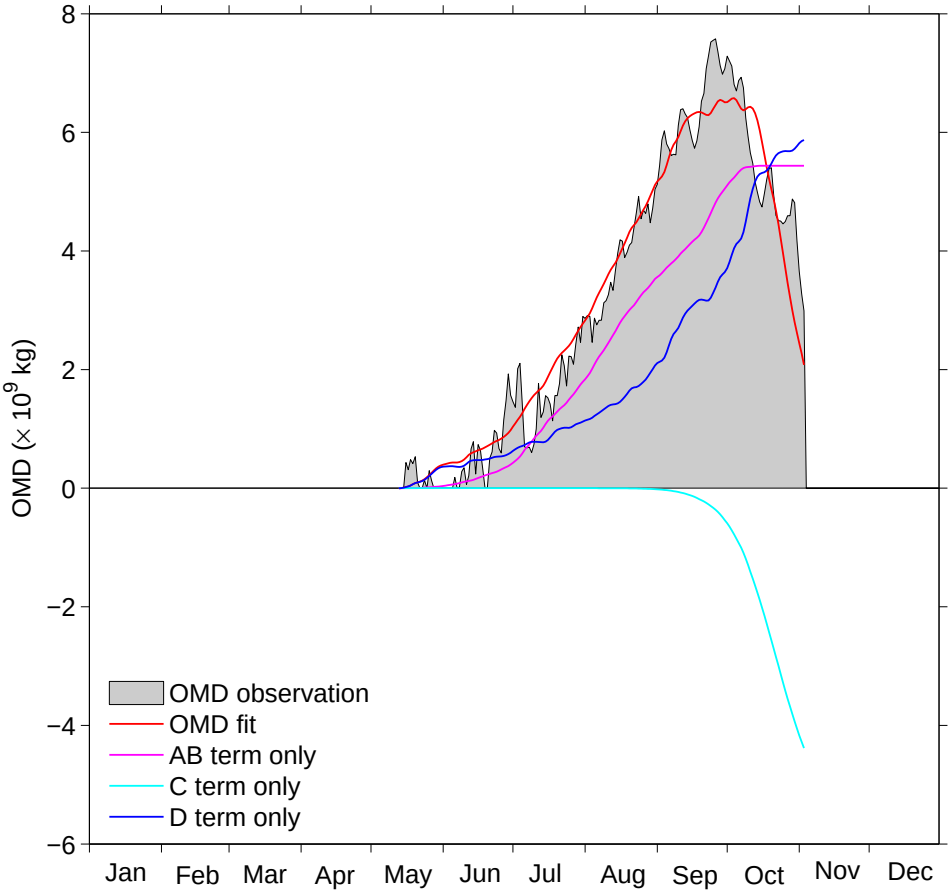

Figure 4.10: OMD observation (grey area) and model fit (red) for 2003. Contributions from each term separately are indicated in colours as specified in legend.

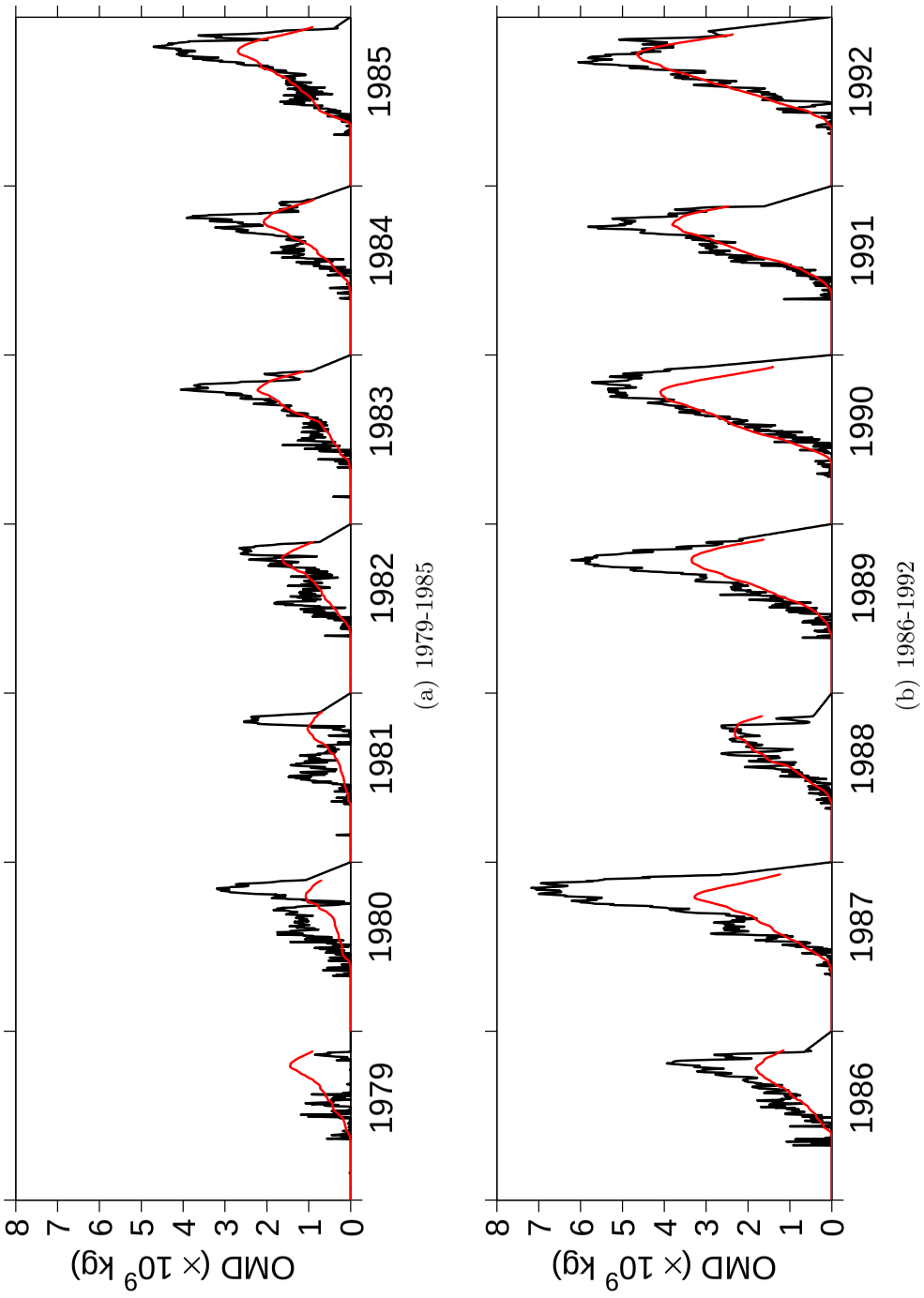

(a) 1979-1985

(b) 1986-1992

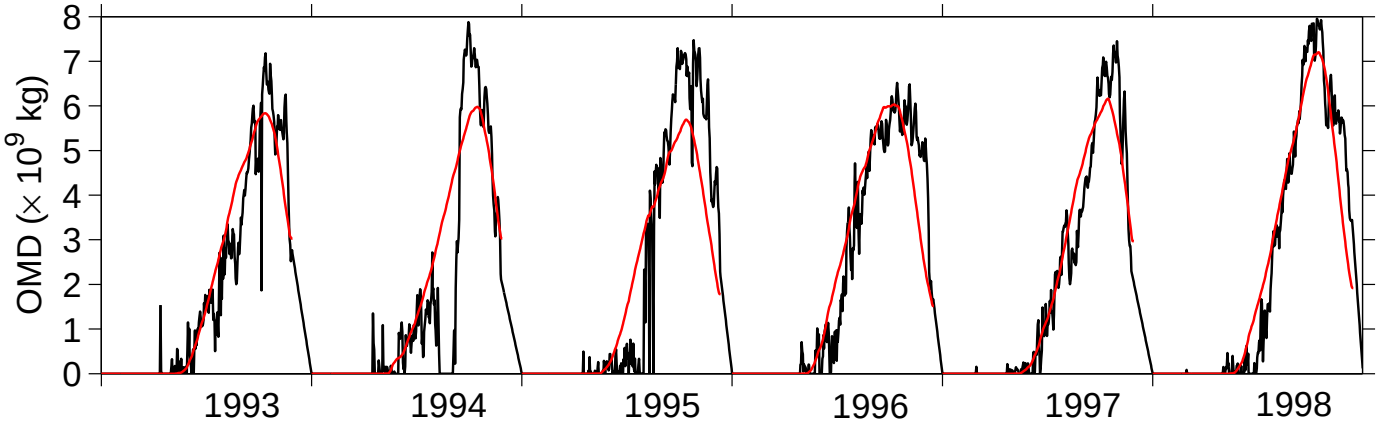

(c) 1993-1998

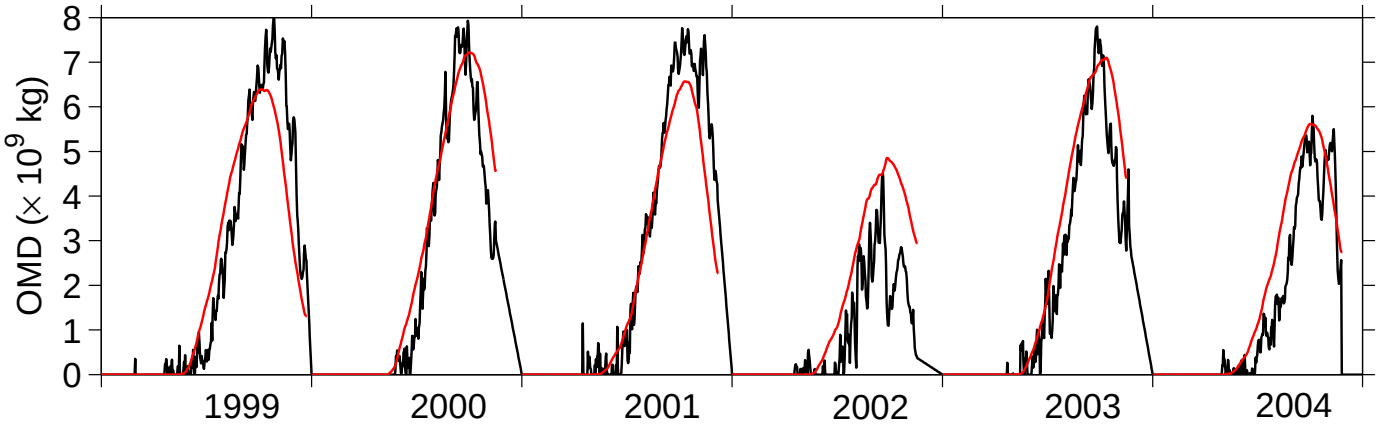

(d) 1999-2004

Figure 4.11: OMD observations (black) and OMD fit (red), with one set of parameters for 20 years applied to data from 1979-2004 distributed over four panels.

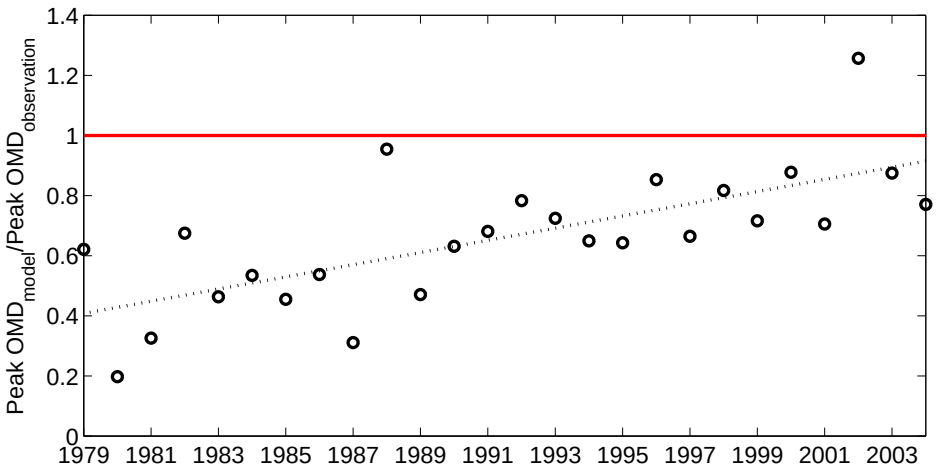

Figure 4.12: Peak values of the OMD model divided by the peak values of OMD observations are displayed in the black circles. The dashed line indicates a linear fit through the data, and the red lines marks where the model peak would reach the same value as the observation.

When fitting the OMD model to all 20 years of observational data together, the coefficients result in A=0.0064, B=1.5795, C=0.0532 and D=0.0002. It should be noted that B falls in the range where it is theoretically expected. The model coefficients were then applied to all the years from 1979-2004 and the model fits in comparison with the OMD observations are displayed in Figures 4.11(a)-4.11(d). Overall, the model output shows good agreement with the observations. The inter-annual variability is reflected in the fits and the seasonal evolution for each year is well represented. The short-term variability as seen in the observations is not reflected in the modelled OMD, but intra-annual features, for example a slow onset of ozone depletion before the rapid increase is captured by the model. The standard deviation of the residual is 0.84 $\times 10^9$ kg. When integrating over all the years, the model reproduces 91 % of the OMD from observations. Even the dynamically unusual years (1988, 2002 and 2004) are captured well by the model. However, in Figure 4.12 it can be seen that the peak value for these years gets overestimated in comparison with the other years. This indicates that the model does not capture dynamical resupply, as was expected.

Large deviations between model output and measurements are observed for 1987 and 1989. In these years the amount of total activated chlorine seems to be underestimated by the chlorine model which might be due to an underestimation of PSC area in those years. Overall, the later years (after 1990) show better agreement between model and observations. Especially the peak values of the modelled OMD, which get underestimated in the earlier years are much closer to the peak values in the observations for the second half of the data (Figure 4.12). This is not surprising since the coefficients in the chlorine activation model were derived only for the later years which might cause a bias in the model.

4.4 Predictive Capability

Prediction of intra- and inter-annual variability in Antarctic ozone depletion has important applications, for example to investigate the recovery of the Antarctic ozone hole and the role of the ozone hole in climate change. Chemistry-climate models have been developed to simulate detailed processes in the stratosphere, however, they are expensive to develop and take a long time to run. In addition, large deviations between different models complicate predictions of the development of the Antarctic ozone hole [*Eyring et al.*, 2006]. The semi-empirical models for Antarctic stratospheric chlorine activation and ozone depletion derived in the previous sections provide an easy, inexpensive and fast approach to projecting the inter- and intra-annual development of the Antarctic ozone hole into the future.

In Section 4.3, the predictive capability of the model was tested by applying the regression coefficients to six years (1979, 1988, 1994-1995, 2002 and 2004) which were not used to derive the coefficients. However, these years were within the time span over which the regression coefficients had been determined. In this section the semi-empirical models for chlorine activation and ozone depletion were used to project the seasonal evolution of OMD for 2005 and 2006. In the schematic in Figure 4.13 the application of the derived models to forecasting ozone depletion is shown. The parameters in the coloured boxes need to be determined as indicated

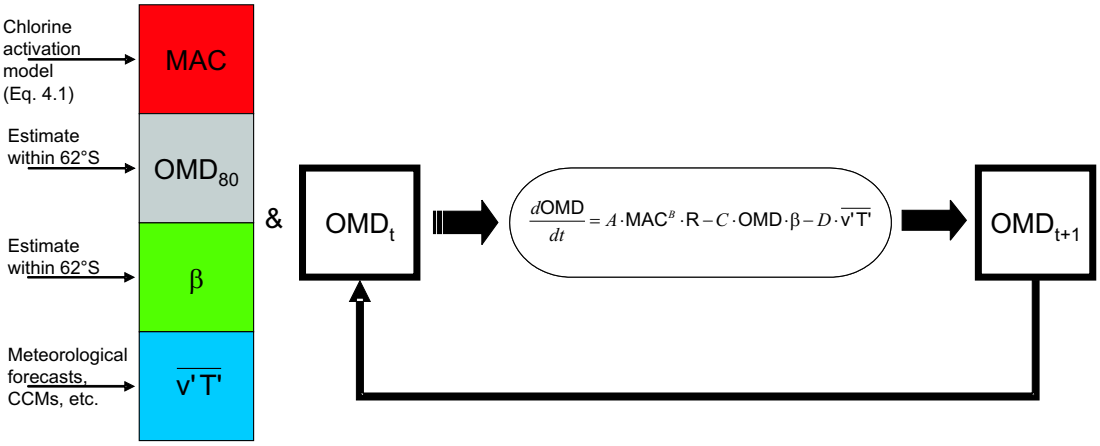

Figure 4.13: Schematic of the ozone model applied to forecasting the intra- and inter-annual evolution of the Antarctic ozone hole.

by the arrows pointing to the boxes. The differential equation can be solved with the fourth order Runge-Kutta method as described above and OMD can be obtained for any year for which the input parameters are available. The input parameters for the chlorine and the ozone models are as follows:

1. EEASC*
2. PSC area: temperature and vortex edge**
3. sun hours*
4. OMD_{150}**
5. β: solar zenith angle*, absorption cross-section of ozone* and vortex area**
6. eddy heat flux: temperature and meridional wind fields

From these parameters, everything marked with a * is a constant and has to be calculated only once or has already been estimated into the future (e.g. EEASC values are available from 1950-2100 [*Newman et al.*, 2006]). The parameters marked with ** can be approximated by using the 62°S latitude circle as the average location of the vortex edge [*Bodeker et al.*, 2002] instead of the inner dynamical vortex edge. This approach has also been applied to the new OMD

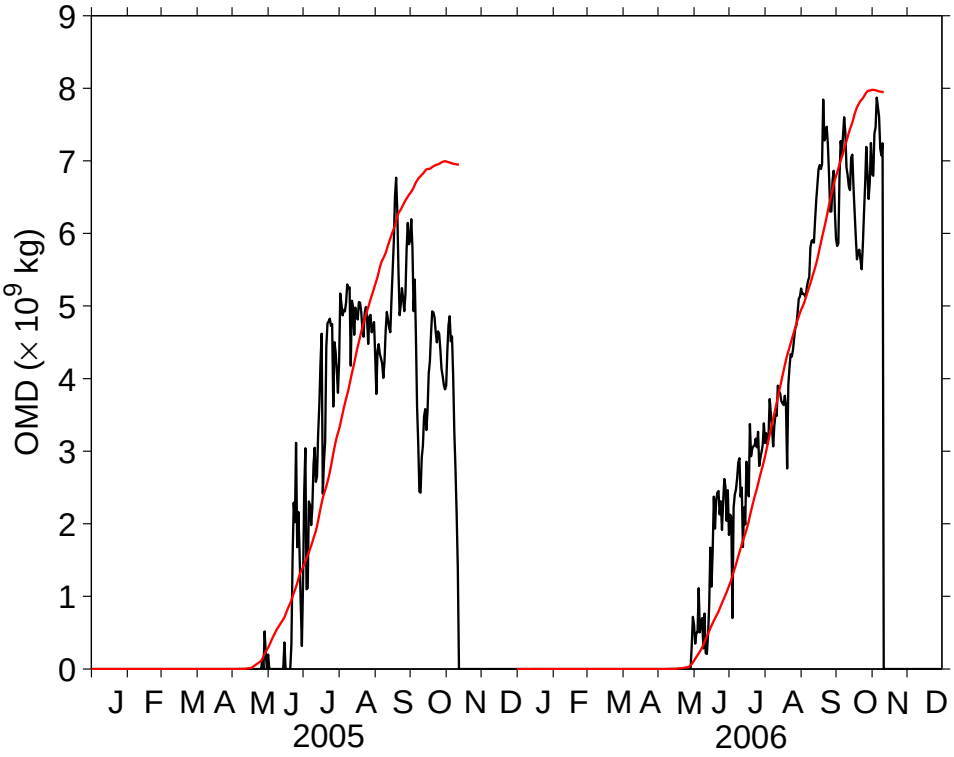

Figure 4.14: Seasonal evolution of ozone projections for 2005 and 2006 in comparison to OMD derived from observations for the area south of 62°S.

measure in Chapter 3, and was used to derive the OMD values from observations for 2005 and 2006 where data to calculate the dynamical inner vortex edge were not available. The only parameters required for each year are temperature and meridional wind fields to obtain estimates for the PSC area and the eddy heat flux. For 2005 and 2006 these parameters were derived from the same sources as for the other years, i.e. NCEP/NCAR reanalyses. In Figure 4.14 OMD estimates south of 62°S from observations are displayed together with the model predictions for 2005 and 2006. Overall, the seasonal development of OMD is represented well in both years, with better agreement between the observations and the model in 2006. When integrating the time series, the model values in 2005 overestimate the total loss of ozone by about 19 %, whereas 98.2 % of the OMD from observations in 2006 is represented by the model. As discussed in Section 4.3.2, the short-term variability in the OMD observations are not represented in the modelled values.

Presumably an additional term in the differential equation (Equation 4.2) to take intrusions of ozone-rich air into the vortex could improve the model and account for some of the short-term fluctuations in OMD.

For projections of the seasonal evolution within a year, temperature and meridional wind fields can be extracted from meteorological forecasts, for example from general circulation models. As long as temperature and wind fields are available, the OMD can be predicted, as indicated above. The seasonal evolution of OMD can be corrected within the year when measurements of temperature and wind fields become available. For example, the forecast in May for the severity of Antarctic ozone depletion from May until November would be based solely on temperature and wind field predictions. In June, one month of temperatures and wind velocities can be replaced with observations and the OMD projection can be improved. While this was outside the scope of this thesis, in future work, the improvement of the models for chlorine activation and ozone depletion over the course of one season will be tested together with the predictive capability of the models over longer time-scales.

4.5 Conclusions

In the study presented above, semi-empirical models for Antarctic chlorine activation and ozone depletion in the stratosphere were derived. The chlorine activation model was regressed against MLS ClO data for five years (1992-1996). The seasonal pattern and the amount of elevated ClO from the model is in excellent agreement with the observations. After applying the derived coefficients to seven pressure levels over the pressure range of PSC occurrence, the total mass of activated chlorine relative to pre-ozone hole activated chlorine was derived. This metric in turn provides a measure for the rate of change in Antarctic ozone depletion. The ozone depletion model was regressed against 20 years of OMD from observations, excluding years with anomalous dynamical activity or problems in the observational database. The derived coefficients were applied to 26 years of

data (1979-2004; including the 20 years of data from the fitting). Especially for more recent years (after 1990) the seasonal pattern and the amount of depleted ozone from the model is in good agreement with the observations. Larger deviations between the amount of modelled OMD and measurements are observed for the earlier years. However, the seasonal evolution is still well represented, only the maximum of OMD is underestimated in the model for most of the years. In the years of unusual high dynamical activity (1988, 2002 and 2004), peak values are higher than in the other years, indicating that dynamical resupply is not captured by the model as was expected. In addition, short-term variability in OMD as seen in the observations is not reproduced in the model. This leads to the conclusion that most likely an additional term for intrusions of ozone-rich air from lower latitudes into the polar region has to be considered if the fluctuations are to be represented in the model. The ability of this regression model to capture the seasonal evolution of OMD and to a large extent the year-to-year variability, confirms that the chemical and dynamical processes controlling Antarctic stratospheric ozone depletion are in general well described by the model. Overall when integrating over all 26 years, the prediction is 91 % of the OMD from observations.

The predictive capability of the chlorine activation and ozone depletion models was tested by applying the derived regression coefficients to temperature and wind data for 2005 and 2006. The seasonal evolution for both years is in good agreement with the observations. The magnitude of total OMD in the model is overestimated by about 19 % in 2005, however in 2006, 98 % of the total OMD can be explained by the model. Projections of OMD into the future can be performed with the semi-empirical models presented above as long as temperature and wind fields are available. These can be obtained, for example, from general circulation models. Future work will examine the ability of the derived models to project the seasonal evolution of OMD based on temperature and wind velocity forecast data and the predictive capability of both models over longer time-scales will be tested.

Chapter 5

Summary, Conclusions and Future Work

5.1 Summary and Conclusions

The aim of this thesis was to study the coupling of dynamics and chemistry in the Antarctic stratosphere and evaluate its influence on the Antarctic ozone hole. Indices of dynamical activity and chemical processes were derived and analysed. Inter- and intra-annual variability in Antarctic stratospheric ozone depletion was explained with simple regression models parameterising the dynamical and chemical processes. Furthermore, these indices were applied to quantify inter-annual variability and intra-seasonal evolution of Antarctic stratospheric ozone depletion in the past, present and future.

In the first part of this thesis (Chapter 2) a simple statistical model was developed to explain inter-annual variability in Antarctic stratospheric ozone depletion based on equivalent effective stratospheric chlorine, South Pole temperatures, and mid-latitude planetary wave activity. The primary driver of the severity of Antarctic ozone depletion was confirmed to be halogen loading in the stratosphere. Year-to-year variability on top of this secular change is dominated by the inter-annual variability in South Pole temperatures. However, the most representative model of inter-annual variability in Antarctic ozone depletion could be derived when taking midlatitude planetary wave activity as an additional explanatory variable into account. A high correlation between this statistical model output and observations was observed. Furthermore, the model coefficients were applied to chemistry-climate model output to estimate how the Antarctic ozone

hole will develop in the future assuming that the relative effects of temperature and wave activity will not change. This application suggests that inter-annual variability in ozone over the Antarctic may increase slightly in the future. More variability is observed when natural forcings are included. Simulations for 2020-2050, in which natural forcings are not included, show less occurrences of extreme events, like the vortex split-up in 2002.

Expansion of these studies to intra-annual variability required the consideration of more detailed processes in chemistry and dynamical activity which can be neglected when averaging over the Antarctic vortex period to investigate year-to-year variability. To this end, an improved version of the ozone depletion measure, OMD, was developed in Chapter 3 of this thesis. The 220 DU constant background, formerly used as the threshold to decide whether a region is considered to be depleted of ozone, was replaced with a seasonally varying pre-ozone hole background. Since the 220 DU threshold also provided the spatial integration limit for the calculation of OMD, in this study the dynamical inner vortex edge, as well as a simpler approach of 62°S, the average location of the vortex edge, were used as the spatial integration limits, respectively. This method was also applied to the calculation of ozone hole area. The new method applied to calculate these indices keeps much of the simplicity of the earlier method which used 220 DU as the unperturbed background and as spatial integration limit but the new ozone depletion measures better capture the true extent of depleted mass of ozone. The new versions of OMD and OHA show closer correspondence with the timing of the return of sunlight to the vortex and the onset of ozone depletion. In addition, through comparisons of the new OMD and OHA indices with tracer-tracer correlation derived accumulated Antarctic chemical ozone loss, it could be demonstrated that with the new method (compared to the 220 DU-based method) the chemical ozone loss within the Antarctic vortex is better represented. Exceptions occur for unusually dynamically perturbed years since the new method cannot distinguish between chemically and dynamically induced changes in ozone. Dynamically unusual years can be identified by investigating temperatures, zonal

mean winds or total wave power. Therefore, the newly proposed Antarctic ozone depletion indices will only be representative of the chemical depletion of ozone in years when dynamical contributions to ozone variability within the vortex are small. However, the new OMD and OHA provide improved metrics of the severity of Antarctic ozone depletion and for impact studies of ozone depletion on the biosphere since they better capture the true extent of the ozone hole. The new methods for calculating OMD and OHA require data that are more readily available than for the tracer-tracer correlation method. The new method requires total column ozone fields and, only for the approach that uses the vortex edge, potential vorticity fields, whereas the tracer-tracer correlation method requires ozone and passive tracer profile measurements. Thus, with the new method, accurate measures of Antarctic ozone depletion can be obtained over longer periods. These new definitions of OHA and OMD should also aid chemistry-climate model intercomparisons. The new measures will be less sensitive to ozone bias since the pre-ozone hole background from which the OMD and OHA are calculated, will be specific to each model and will result in some cancellation of any ozone bias.

In the third part of this thesis (Chapter 4), two semi-empirical models were developed which parameterise chemical and dynamical processes to describe the seasonal evolution of stratospheric chlorine activation and the rate of change of stratospheric ozone depletion. The rate of change of chlorine activation was modelled based on the area containing polar stratospheric clouds, the hours of sunlight illuminating this area, and the rate of chlorine deactivation which includes the half-life of chlorine monoxide and the availability of polar stratospheric clouds which remove nitric acid and water vapour from the reaction cycle. The model was fit to chlorine monoxide observations from the Microwave Limb Sounder onboard the Upper Atmosphere Research Satellite from 1992 to 1996. Excellent agreement between the chlorine activation model and observations could be achieved. Activated chlorine abundances were then calculated for seven layers, centred on pressure levels between 250 and 30 hPa, the region where most polar stratospheric clouds occur. The total mass of activated chlorine was estimated by

integrating over all the layers after subtracting the amount of activated chlorine at pre-ozone hole conditions (equivalent to calculating the new OMD relative to pre-ozone hole conditions). This measure in turn was used to describe the rate of change of ozone destruction. In addition, saturation of ozone depletion, in-situ production and dynamical disturbances were considered as further drivers. To determine proportionality constants, the OMD model was fit to 20 years of observations, excluding years with unusual dynamical activity or with problems in the observational database. The derived regression coefficients were then applied to meteorological and chemical data from 1979-2004, including the 20 years of data from the fitting. It was shown that good agreement between the seasonal evolution of measured and modelled OMD could be achieved using this semi-empirical approach. Better representation of the magnitude in OMD is observed after 1990, however, the seasonal evolution is well represented for all years. In the model for ozone depletion the short-term variability in OMD as seen in the observations is not reproduced in the model. An additional term for intrusions of ozone-rich air from lower latitudes into the polar region would most likely help to model these fluctuations. A slight over-estimation of the peaks in OMD in the dynamically unusual years (1988, 2002 and 2004) also suggests that an additional term to account for dynamical resupply could improve the model. The predictive capability of the model was evaluated on data for 2005 and 2006. Only temperature and meridional wind velocity fields need to be obtained to apply the regression coefficients. The remaining data are either constants, can be estimated by replacing the dynamical vortex edge with the average location of the vortex edge at 62°S, or can be obtained from already available future estimates (e.g. EEASC). The model was able to reproduce the intra-annual variability and magnitude of the depleted mass of ozone in good agreement with OMD estimates from observations.

Based on the atmospheric processes affecting the inter- and intra-annual variability in the severity of Antarctic ozone depletion, a pair of semi-empirical models were designed that can describe the seasonal evolution of OMD, given readily

available meteorological fields. For projections of the seasonal evolution of OMD into the future, forecasts of the required temperature and wind fields need to be obtained. In Chapter 2 it was shown that a two week time lag between mid-latitude wave activity and Antarctic ozone depletion leads to highest correlations between the two measures. This time lag suggests some predictive capability when looking at wave activity. Further options are to get projections from a numerical weather prediction model.

Overall, the linear regression model and the two semi-empirical models presented in this thesis provide fast and inexpensive tools to describe and study inter- and intra-annual variability in Antarctic stratospheric ozone depletion. The ability of the empirical models to represent year-to-year variations in the Antarctic ozone hole and the seasonal evolution of chlorine activation and ozone depletion was shown to be in good agreement with observations.

5.2 Future Work

Future work can cover a number of issues to improve the methods presented, to examine the presented methods further, and to expand these methods to new applications.

For the application of the regression coefficients from the linear regression model in Chapter 2, it would be desirable to have more CCM data. In particular, it would be very interesting to have a number of CCM runs for the past and present with different forcings, and the same model runs for the same forcings for a period into the future. With these data sets, it would be possible to better estimate the effect of different forcings on Antarctic stratospheric ozone depletion. Furthermore, a larger number of CCM runs would allow a statistically more significant conclusion on how the Antarctic ozone hole will develop in the near future, assuming that the impact of temperature and wave activity will remain unchanged.

A possible further application of the newly derived OMD and OHA measures in

Chapter 3 is to use this method for chemistry-climate model intercomparison as already indicated in the chapter. This would have the advantage that ozone biases in the different models could be avoided by defining a model specific climatology. Furthermore, these measures can be used to study the impact of the Antarctic ozone hole on the biosphere since they better represent the true extent of ozone depletion. It would be interesting to compare correlations between UV-impact at the surface and the old ozone measures with correlations between UV-impact at the surface and the new ozone measures.

The semi-empirical model for Antarctic stratospheric chlorine activation can be improved when more observational data to fit the model become available. ClO profile measurements on pressure levels between 250-30 hPa would be preferable so that the possible altitude dependence of the coefficients can be investigated. The semi-empirical model for the rate of change in OMD could be improved by including an additional term to capture short-term variability due to intrusions of ozone-rich air from lower latitudes. A possible approach could be to define a threshold to distinguish between wave activity causing an increase in ozone depletion due to vortex distortion and/or deformation and wave activity causing a decrease of ozone depletion due to an increase in heat flux and transport of ozone-rich air into the vortex.

Furthermore, the predictive capability of the model can be tested further as indicated in Section 4.4. Application of the derived model to meteorological forecasts of temperature and wave activity was outside the scope of this thesis. The ability of the OMD model to project Antarctic stratospheric ozone depletion into the future, based on temperature and wind data from general circulation models, could be evaluated. In addition, the increase of accuracy of the model with increasing availability of observational data over the course of the year should be tested.

With additional resources, profile measurements of the meteorological and chemical parameters could be obtained and the models could be expanded in a third dimension which could lead to higher accuracy in the modelled values. For ex-

ample, effects of diabatic descent on Antarctic ozone loss could be quantified and separated from chemical ozone depletion. Chlorine activation could be estimated with a vertical distribution, which would lead to better representation of the atmospheric conditions. When looking at the vertical resolution of ozone depletion additional catalytic destruction cycles could be considered and the relative importance could be evaluated. In addition, the semi-empirical models for chlorine activation and ozone destruction could be expanded for Arctic conditions. Since the Arctic polar vortex is less stable than the Antarctic vortex, terms to account for intrusion into the vortex would need to be added to the equations.

The coefficients derived when fitting the semi-empirical model to observations capture key sensitivities of dynamical and chemical processes in the atmosphere. Similar coefficients can be estimated for CCMs and comparison of the sensitivities may provide new insights into potential sources of differences in CCM projections of Antarctic ozone depletion. Application of the semi-empirical models developed in this thesis could help to quantify the severity of Antarctic ozone depletion in the future and therefore help to assess the potential recovery of the Antarctic ozone hole.

Appendix A

Physical and Chemical Formulas

A.1 Physical Formulas

α	efficiency factor for bromine vs. chlorine
β-effect	variation in Coriolis effect with latitude
λ	wavelength
ρ_0	density
ϕ	latitude
a	mean radius for distance from any point in the atmosphere to the centre of Earth
F	Eliassen-Palm flux
$\frac{FC_x}{FC_{CFC-11}}$	relative fractional release of chlorine/bromine
FC_{CFC_11}	absolute fractional release of CFC-11
n_x	number of chlorine or bromine atoms in each halocarbon
T	temperature
u, v, w	wind components
$\overline{u'v'}$	momentum flux
$\overline{v'T'}$	heat flux
z	longitude

A.2 Chemical Formulas

Br	bromine atom
$BrNO_3$	bromine nitrate
BrO	bromine monoxide
$BrONO_2$	bromine nitrate
CBr_2F_2	H-1202
$CBrClF_2$	H-1211
$CBrF_3$	H-1301
CCl_2F_2	CFC-12
CCl_2FCClF_2	CFC-113
CCl_3F	CFC-11
CCl_4	carbon tetrachloride
$CClF_2CClF_2$	CFC-114
$CClF_2CF_3$	CFC-115
CH_3Br	methyl bromide
CH_3CCl_2F	HCFC-141b
CH_3CCl_3	methyl chloroform
CH_3CClF_2	HCFC-142b
CH_3Cl	methyl chloride
CH_4	methane
$CHClF_2$	HFCF-22
Cl	chorine atom
Cl, Br, ClO, BrO	halogens
Cl_2	chlorine molecule
Cl_2O_2	chlorine dimer
ClBr	photochemically labile state of chlorine/bromine
ClO	chlorine monoxide
$ClONO_2$	chlorine nitrate
HBr	hydrogen bromide
HCl	hydrogen chloride

HF	hydrofluoric acid
HNO_3	nitric acid
HOBr	hypobromous acid
HOCl	hypochlorous acid
N_2O	nitrous oxide
NAT	nitric acid trihydrate ($HNO_3(H_2O)_3$)
NO_2	nitrogen dioxide
NO_x	nitrogen oxides (NO + NO_2 + NO_3)
NO_y	total reactive nitrogen
	(NO, NO_2, NO_3, N_2O_5, $ClONO_2$, HNO_4, HNO_3)
O	oxygen atom
O_2	oxygen molecule
O_3	ozone
OClO	symmetric chlorine dioxide
OH	hydroxide radical
STS	supercooled ternary solution ($H_2SO_4/HNO_3/H_2O$)
X	catalyst

Appendix B

Symbols and Acronyms

AMTRAC	Atmospheric Model with Transport and Chemistry
AVP	Antarctic Vortex Period
CCM	Chemistry-Climate Model
CCMVal	Chemistry-Climate Model Validation
CCSTNIES	Center for Climate System Research/
	National Institute for Environmental Studies
CFCs	Chlorofluorocarbons
CMAM	Canadian Middle Atmosphere Model
DU	Dobson Unit
EEASC	Equivalent Effective Antarctic Stratospheric Chlorine
EESC	Equivalent Effective Stratospheric Chlorine
GEOSCCM	Goddard Earth Observing System Chemistry-Climate Model
GOME	Global Monitoring Experiment
HALOE	Halogen Occultation Experiment
ILAS	Improved Limb Atmospheric Spectrometer
LMDZ	Laboratoire de Meteorologie Dynamique
	General Circulation System
MAC	Mass of Activated Chlorine
MAECHAM	Middle Atmosphere European Center Hamburg Model
MLS	Microwave Limb Sounder
MRI	Meteorological Research Institute Model
NCAR	National Center of Atmospheric Research
NCEP	National Center of Environmental Prediction

NIWA	National Institute of Water and Atmospheric Research
OHA	Ozone Hole Area
OMD	Ozone Mass Deficit
PSCs	Polar Stratospheric Clouds
PV	Potential Vorticity
QBO	Quasi-Biennial Oscillation
SAO	Semi-Annual Oscillation
SOCOL	Solar Climate Ozone Links
STP	Standard Temperature and Pressure
SZA	Solar Zenith Angle
TOMS	Total Ozone Mapping Spectrometer
UARS	Upper Atmosphere Research Satellite
ULAQ	University of l'Aquila Model
UMETRAC	Unified Model with Eulerian Transport and Chemistry
UMSLIMCAT	Unified Model - Single Level Isentropic Model of Chemistry and Transport
UV	Ultra-Violet
WACCM	Whole Atmosphere Community Climate Model
WMO	World Meteorological Organisation

Appendix C

Rossby Waves

Atmospheric waves are excited when air is disturbed from equilibrium, for example when air is displaced over elevated terrain or heated inside convection. The conservation of absolute vorticity can be expressed by equation C.1, and the perturbation vorticity equation (Equation C.2) is obtained by linearising about a basic state that is barotropically stratified and in uniform motion. As this motion is non-divergent it can be represented in terms of a stream function (Equation C.3) and the perturbation equation (Equation C.2) results in equation C.4 which is also known as the Rossby wave equation. It reflects a balance between changes in the relative vorticity of an air parcel and changes in its planetary vorticity due to meridional displacement.

$$\frac{d\zeta}{dt} + \beta v = 0 \tag{C.1}$$

$$\frac{D\zeta'}{Dt} + \beta v' = 0 \tag{C.2}$$

$$\vec{v}'_h = \vec{k} \times \nabla\psi' \tag{C.3}$$

$$\frac{D}{Dt}\nabla^2\psi' + \beta\frac{\partial\psi'}{\partial x} = 0 \tag{C.4}$$

where ζ is the absolute vorticity, β is the meridional gradient of the Coriolis term, v is the meridional wind velocity, primed quantities denote departure from the zonal mean, v_h indicates the motion described by a stream function, k is a unit vector and ψ represents the stream function.

Rossby waves are observed on horizontal scales of thousands of kilometres and

with periods of several days. They occur on large horizontal wavelengths and with low frequencies, therefore it is reasonable to use quasi-geostrophic equations to model these waves. With the uniform zonal background flow $(U, 0, 0)$ (U is constant), the linearised quasi-geostrophic potential vorticity equation results in equation (C.5).

$$\left(\frac{\partial}{\partial t} + U\frac{\partial}{\partial x}\right)\left(\frac{\partial^2}{\partial x^2} + \frac{\partial^2}{\partial y^2} + \frac{\partial}{\partial z}\left(\frac{f_0^2}{N_B^2}\frac{\partial}{\partial z}\right)\right)\psi' + \beta\frac{\partial \psi'}{\partial x} = 0, \tag{C.5}$$

where N_B is the buoyancy frequency. Choosing N_B to be constant and substituting ψ' with equation (C.6) the dispersion relation for Rossby waves is obtained (Equation C.7) [*Andrews*, 2000].

$$\psi' = \mathrm{Re}\left(\hat{\psi}\right) e^{i(kx+ly+mz-\omega t)} \tag{C.6}$$

$$\omega = kU - \frac{\beta k}{k^2 + l^2 + f_0^2 m^2/N_B^2}, \tag{C.7}$$

where $\hat{\psi}$ is the complex amplitude and m is the vertical wavenumber.

The dispersion relation reveals several features [*Andrews*, 2000]:

- The crucial effect for the existence of Rossby waves is the β-effect. If $\beta = 0$, it would lead to $\omega = kU$ and the waves would just be carried along with the background flow U.
- $\beta > 0$ leads to $U - c > 0$ and therefore Rossby waves always move westward with respect to the background flow.
- Considering vertical propagation for given real values of the horizontal wavenumbers k and l, as well as $m^2 > 0$, the relation $0 < U - c < U_c$ is found, where U_c depends on the horizontal wavelengths of the wave. In particular, for stationary waves, whose crests and troughs do not move with respect to the ground $c = 0$. The derived relation $0 < U < U_c$ is

known as the **Charney-Drazin** criterion. It states that stationary waves propagate vertically only in eastward background flows ($U > 0$) and that those background flows should not be too strong ($U < U_c$). In consistence with observations in the northern hemisphere, this criterion gives an explanation why stationary Rossby waves have large horizontal scales in the eastward winds of the winter stratosphere, whereas the waves are absent in the westward winds of the summer stratosphere.

- Rossby waves show strong variations of phase speed with wavelength: large horizontal scales have small values of $k^2 + l^2$ and the zonal phase speed approaches $c_{long} = U - (\beta N_B^2)/(f_0^2 m^2)$, whereas for short horizontal scales the zonal phase speed approaches U, the speed of the background flow. This indicates that these waves are strongly dispersive and therefore a composure of different wavelengths will tend to break up or disperse in time.

- The definition of a group velocity vector $\vec{c_g} = (c_g^{(x)}, c_g^{(y)}, c_g^{(z)}) = (\frac{\partial\omega}{\partial k}, \frac{\partial\omega}{\partial l}, \frac{\partial\omega}{\partial m})$, shows that the vertical component of the group velocity

$$c_g^{(z)} = \frac{\partial\omega}{\partial m} = \frac{2f_0^2\beta km}{N_B^2\left(k^2 + l^2 + \frac{f_0^2 m^2}{N_B^2}\right)^2} \tag{C.8}$$

  is positive (with convention $k, m > 0$) and therefore the waves propagate momentum upwards.

To demonstrate how the β-effect is the restoring force for planetary waves, the disturbance vorticity without a z-dependence is considered:

$$\zeta' = \frac{\partial^2\psi'}{\partial x^2} + \frac{\partial^2\psi'}{\partial y^2} \tag{C.9}$$

The total quasi-geostrophic potential vorticity is then $q = f_0 + \beta y + \zeta'$, and q is conserved following the geostrophic flow [*Andrews*, 2000]. Therefore, if an air parcel A along a certain latitude is moving equatorward (Figure C.1), its value of ζ' increases and the local velocity field experiences a cyclonic rotation. Considering a second air parcel B of the same latitude, west of the first one, B

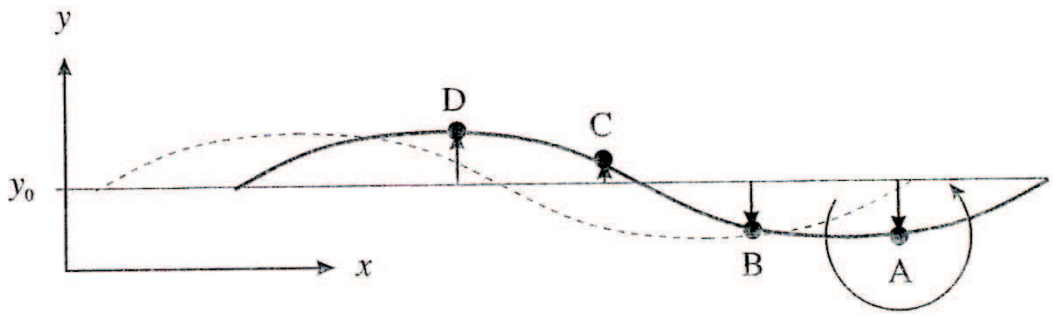

Figure C.1: Illustration of a Rossby wave, considering the conservation of potential vorticity at a certain latitude-circle y_0. See text for details.

is now encouraged by the local velocity field to move equatorward and its value of ζ' increases. This again forces the air parcel C of the same latitude west of B to move equatorward and the air parcel A to move poleward. Imagining this for an infinite number of air parcels, a self-sustaining, westward-moving Rossby-wave pattern emerges.

Appendix D

Chemical Reaction Equations

D.1 Production and Destruction of Ozone in the Stratosphere

The main production of the stratospheric ozone takes place in tropical latitudes in two main steps. The first step is photolysis of molecular oxygen which results in two highly reactive oxygen atoms (Reaction D.1). The second step is recombination of atomic and molecular oxygen to form ozone (Reaction D.2).

$$\mathrm{O_2} + h\nu \longrightarrow \mathrm{O} + \mathrm{O} \quad (\lambda < 242 \text{ nm}) \tag{D.1}$$

$$\mathrm{O} + \mathrm{O_2} + M \longrightarrow \mathrm{O_3} + M \tag{D.2}$$

$$Net: \ 3\ \mathrm{O_2} + h\nu \longrightarrow 2\ \mathrm{O_3} \tag{D.3}$$

where $h\nu$ is the energy of a photon with the frequency ν, λ is the wavelength and M the catalyst which does not change its chemical properties and absorbs excess energy and momentum during the reaction. Photochemical destruction of ozone is caused by photolysis of ozone molecules (Reaction D.4) which again results in a highly reactive oxygen atom and an oxygen molecule. The oxygen atom can react with ozone to form two oxygen molecules (Reaction D.5).

$$O_3 + h\nu \longrightarrow O + O_2 \quad (\lambda < 320\ nm) \tag{D.4}$$

$$O + O_3 \longrightarrow 2\ O_2 \tag{D.5}$$

$$Net:\ 2\ O_3 + h\nu \longrightarrow 3\ O_2 \tag{D.6}$$

Chemical reactions D.1 to D.6 are known as the **Chapman Cycle** after *Chapman* [1930]. In addition, catalytic cycles have to be taken into account. Different catalytic cycles happen with different radicals, for example hydroxide radical (OH), nitrogen oxides (NO_x), halogens (Cl, Br, ClO, BrO), etc. The importance of the different catalytic cycles depends on altitude, meteorological conditions and the concentration of the radicals which react with ozone [*WMO*, 1999].

In the upper stratosphere (between 30 and 50 km), with the exception of the region poleward of about 45 °, ozone is in photochemical steady state, which means that the photochemical reactions are sufficiently fast that the concentrations of ozone are determined by a local balance of photochemical production and loss. However, longer lived gases, such as methane (CH_4), water vapour (H_2O), CFCs and nitrous oxide (N_2O) are affected by transport. Therefore transport has an indirect effect on ozone since the above mentioned gases all act as radical precursors [*WMO*, 1999].

The most important catalytic cycles in the upper stratosphere are those involving NO_x radicals (Reaction D.7), chlorine/bromine radicals (Reaction D.8) and OH radicals (Reactions D.9 to D.11).

$$\begin{aligned} NO_2 + O &\longrightarrow NO + O_2 \\ NO + O_3 &\longrightarrow NO_2 + O_2 \end{aligned}$$

$$Net: \ O + O_3 \longrightarrow 2\ O_2 \tag{D.7}$$

$$\begin{aligned} ClO^* + O &\longrightarrow Cl + O_2 \quad (^*\text{or BrO}) \\ Cl + O_3 &\longrightarrow ClO + O_2 \end{aligned}$$

$$Net: \ O + O_3 \longrightarrow 2\ O_2 \tag{D.8}$$

$$\begin{aligned} OH + O &\longrightarrow H + O_2 \\ H + O_3 &\longrightarrow OH + O_2 \end{aligned}$$

$$Net: \ O + O_3 \longrightarrow 2\ O_2 \tag{D.9}$$

$$\begin{aligned} OH + O &\longrightarrow H + O_2 \\ H + O_2 + M &\longrightarrow HO_2 + M \\ HO_2 + O &\longrightarrow OH + O_2 \end{aligned}$$

$$Net: \ O + O \longrightarrow O_2 \tag{D.10}$$

$$\begin{aligned} HO_2 + O &\longrightarrow OH + O_2 \\ OH + O_3 &\longrightarrow HO_2 + O_2 \end{aligned}$$

$$Net: \ O + O_3 \longrightarrow 2\ O_2 \tag{D.11}$$

D.2 Heterogeneous Reactions

The role of heterogeneous reactions was described in detail in Section 1.3.3. The most important reactions in the ozone depletion cycle are listed below. The first step of the process is the gaseous absorption of HCl by PSCs, followed by the heterogeneous reaction of $ClONO_2$ (gas-phase) with the particle (Reaction D.12). All heterogeneous reactions (Reaction D.12-D.15) would be extremely slow in gas-phase [*Seinfeld and Pandis*, 1998]. The reaction product HOCl from Reaction D.13 can undergo a subsequent heterogeneous reaction (Reaction D.14) as discovered by *Abbatt and Molina* [1992].

$$ClONO_2^{(g)} + HCl^{(s)} \longrightarrow Cl_2^{(g)} + HNO_3^{(s)} \quad \text{(D.12)}$$

$$ClONO_2^{(g)} + H_2O^{(s)} \longrightarrow HOCl^{(g)} + HNO_3^{(s)} \quad \text{(D.13)}$$

$$HOCl^{(g)} + HCl^{(s)} \longrightarrow Cl_2^{(g)} + H_2O^{(s)} \quad \text{(D.14)}$$

$$HOBr^{(g)} + HCl^{(s)} \longrightarrow ClBr^{(g)} + H_2O^{(s)} \quad \text{(D.15)}$$

with (s) denoting a species on the ice and (g) a species in gas-phase.

References

Abbatt, J. P. D., and M. J. Molina, The heterogeneous reaction of HOCl+HCl-] Cl_2+H_2O on ice and nitric-acid trihydrate - reaction probabilities and stratospheric implications, *Geophysical Research Letters*, *19*(5), 461–464, 1992.

Akiyoshi, H., T. Sugita, H. Kanzawa, and N. Kawamoto, Ozone perturbations in the Arctic summer lower stratosphere as a reflection of NOx chemistry and planetary scale wave activity, *Journal of Geophysical Research*, *109*, D03304, doi:10.1029/2003JD003632, 2004.

Allaart, M. A. F., H. Kelder, and L. C. Hejboer, On the relation between ozone and potential vorticity, *Geophysical Research Letters*, *20*, 811–814, 1993.

Alvarez-Madrigal, M., and J. Pérez-Peraza, Analysis of the evolution of the Antarctic ozone hole size, *Journal Geophysical Research*, *110*, D02107, doi:10.1029/2004JD004944, 2005.

Andrews, D. G., *An Introduction to Atmospheric Physics*. University Press, Cambridge, 2000.

Andrews, D. G., J. R. Holton, and C. B. Leovy, *Middle Atmosphere Dynamics*. Academic Press, 1987.

Austin, J., A three-dimensional coupled chemistry-climate model simulation of past stratospheric trends, *Journal of the Atmospheric Sciences*, *59*(2), 218–232, 2002.

Austin, J., and N. Butchart, A three-dimensional modelling study of the influ-

ence of planetary wave dynamics on polar ozone photochemistry, *Journal of Geophysical Research*, *97*(D9), 10165–10186, doi:10.1029/92JD00505, 1992.

Austin, J., and N. Butchart, Coupled chemistry-climate model simulations for the period 1980 - 2020: Ozone depletion and the start of the ozone recovery, *Quarterly Journal of the Royal Meteorological Society*, *129*, 32253249, 2003.

Austin, J., and J. Wilson, Ensemble simulations of the decline and recovery of stratospheric ozone, *Journal of Geophysical Research*, *111*(D16314), doi:10.1029/2005JD006907, 2006.

Austin, J., et al., Uncertainties and assessments of chemistry-climate models of the stratosphere, *Atmospheric Chemistry Physics*, *3*, 1–27, 2003.

Austin, J., J. Wilson, F. Li, and H. Vömel, Evolution of water vapor concentrations and stratospheric age of air in coupled chemistry-climate model simulations, *Journal of Atmospheric Science*, *64*(3), 905–921, 2007.

Baldwin, M., and T. Dunkerton, Quasi-biennial modulation of the southern hemisphere stratospheric polar vortex, *Geophysical Research Letters*, *25*(17), 3343–3346, 1998.

Baldwin, M. P., et al., The quasi-biennial oscillation, *Reviews of Geophysics*, *39*(2), 179–229, 2001.

Beagley, S. R., J. deGrandpre, J. N. Koshyk, N. A. McFarlane, and T. G. Shepherd, Radiative-dynamical climatology of the first-generation Canadian Middle Atmosphere Model, *Atmosphere-Ocean*, *35*(3), 293–331, 1997.

Bloom, S., et al., Documentation and validation of the Goddard Earth Observing System (GEOS) data assimilation system - version 4, *Technical Report Seies on Global Modeling and Data Assimilation*, *26*(104606), 2005.

Bodeker, G. E., and M. W. J. Scourfield, Planetary waves in total ozone and their relation to Antarctic ozone depletion, *Geophysical Research Letters*, *22*(21), 2949–2952, doi:10.1029/95GL01778, 1995.

Bodeker, G. E., B. J. Connor, J. B. Liley, and W. A. Matthews, The global mass of ozone: 1978-1998, *Geophysical Research Letters*, *28*(14), 2819–2822, 2001.

Bodeker, G. E., H. Struthers, and B. J. Connor, Dynamical containment of Antarctic ozone depletion, *Geophysical Research Letters*, *29*(7), 2002.

Bodeker, G. E., H. Shiona, and H. Eskes, Indicators of Antarctic ozone depletion, *Atmospheric Chemistry and Physics*, *5*, 2603–2615, 2005.

Boyce, W. E., and R. C. DiPrima, *Elementary Differential Equations and Boundary Value Problems*. John Wiley & Sons, Inc., 2001.

Brasseur, G., and S. Solomon, *Aeronomy of the Middle Atmosphere*. D. Reidel, 1984.

Brewer, A. M., Evidence for a world circulation provided by the measurements of helium and water vapor distribution in the stratosphere, *Quarterly Journal of the Royal Meteorological Society*, *75*, 351–363, 1949.

Butchart, N., and E. Remsberg, The area of the stratospheric polar vortex as a diagnostic for tracer transport on an isentropic surface, *Journal of the Atmospheric Sciences*, *43*(13), 1319–1339, 1986.

Butchart, N., and A. Scaife, Removal of chlorofluorocarbons by increased mass exchange between the stratosphere and troposphere in a changing climate, *Nature*, *410*, 799–802, 2001.

Chandra, S., and R. D. McPeters, Some observations on the role of planetary waves in determining the spring time ozone distribution in the Antarctic, *Geophysical Research Letters*, *13*(12), 1224–1227, 1986.

Chapman, S., A theory of upper atmospheric ozone, *Mem. Roy. Soc.*, *3*, 103–109, 1930.

Charney, J., The dynamics of long waves in a baroclinic westerly current, *J. Meteor.*, *4*, 135–163, 1947.

Chipperfield, M. P., and R. L. Jones, Relative influences of atmospheric chemistry and transport on Arctic ozone trends, *Nature*, *400*, 551–554, 1999.

Chipperfield, M. P., and J. A. Pyle, Model sensitivity studies of Arctic ozone depletion, *Journal of Geophysical Research-Atmospheres*, *103*(D21), 28389–28403, 1998.

Coleman, T. F., and Y. Li, On the convergence of reflective Newton methods for large-scale nonlinear minimization subject to bounds, *Mathematical Programming*, *67*(2), 189–224, 1994.

Coleman, T. F., and Y. Li, An interior, trust region approach for nonlinear mnimization subject to bounds, *SIAM Journal on Optimization*, *6*, 418–445, 1996.

Coy, L., E. Nash, and P. Newman, Meteorology of the polar vortex: Spring 1997, *Geophysical Research Letters*, *24*(22), 2693–2696, 1997.

Crutzen, P., The influence of nitrogen oxides on the atmospheric ozone content, *QJR Meteorol. Soc*, 1970.

Dameris, M., et al., Long-term changes and variability in a transient simulation with a chemistry-climate model employing realistic forcing, *Atmospheric Chemistry and Physics*, *5*, 2121–2145, 2005.

Dameris, M., S. Matthes, R. Deckert, V. Grewe, and M. Ponater, Solar cycle effect delays onset of ozone recovery, *Geophysical Research Letters*, *33*(3), L03806, 2006.

Daniel, J., S. Solomon, and D. Albritton, On the evaluation of halocarbon radiative forcing and global warming potentials, *Journal of Geophysical Research*, *100*(D1), 1271–1285, doi:10.1029/94JD02516, 1995.

de Grandpre, J., S. R. Beagley, V. I. Fomichev, E. Griffioen, J. C. McConnell, A. S. Medvedev, and T. G. Shepherd, Ozone climatology using interactive

chemistry: Results from the canadian middle atmosphere model, *Journal of Geophysical Research-Atmospheres*, *105*(D21), 26475–26491, 2000.

Dobson, G. M. B., Origin and distribution of polyatomic molecules in the atmosphere, *Proceedings of the Royal Society London*, *A236*, 187–193, 1956.

Douglass, A., et al., A 3D simulation of the early winter distribution of reactive chlorine in the north polar vortex, *Geophysical Research Letters*, *20*(12), 1271–1274, 1993.

Dunkerton, T. J., and M. P. Baldwin, Modes of interannual variability in the stratosphere, *Geophysical Research Letters*, *19*, 49–52, 1992.

Eady, E., Long waves and cyclone waves, *Tellus*, *1*, 33–52, 1949.

Egorova, T., E. Rozanov, V. Zubov, E. Manzini, W. Schmutz, and T. Peter, Chemistry-climate model SOCOL: A validation of the present-day climatology, *Atmospheric Chemistry and Physics*, *5*, 1557–1576, 2005.

Eyring, V., et al., Assessment of temperature, trace species and ozone in chemistry-climate model simulations of the recent past, *Journal of Geophysical Research*, *111*(D22308), doi:10.1029/2006JD007327, 2006.

Farman, J. C., R. J. Murgatroyd, A. M. Silnickas, and B. A. Thrush, Ozone photochemistry in the Antarctic stratosphere in summer, *Quarterly Journal of the Royal Meteorological Society*, *111*, 1013–1028, 1985.

Fels, S. B., A parameterisation of scale-dependent radiative damping rates in the middle atmosphere, *Journal of Atmospheric Sciences*, *39*, 1141–1152, 1982.

Fritz, S., and D. Soules, Planetary variations of stratospheric temperature, *Monthly Weather Review*, *100*, 582–589, 1972.

Fusco, A. C., and M. L. Salby, Interannual variations of total ozone and their relationship to variations of planetary wave activity, *Journal of Climate*, pp. 1619–1629, 1999.

Garcia, R. R., and S. Solomon, A possible relationship between interannual variability in Antarctic ozone and the quasi-biennial oscillation, *Geophysical Research Letters*, *14*, 848–851, 1987.

Garcia, R. R., D. R. Marsh, D. E. Kinnison, B. A. Boville, and F. Sassi, Simulations of secular trends in the middle atmosphere, 1950-2003, *Journal of Geophysical Research*, *112*(D09301), doi:10.1029/2006JD007485, 2007.

Gray, L. J., S. J. Phipps, T. J. Dunkerton, M. P. Baldwin, E. F. Drysdale, and M. R. Allen, A data study of the influence of the equatorial upper stratosphere on northern-hemisphere stratospheric sudden warmings, *Quarterly Journal of the Royal Meteorological Society*, *127*(576), 1985–2003, Part B, 2001.

Hadley, G. S., Concerning the cause of the general trade winds, *Phil. Trans.*, *29*, 58–62, 1735.

Halley, E., *Philosophical Transactions of the Royal Society*, *11*(683), 1676.

Haynes, P. H., C. J. Marks, M. R. McIntyre, T. G. Shepherd, and K. P. Shine, On the 'downward control' of extratropical diabatic circulations by eddy-induced mean zonal forces, *Journal of Atmospheric Science*, *48*, 651–678, 1991.

Holton, J. R., *An Introduction to Dynamic Meteorology*. Academic Press, London, 3rd edn., 1992.

Holton, J. R., and M. J. Alexander, The role of waves in the transport circulation of the middle atmosphere, *Geophysical Monograph*, *123*, 21–35, 2000.

Holton, J. R., P. H. Haynes, M. E. Mcintyre, A. R. Douglass, R. B. Rood, and L. Pfister, Stratosphere-troposphere exchange, *Reviews of Geophysics*, *33*(4), 403–439, 1995.

Hoppel, K., R. Bavilacqua, D. R. Allen, G. E. Nedoluha, and C. Randall, POAM III observations of the anomalous 2002 Antarctic ozone hole, *Geophysical Research Letters*, *30*(7), 1394, doi:10.1029/2003GL016899, 2003.

Hoppel, K., G. Nedoluha, M. Fromm, D. Allen, R. Bevilacqua, J. Alfred, B. Johnson, and G. Konig-Langlo, Reduced ozone loss at the upper edge of the Antarctic ozone hole during 2001-2004, *Geophysical Research Letters*, *32*(20), L20816, 2005.

Huck, P. E., A. J. McDonald, G. E. Bodeker, and H. Struthers, Interannual variability in Antarctic ozone depletion controlled by planetary waves and polar temperature, *Geophysical Research Letters*, *32*(13), doi:10.1029/2005GL022943, L13819, 2005.

Jiang, Y. B., Y. L. Yung, and R. W. Zurek, Decadal evolution of the Antarctic ozone hole, *Journal of Geophysical Research-Atmospheres*, *101*(D4), 8985–8999, 1996.

Julian, P., Midwinter stratospheric warmings in the southern hemisphere: General remarks and a case study, *J. Apl. Met*, (6), 557563, 1967.

Kim, Y., W. Choi, K.-M. Lee, J. H. Park, S. T. Massie, Y. Sasano, H. Nakajima, and T. Yokota, Polar stratospheric clouds observed by the ILAS-II in the Antarctic region: Dual compositions and variation of compositions during June to August of 2003, *Journal of Geophysical Research*, *111*(D135890), doi:10.1029/2005JD006445, 2006.

Kraus, H., *Die Atmosphäre der Erde*. Verlag Vieweg, 2000.

Kröger, C., M. Hervig, B. Nardi, L. Oolman, T. Deshler, S. Wood, and S. Nichol, Stratospheric ozone reaches new minima above McMurdo Station, Antarctica, between 1998 and 2001, *Journal of Geophysical Research*, *108*(D17), 4555, doi:10.1029/2002JD002904, 2003.

Kurokawa, J., H. Akiyoshi, T. Nagashima, H. Masunaga, T. Nakajima, M. Takahashi, and H. Nakane, Effects of atmospheric sphericity on stratospheric chemistry and dynamics over Antarctica, *Journal of Geophysical Research-Atmospheres*, *110*(D21), D21305, 2005.

Labitzke, K., Midwinter warmings in the stratosphere and lower mesosphere, *Zeitschr. Geophys.*, (34), 555561, 1968.

Labitzke, K., and M. Kunze, Stratospheric temperatures over the Arctic: Comparison of three data sets, *Meteorologische Zeitschrift*, *14*(1), 65–74, 2005.

Lait, l. R., M. R. Schoeberl, and P. A. Newman, Quasi-biennial modulation of Antarctic ozone depletion, *Journal of Geophysical Research*, *94*, 11559–11571, 1989.

Lee, A. M., H. K. Roscoe, A. E. Jones, P. H. Haynes, E. F. Shuckburgh, M. W. Morrey, and H. C. Pumphrey, The impact of the mixing properties within the Antarctic stratospheric vortex on ozone loss in spring, *Journal of Geophysical Research-Atmospheres*, *106*(D3), 3203–3211, 2001.

Lefevre, F., G. P. Brasseur, I. Folkins, A. K. Smith, and P. Simon, Chemistry of the 1991-1992 stratospheric winter - 3-dimensional model simulations, *Journal of Geophysical Research-Atmospheres*, *99*(D4), 8183–8195, 1994.

Manney, G. L., J. L. Sabutis, S. Pawson, M. L. Santee, B. Naujokat, R. Swinbank, M. E. Gelman, and W. Ebisuzaki, Lower stratospheric temperature differences between meteorological analyses in two cold Arctic winters and their impact on polar processing studies, *Journal of Geophysical Research-Atmospheres*, *108*(D5), 8328, 2003.

Manzini, E., B. Steil, C. Bruhl, M. A. Giorgetta, and K. Kruger, A new interactive chemistry-climate model: 2. Sensitivity of the middle atmosphere to ozone depletion and increase in greenhouse gases and implications for recent stratospheric cooling, *Journal of Geophysical Research-Atmospheres*, *108*(D14), 4429, 2003.

McCormick, M. P., H. M. Steele, P. Hamill, W. P. Chi, and T. J. Swissler, Polar stratospheric cloud sightings by SAM II, *Journal of Atmospheric Sciences*, *39*, 1387–1397, 1982.

McElroy, M. B., R. J. Salawitch, S. C. Wofsy, and J. A. Logan, Reductions of Antarctic ozone due to synergistic interactions of chlorine and bromine, *Nature*, *321*(6072), 759–762, 1986.

McKenzie, R., B. Conner, and G. Bodeker, Increased summertime UV radiation in New Zealand in response to ozone loss, *Science*, *285*(5434), 1709–1711, 1999.

Molina, L. T., and M. J. Molina, Production of Cl_2O_2 from the self-reaction of the ClO radical, *Journal of Physical Chemistry*, *91*(2), 433–436, 1987.

Molina, M. J., and F. S. Rowland, Stratospheric sink for chlorofluoromethanes: Chlorine atom-catalysed destruction of ozone, *Nature*, *249*(doi:10.1038/249810a0), 810 – 812, 1974.

Müller, R., U. Schmidt, A. Engel, D. S. McKenna, and M. H. Proffitt, The O_3/N_2O relation from balloon-borne observations as a measure of Arctic ozone loss in 1991/92, *Quarterly Journal of the Royal Meteorological Society*, *127*(574), 1389–1412, Part B, 2001.

Müller, R., S. Tilmes, P. Konopka, J. U. Grooß, and H. J. Jost, Impact of mixing and chemical change on ozone-tracer relations in the polar vortex, *Atmospheric Chemistry and Physics*, *5*, 3139–3151, 2005.

Nakajima, H., Preface to special section on ILAS-II: The Improved Limb Atmospheric SpectrometerII, *Journal of Geophysical Research*, *111*(D20, D20S90), doi:10.1029/2006JD007412, 2006.

Nakajima, H., et al., Characteristics and performance of the Improved Limb Atmospheric Spectrometer-II (ILAS-II) onboard the ADEOS-II satellite, *Journal of Atmospheric Research*, *111*(D11S01), doi:10.1029/2005JD006334, 2006.

Nash, E. R., P. A. Newman, J. E. Rosenfield, and M. R. Schoeberl, An objective determination of the polar vortex using Ertel's potential vorticity, *Journal of Geophysical Research-Atmospheres*, *101*(D5), 9471–9478, 1996.

Nathan, T., E. C. Cordero, L. Li, and D. J. Wuebbles, Effects of planetary wave-breaking on the seasonal variation of total column ozone, *Geophysical Research Letters*, *27*(13), 1907–1910, 2000.

Naujokat, B., and H. K. Roscoe, Evidence against an Antarctic stratospheric vortex split during the periods of pre-IGY temperature measurements, *Journal of the Atmospheric Sciences*, *62*(3), 885–889, 2005.

Newman, P., E. Nash, and J. Rosenfield, What controls the temperature of the Arctic stratosphere during the spring?, *Journal of Geophysical Research*, *106*(D17), 19999–20010, 2001.

Newman, P. A., and E. R. Nash, The unusual Southern Hemisphere stratosphere winter of 2002, *Journal of the Atmospheric Sciences*, *62*(3), 614–628, 2005.

Newman, P. A., and W. J. Randel, Coherent ozone dynamical changes during the southern hemisphere spring 1979-1986, *Journal of Geophysical Research*, *93*, 12585–12606, 1988.

Newman, P. A., M. R. Schoeberl, and L. R. Lait, Comparison of the southern hemisphere springs of 1988 and 1987, *Kluwer Academic Publishers*, pp. 71–89, 1990.

Newman, P. A., S. R. Kawa, and E. R. Nash, On the size of the Antarctic ozone hole, *Geophys. Res. Lett.*, *31*(21), doi:/10.1029/2004GL020596, 2004.

Newman, P. A., E. R. Nash, S. R. Kawa, S. A. Montzka, and S. M. Schauffler, When will the Antarctic ozone hole recover?, *Geophysical Research Letters*, *33*(12), 2006.

O'Sullivan, D., and T. J. Dunkerton, Seasonal development of the extratropical QBO in a numerical model of the middle atmosphere, *Journal of Geophysical Research*, *151*, 3706–3721, 1995.

Pitari, G., E. Mancini, and V. Grewe, Deep convective transport in a two-dimensional model: Effects on lower stratospheric aerosols and ozone, *Meteorologische Zeitschrift*, *11*(3), 187–196, 2002.

Press, W. H., S. A. Teukolsky, W. T. Vetterling, and B. P. Flannery, *Numerical recipes in C - The art of scientific computing*. Cambridge University Press, second edn., 1997.

Proffitt, M. H., J. J. Margitan, K. K. Kelly, M. Loewenstein, J. R. Podolske, and K. R. Chan, Ozone loss in the Arctic polar vortex inferred from high-altitude aircraft measurements, *Nature*, *347*(6288), 31–36, 1990.

Randel, W. J., Global atmospheric circulation statistics 1000-1, *NCAR Technical Note*, *NCAR/TN-295*, 245 pp., 1987.

Randel, W. J., Global variations of zonal mean ozone during stratospheric warming events, *Journal of Atmospheric Sciences*, *50*, 3308–331, 1993.

Randel, W. j., and J. B. Cobb, Coherent variations of monthly mean total ozone and lower stratospheric temperature, *Journal of Geophysical Research*, *99*, 5433–5447, 1994.

Randel, W. J., F. Wu, and R. Stolarski, Changes in column ozone correlated with the stratospheric EP flux, *Journal of the Meteorological Society of Japan*, *80*(4B), 849–862, 2002.

Reid, S., *Ozone and Climate Change - A Beginner's Guide*. Gordon and Breach Science Publishers, 2000.

Richard, E. C., et al., Severe chemical ozone loss inside the Arctic polar vortex during winter 1999-2000 inferred from in-situ airborne measurements (vol 28, pg 2197, 2001), *Geophysical Research Letters*, *28*(16), 3167–3167, 2001.

Rodriguez, J. M., Probing stratospheric ozone, *Science*, *261*(5125), 1128–1129, 1993.

Roscoe, H. K., J. D. Shanklin, and S. R. Colwell, Has the Antarctic vortex split before 2002?, *Journal of the Atmospheric Sciences*, *62*(3), 581–588, 2005.

Rossby, C. G., Relation between variations in the intensity of the zonal circulation of the atmosphere and the displacements of the semipermanent centers of action, *Journal of Marine Research*, *2*(1), 38–55, 1939.

Rozanov, E., M. Schraner, C. Schnadt, T. Egorova, M. Wild, A. Ohmura, V. Zubov, W. Schmutz, and T. Peter, Assessment of the ozone and temperature variability during 1979-1993 with the chemistry-climate model SOCOL, *35*, 1375–1384, 2005.

Russell III, J. M., L. Gordley, J. Park, S. R. Drayson, A. F. Tuck, J. Harries, R. J. Cicerone, P. J. Crutzen, and J. E. Frederick, The Halogen Occultation Experiment, *Journal of Geophysical Research*, *98*, 10777–10797, 1993.

Saitoh, N., S. Hayashida, Y. Sasano, and L. L. Pan, Characteristics of Arctic polar stratospheric clouds in the winter of 1996/1997 inferred from ILAS measurements, *Journal of Geophysical Research-Atmospheres*, *107*(D24), 8205, 2002.

Salawitch, R., et al., Chemical loss of ozone in the Arctic polar vortex in the winter of 1991-1992, *Science*, *261*, 1146–1149, 1993.

Salby, M. L., *Fundamentals of Atmospheric Physics*. Academic Press, San Diego, 1996.

Santee, M. L., G. L. Manney, J. W. Waters, and N. J. Livesey, Variations and climatology of ClO in the polar lower stratosphere from UARS Microwave Limb Sounder measurements, *Journal of Geophysical Research-Atmospheres*, *108*(D15), 2003.

Sasano, Y., M. Suzuki, T. Yokota, and H. Kanzawa, Improved limb atmospheric spectrometer (ILAS) for stratospheric ozone layer measurements by solar occultation technique, *Journal of Geophysical Research*, *26*, 197–200, doi:10.1029/1998GL900276, 1999.

Schoeberl, M. R., and D. L. Hartmann, The dynamics of the stratospheric polar vortex and is relation to springtime ozone depletions, *Science*, *251*, 46–52, 1991.

Schubert, S. D., and M. J. Muntenau, An analysis of tropopause pressure and total ozone correlations, *Monthly Weather Review*, *116*, 569–582, 1988.

Seinfeld, J., and S. Pandis, *Atmospheric Chemistry and Physics - from air pollution to climate change*. John Wiley & Sons, Inc., 1998.

Shibata, K., and M. Deushi, Partitioning between resolved wave forcing and unresolved gravity wave forcing to the quasi-biennial oscillation as revealed with a coupled chemistry-climate model, *Geophysical Research Letters*, *32*(12), L12820, 2005.

Shibata, K., M. Deushi, T. T. Sekiyama, and H. Yoshimura, Development of an MRI chemical transport model for the study of stratospheric chemistry, *Papers in Meteorology and Geophysics*, *55*, 75–119, 2005.

Shindell, D. T., S. Wong, and D. Rind, Interannual variability of the Antarctic ozone hole in a GCM. Part I: The influence of tropospheric wave variability, *Journal of the Atmospheric Sciences*, *54*, 2308–2319, 1997.

Shine, K. P., The middle atmosphere in the absence of dynamic heat fluxes, *Quarterly Journal of the Royal Meteorological Society*, *113*, 603–633, 1987.

Sinnhuber, B.-M., M. Weber, A. Amankwah, and J. Burrows, Total ozone during the unusual Antarctic winter of 2002, *Geophysical Research Letters*, *30*(11), 1580, doi:10.1029/2002GL016798, 2003.

Solomon, P., J. Barrett, T. Mooney, B. Connor, A. Parrish, and D. E. Siskind, Rise and decline of active chlorine in the stratosphere, *Geophysical Research Letters*, *33*(18), 2006.

Solomon, S., Stratospheric ozone depletion: A review of concepts and history, *Rev. Geophys.*, *37*(3), 275–316, doi:10.1029/1999RG900008, 1999.

Solomon, S., R. R. Garcia, F. S. Rowland, and D. J. Wuebbles, On the depletion of Antarctic ozone, *Nature*, *321*(6072), 755–758, 1986.

Solomon, S., J. Smith, R. Sanders, L. Perliski, H. Miller, G. Mount, J. Keys, and A. Schmeltekopf, Visible and near-ultraviolet spectroscopy at McMurdo Station, Antarctica 8. observations of nighttime NO_2 and NO_3 from April to October 1991, *Journal of Geophysical Research*, *98*(D1), 993–1000, doi:10.1029/92JD02390, 1993.

Solomon, S., R. W. Portmann, T. Sasaki, D. J. Hofmann, and D. W. J. Thompson, Four decades of ozonesonde measurements over Antarctica, *Journal of Geophysical Research-Atmospheres*, *110*(D21), D21311, 2005.

Steil, B., C. Bruhl, E. Manzini, P. J. Crutzen, J. Lelieveld, P. J. Rasch, E. Roeckner, and K. Kruger, A new interactive chemistry-climate model: 1. Present-day climatology and interannual variability of the middle atmosphere using the model and 9 years of HALOE/UARS data, *Journal of Geophysical Research-Atmospheres*, *108*(D9), 4290, 2003.

Steinbrecht, W. e. a., Correlations between tropopause height and total ozone: Implications for long term changes, *Journal of Geophysical Research*, *103*, 19183–19192, 1998.

Stolarski, R., M. Schoeberl, P. Newman, R. McPeters, and A. Krueger, The 1989 Antarctic ozone hole as observed by TOMS, *Geophysical Research Letters*, *17*(9), 1267–1270, 1990.

Stolarski, R. S., A. R. Douglass, S. Steenrod, and S. Pawson, Trends in stratospheric ozone: Lessons learned from a 3D chemical transport model, *Journal of the Atmospheric Sciences*, *63*(3), 1028–1041, 2006.

Strahan, S., Influence of planetary wave transport on Arctic ozone as observed by polar ozone and aerosol measurement (POAM) III, *Journal of Geophysical Research*, *107*(D20), 4417, doi:10.1029/2002JD002189, 2002.

Struthers, H., K. Kreher, J. Austin, R. Schofield, G. Bodeker, P. Johnston, H. Shiona, and A. Thomas, Past and future simulations of NO_2 from a coupled chemistry-climate model in comparison with observations, *Atmospheric Chemistry and Physics*, *4*, 2227–2239, 2004.

Suzuki, M. A., A. Matsuzaki, T. Ishigaki, N. Kimura, N. Araki, T. Yokota, and Y. Sasano, ILAS, the improved limb atmospheric spectrometer, on the advanced Earth observing satellite, *IEICE TRANS Commun*, *E78-B,12*, 1560–1570, 1995.

Tian, W. S., and M. P. Chipperfield, A new coupled chemistry-climate model for the stratosphere: The importance of coupling for future O-3-climate predictions, *Quarterly Journal of the Royal Meteorological Society*, *131*(605), 281–303, Part A, 2005.

Tilmes, S., R. Müller, J.-U. Grooß, R. Spand, T. Sugita, H. Nakajima, and Y. Sasano, Chemical ozone loss and related processes in the Antarctic winter 2003 based on ILAS-II observations, *Journal of Geophysical Research*, *111*(D11S12), doi:/10.1029/2005JD006260, 2006a.

Tilmes, S., R. Müller, A. Engel, M. Rex, and J. M. Russell, Chemical ozone loss in the Arctic and Antarctic stratosphere between 1992 and 2005, *Geophysical Research Letters*, *33*(20), L20812, 2006b.

Uchino, O., R. D. Bojkov, D. S. Balis, K. Akagi, M. Hayashi, and R. Kajihara, Essential characteristics of the Antarctic-spring ozone decline: Update to 1998, *Geophysical Research Letters*, *26*(10), 1377–1380, 1999.

Wagner, T., C. Leue, K. Pfeilsticker, and U. Platt, Monitoring of the stratospheric chlorine activation by Global Ozone Monitoring Experiment (GOME) OClO measurements in the austral and boreal winters 1995 through 1999, *Journal of Geophysical Research-Atmospheres*, *106*(D5), 4971–4986, 2001.

Wagner, T., F. Wittrock, A. Richter, M. Wenig, J. P. Burrows, and U. Platt, Continuous monitoring of the high and persistent chlorine activation during

the Arctic winter 1999/2000 by the GOME instrument on ERS-2, *Journal of Geophysical Research-Atmospheres*, *107*(D20), 8267, 2002.

Wallace, J., and P. Hobbs, *Atmospheric Science - An introductory survey*. Elsevier Inc., 2006.

Waugh, D. W., and T. M. Hall, Age of stratospheric air: Theory, observations, and models, *Rev. of Geophys.*, *40*(4), 1010, doi:10.1029/2000RG000101, 2002.

Wirth, V., Quasi-stationary planetary waves in total ozone and their correlation with lower stratospheric temperature, *Journal of Geophysical Research*, *98*(D5), 8873–8882, 1993.

WMO, *Atmospheric ozone 1985: Assessment of our understanding of the processes controlling its present distribution and change*. World Meteorological Organisation Global Ozone Research and Monitoring Project Report No. 16, Geneva, 1985.

WMO, *Scientific Assessment of ozone depletion: 1998*. World Meteorological Organisation Global Ozone Research and Monitoring Project Report No. 44, 1999.

WMO, *Scientific Assessment of ozone depletion: 2002*. World Meteorological Organisation Global Ozone Research and Monitoring Project Report No. 47, 2003.

WMO, *Scientific Assessment of Ozone Depletion: 2006*. World Meteorological Organization Global Ozone Research and Monitoring Project Report No. 50, Geneva, 2007.